

FAR-INFRARED STUDIES OF INORGANIC COMPLEXES
IN THE SOLID STATE BY SPECTROSCOPIC AND
INTERFEROMETRIC METHODS

A Thesis

presented for the degree of

Doctor of Philosophy in the Faculty of Science

of the

University of Leicester

by

Donald Michael Morris

The University of Leicester
July 1967

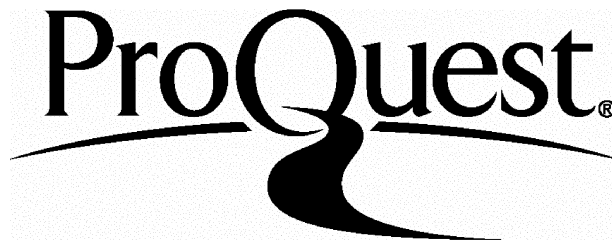
ProQuest Number: U622481

All rights reserved

INFORMATION TO ALL USERS

The quality of this reproduction is dependent upon the quality of the copy submitted.

In the unlikely event that the author did not send a complete manuscript and there are missing pages, these will be noted. Also, if material had to be removed, a note will indicate the deletion.



ProQuest U622481

Published by ProQuest LLC(2015). Copyright of the Dissertation is held by the Author.

All rights reserved.

This work is protected against unauthorized copying under Title 17, United States Code.
Microform Edition © ProQuest LLC.

ProQuest LLC
789 East Eisenhower Parkway
P.O. Box 1346
Ann Arbor, MI 48106-1346

X752984585

541.4
318640
23-268



This thesis is humbly dedicated, somewhat topically,
to Claudio, source and inspiration of much pleasure.

Statement

The experimental work in this thesis has been carried out at the University of Leicester under the supervision of Dr. D. M. Adams.

This thesis has not been presented and is not being currently presented for any other degree.

D. Morris

July, 1967.

I wish to express my gratitude to Dr. D. M. Adams for his help and encouragement throughout the course of this work.

My thanks are also due to my colleagues for their interest, assistance and tolerance, and to Mrs. J. Kempston for the hours spent typing this thesis.

I also wish to thank S. R. C. for a maintenance grant.

CONTENTS

CHAPTER 1	Interferometry-theory and practice	1
CHAPTER 2	Slit spectrometry	46
CHAPTER 3	Octahedral anions	61
CHAPTER 4	Square-planar ions	113
CHAPTER 5	Tetrahedral anions	139
CHAPTER 6	Tungsten chloride pentafluoride	147
CHAPTER 7	Cupric halide-quinoxaline complexes	173

CHAPTER I INTERFEROMETRY - THEORY AND PRACTICE1.1 Introduction

The study of far-infrared spectra by interferometric methods is a fairly recent development, although the theory has been known for over sixty years. It is probably true to say that the chemical spectroscopist has not yet accepted the interferometer as an every day tool.

Defining the far-infrared region as those frequencies between 375 cm^{-1} (KBr cutoff) and 10 cm^{-1} (1 mm), there are a number of reasons why this region has not been extensively explored. The most important reason is due to the fact that no source adequately emits in this region. A black body radiator has the energy-wavelength distribution shown in figure [1.1]. The far-infrared part of this curve is shaded. The minute percentage of far-infrared radiation emitted by a black body means that the available energy in this region must be used as efficiently as possible. This, until recently, has unfortunately not been achieved. It was not until 1947 that Golay¹ invented the detector that now bears his name. The limitation on the detectivity of the Golay detector is set by the intrinsic noise of any device operating at 300°K . The liquid helium bolometer which operates at 1.5°K is a far more sensitive detector

but is not generally available. Besides the lack of suitable detectors the poor use of the available energy was due ^{to} the absence of good and suitable dispersive materials for use in prisms. Fortunately rock salt crystals could be found naturally but this only allowed spectra to be measured down to 650 cm^{-1} . Only in 1930² were the first synthetic crystals of potassium bromide made, extending the spectral region down to 375 cm^{-1} .

The alternative method of dispersion to the prism is the grating. The first one for use in an infrared spectrometer was made by Wood and Trowbridge in 1910³. There is a distinct energy gain with a grating compared to a prism. For instance at 1000 cm^{-1} a 2,500 lines per inch grating has six fold energy gain compared with a 60° NaCl prism. When the Merton screw for reproduction of gratings became available it was inevitable that grating instruments would replace prism ones except for the simplest applications. Even allowing for the energy gain obtained using a grating it can be shown that slit spectrometers do not use this available energy in the most economical manner. In fact the lower the frequency of radiation considered the lower is the light grasp of a prism spectrometer. By light grasp we mean the relative quantity of radiation

from a source, as measured by the product of source area and solid angle subtended by the source, which each spectroscopic system can transmit to a detector for the same spectroscopic resolution. A grating spectrometer has a slightly higher light grasp than a prism instrument but is still not a great deal more efficient. Because of the unsatisfactory nature of the prism and grating spectrometer in the very far -infrared other types of spectrometer have been sought as an alternative. One alternative that has proved particularly successful is the Michelson interferometer. The first spectrum of chemical interest obtained with an interferometer was published in 1956⁴. Thus we see that the raison d'etre for the application of interferometry to the study of the far-infrared region was the inadequacy of the slit spectrometer in this region; the advantages of the interferometer over the slit spectrometer will be given later.

1.2 Brief history of interferometry

In 1891, Michelson⁵ showed that the intensity at the detector of a two beam interferometer of variable path length is the cosine Fourier transform of the spectrum emanating from the source. It follows that the cosine Fourier transform of the interferogram should yield the spectrum itself. Interferogram is the conventional name for the plot of intensity of radiation falling on the detector versus the path difference between the two beams in the interferometer. Generally the calculation of the Fourier transform required to yield all spectral elements is prohibitively long and a computer is really necessary. It is for this reason that Michelson only used the interferogram to resolve the fine structure of certain spectral lines in the visible part of the spectrum. Although his calculations did not yield the exact position of the particular band studied, they did indicate whether the band had structure or not. The first far infrared spectrum obtained interferometrically was calculated by Rubens and Wood⁶ although it is probable that they did not realise the full significance of their work.

Present day interferometry springs from the attempts

by Fellgett to measure the spectrum of the night sky. Apparently in 1949 he communicated to Golay the fundamental advantage of spectrographic measurements over spectrometric ones⁷; this advantage has become known as the Fellgett or multiplex advantage. He used two balanced bolometers to record the interferometric pattern produced by a narrow air wedge between two glass plates, the source being focussed on this wedge. One bolometer recorded the light transmitted, the other that reflected. By recording the interference pattern up to the 100th order of interference and taking the Fourier transform of this pattern observed Fellgett was able to obtain spectra of mercury and carbon arcs in fair agreement with the conventional spectral measurements of these sources. Subsequent studies began independently at John Hopkins University and the Centre Nationale de la Recherche Scientifique, Bellvue, France. The first published far-infrared spectrum of chemical interest came from John Hopkins University; Gebbie and Vanesse⁴ obtained the spectrum of water vapour between 60 and 120 cm^{-1} with reasonable agreement with the theoretically calculated spectrum. The extensive work performed at Bellvue is admirably summarised in a series of articles that appear in *Revue d'Optique*.⁸⁻¹¹ Gebbie continued his interest in interferometry at N.P.L; the

subject developed so rapidly that important Conferences took place at Bellvue in 1957 and N.P.L. in 1959.

Inorganic solids were first investigated interferometrically in 1962; Adams and Gebbie¹² obtained the stretching, bending and lattice mode vibrations of a number of complex halides. Since 1962 there has been considerable increase in the number of papers published each year which have quoted interferometric results. This is mainly due to the availability of the first commercial instrument, the FS-520, manufactured by Research and Industrial Instruments Co. Although this interferometer has been extensively used there has not been to date a critical analysis of its particular advantages and faults.

The key experiment that demonstrated the actual advantage of interferometry over slit spectrometry, as is theoretically predicted, was performed at Bell Telephone Laboratories by Richards.¹³ Three instruments, a diffraction grating monochromator, a lamellar grating interferometer and a Michelson interferometer were all operated with the same source and same detector, thus providing, for the first time a direct comparison on the relative merits of the two types of spectrometer. The detector used was a liquid helium bolometer operated at 1.2°K connected to the exit

slit of the above instrument by a 1 metre light pipe; the source was a conventional high pressure mercury arc lamp in a fused quartz jacket. For the interferometers resolution approaching 0.1 cm^{-1} was obtained in the region $3-80 \text{ cm}^{-1}$. Comparison of the results obtained with the interferometer when used at resolutions equivalent to that of the grating spectrometer showed that the signal to noise ratio of the former instruments were at least three times better than those with the latter. This is entirely in keeping with the Fellgett advantage.

The most promising recent development in commercial interferometers is the use of an analogue computer in conjunction with the interferometer. This system alleviates the tedious time-waste in waiting for the spectrum to be computed on a digital system. Research and Industrial Instruments Company manufactured the FTC-100 system which basically is an FS-620 interferometer and a analogue computer.

1.3 Theory.

Consider as a model a normal two-beam interferometer. Assume that a beam splitter separates the incident radiation into two equal beams causing a path difference Δ when the two beams re-unite. In this hypothetical experiment we shall give Δ a largest value L ; that is to say Δ changes from $-L$ through zero to $+L$. The principle of the interferometer has its origin in the wave theory of light. Simple wave theory states that the phase difference between two beams of monochromatic light after re-uniting is $[(2\pi/\lambda) \times \text{path difference}]$ or $\frac{2\pi\Delta}{\lambda}$; λ is the wavelength of the light. Wave theory also states that a light beam can be represented by a scalar, Φ , with

$$\Phi : = a \sin (\omega t - \delta) \quad [1]$$

[ω = period, t = time, δ = phase constant, a = amplitude constant]

Consider first the interference of two unequal beams of light of the same frequency. Taking equation [1] as a model they can be represented as

$$\Phi_1 = a_1 \sin (\omega t - \delta_1)$$

$$\Phi_2 = a_2 \sin (\omega t - \delta_2)$$

Using the principle of superposition of light the resultant Φ

will be given by

$$\begin{aligned}\phi &= a_1 \sin (\omega t - \delta_1) + a_2 \sin (\omega t - \delta_2) \\ &= \sin \omega t (a_1 \cos \delta_1 + a_2 \cos \delta_2) - \cos \omega t (a_1 \sin \delta_1 + \\ &\quad a_2 \sin \delta_2) \quad [2]\end{aligned}$$

To simplify [2] put

$$\begin{aligned}A \sin \delta &= a_1 \sin \delta_1 + a_2 \sin \delta_2 \\ A \cos \delta &= a_1 \cos \delta_1 + a_2 \cos \delta_2\end{aligned}$$

Equation [2] now reduces to the form

$$\phi = A \sin (\omega t - \delta)$$

where

$$A^2 = a_1^2 + a_2^2 + 2 a_1 a_2 \cos (\delta_2 - \delta_1)$$

and

$$\tan \delta = (a_1 \sin \delta_1 + a_2 \sin \delta_2) / (a_1 \cos \delta_1 + a_2 \cos \delta_2)$$

If now $a_1 = a_2 = a$ (say), as is the case in an interferometer model where both beams have the same source, then A the amplitude constant takes the special form :

$$\begin{aligned}A^2 &= 2a^2 [1 + \cos (\delta_2 - \delta_1)] \\ &= 4a^2 \cos^2 \left(\frac{\delta_2 - \delta_1}{2} \right) \quad [3]\end{aligned}$$

The square of the amplitude constant is of course proportional to the intensity of the light beam. Also $(\delta_2 - \delta_1)$ represents the phase difference between the two beams and is equal to $(2\pi\Delta/\lambda)$ as stated above. It is conventional in chemical spectroscopy to use wave numbers instead of wavelengths ; using the relation $\lambda\sigma = 1$, where σ is the wave number (in cm^{-1}), the phase difference becomes $2\pi\sigma\Delta$ and on substituting this in equation [3] one obtains

$$A^2 = 4a^2 \cdot \cos^2 (\pi\sigma\Delta). \quad [4]$$

Reverting back to the cosine form from this half-cosine form,

$$A^2 = 2a^2 [1 + \cos (2\pi\sigma\Delta)]. \quad [5]$$

The right hand side of this equation consists of a constant part and a variable part. The variable part, if put equal to $I(\Delta)$ gives

$$I(\Delta) = 2a^2 \cdot \cos (2\pi\sigma\Delta) \quad [6]$$

If the path difference between the two beams is changing linearly with time the resultant intensity of the monochromatic beam after self-interference varies sinusoidally with time, and anyway always with path difference.

In a real system the radiation will vary between, say, σ_1 and σ_2 cm^{-1} and there will be an arbitrary spectral input $B(\sigma)$. If the same arguments as above are given equation [7] now takes the form :

$$I(\Delta) = \sum_{\sigma = \sigma_1}^{\sigma_2} B(\sigma) \cos (2\pi \sigma \Delta) \cdot \Delta(\sigma)$$

or in the limit of $\Delta(\sigma) \rightarrow d\sigma$

$$I(\Delta) = \int_{\sigma_1}^{\sigma_2} B(\sigma) \cos (2\pi \sigma \Delta) \cdot d\sigma \quad [8]$$

Equation [8] marks the point where interferometry theory takes over from wave theory. $I(\Delta)$, the signal detected after the radiation has interfered is called the interferogram, and is, as equation [8] implies, the Fourier transform (cosine part) of the spectral input. Since Fourier transformation is a reciprocal operation, that is to say that two functions A and B must be Fourier transforms of each other, if one is known to be the transform of the second, then $B(\sigma)$ must be the Fourier transform of the interferogram $I(\Delta)$.

thus

$$B(\sigma) = \int_{-\infty}^{+\infty} I(\Delta) \cos (2\pi \sigma \Delta) d\Delta \quad [9]$$

This is the fundamental relationship of interferometry, and tells one how to re-create the spectrum from the interferogram.

Since a cosine is an even function (and since theoretically, the experimental interferogram is symmetrical about zero path difference) one can re-write equation [9] as

$$B(\sigma) = 2 \int_0^{\infty} I(\Delta) \cos(2\pi \sigma \Delta) d\Delta.$$

Equation [9] has implied that the path difference has varied from $-\infty$ to $+\infty$. As mentioned above this is not so and varies in fact from a finite $-L$ to $+L$. This means that the spectrum one measures is not $B(\sigma)$ but $B'(\sigma)$ where

$$B'(\sigma) = \int_{-L}^{+L} I(\Delta) \cos(2\pi \sigma \Delta) d\Delta.$$

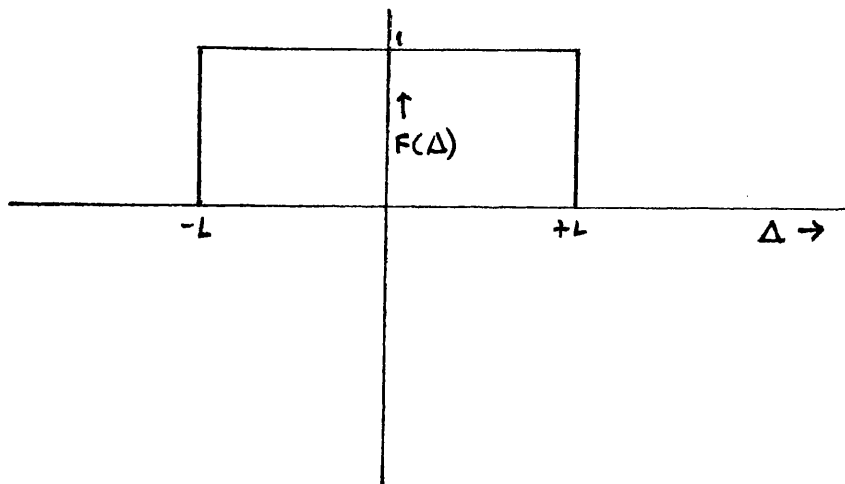
It is convenient to represent this as in equation [10] to introduce the important term APODIZATION.

$$B'(\sigma) = \int_{-\infty}^{+\infty} I(\Delta) \cdot F(\Delta) \cdot \cos(2\pi \sigma \Delta) d\Delta. \quad [10]$$

$F(\Delta)$ is the rectangular function defined by :

$$F(\Delta) = 1, \quad -L \leq \Delta \leq L, \quad F(\Delta) = 0, \quad |\Delta| > L$$

The shape of this function is shown below.



The right hand side of equation [10] involves the product of two functions of Δ ; $B'(\sigma)$ equals the Fourier transform of this product. The convolution theorem states that the Fourier transform of a product of two functions is equal to the convolution of the two individual Fourier transforms. The convolution of two functions $h(t)$ and $g(t)$ is $k(r)$ where

$$k(r) = \int_{-\infty}^{+\infty} g(r) h(t-r) dr.$$

Now the Fourier transform of $I(\Delta)$ is $B(\sigma)$ precisely. Putting the Fourier transform of $F(\Delta)$ equal to $G(\sigma)$ for the moment we see on applying the convolution theorem

$$B'(\sigma_1) = \int_{-\infty}^{+\infty} B(\sigma) \cdot G(\sigma - \sigma_1) \cdot d\Delta \quad [11]$$

The observed spectrum is therefore the convolution of the

actual spectrum with the function $G(\sigma)$. This function is commonly called the INSTRUMENTAL FUNCTION. The ideal instrumental function would be $G(\sigma) = \delta_{\sigma_1, \sigma}$ where $\delta_{\sigma_1, \sigma}$ is the Kronecker delta. The Kronecker delta $\delta_{a, b}$ is defined by $\delta_{a, b} = 1$ if $a = b$ and zero otherwise. In this case one would find $B'(\sigma) = B(\sigma)$.

In interferometry the form of the instrumental function arises to a large extent from the fact that only a finite maximum path difference can be taken and thus it is very important to consider the Fourier transform of $F(\Delta)$. This function was defined earlier as a rectangular function; the Fourier transform of this is given by

$$G(\sigma) = \frac{\sin(K\sigma)}{K\sigma} = \text{Si}(K\sigma)$$

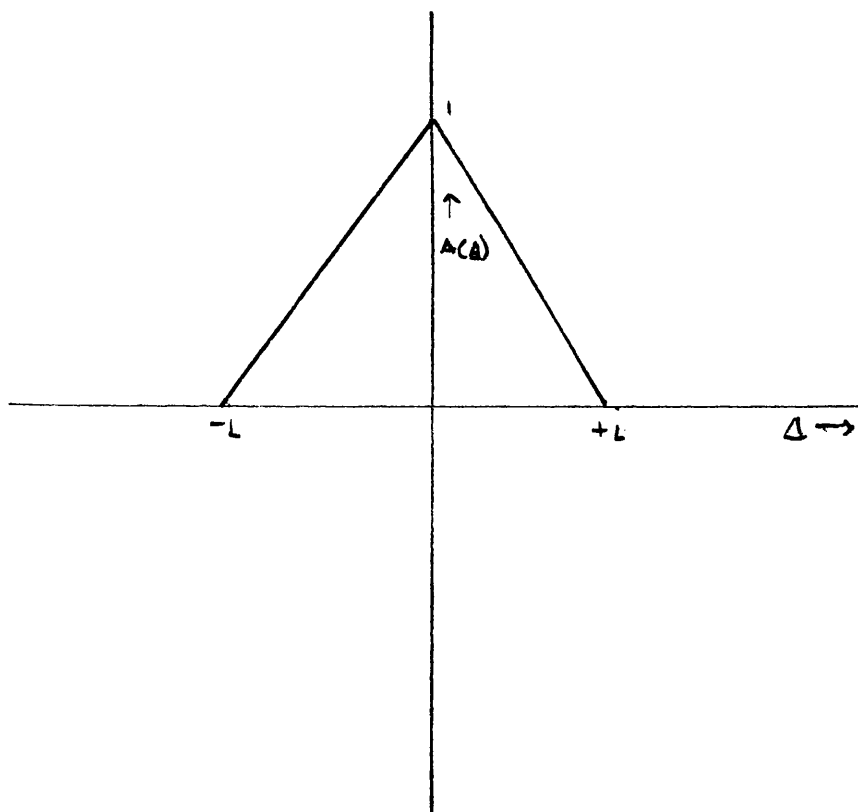
where K is an arbitrary constant. $\text{Si}(K\sigma)$ contributes to a large extent to the instrumental function. The convolution of the spectrum with $\text{Si}(K\sigma)$ is automatically implied when the Fourier transform of a finite maximum path length interferogram is computed numerically. This function $[\text{Si}(K\sigma)]$ is plotted in Figure [1.2]. From this Figure it is seen that the instrumental function $\text{Si}(K\sigma)$ quickly goes to zero as one moves along the abscissa but that there is a quite large secondary maximum which would considerably distort an absorption band.

It is possible to replace the rectangular function $F(\Delta)$, which as stated above is implicit in numerical calculations, by another function $A(\Delta)$ which is more suited to spectroscopic problems; such a function is called an APODISING function. The value of $I(\Delta)$ is merely replaced by $I(\Delta) \cdot A(\Delta)$ before the numerical transform is performed. The most common apodising function is the co-called triangular function defined by

$$A(\Delta) = 1 - \left| \frac{\Delta}{L} \right|, \quad -L \leq \Delta \leq L$$

$$A(\Delta) = 0, \quad |\Delta| > |L|$$

The shape of this function is shown below :



This apodising function causes the instrumental function to be of the form

$$G(\sigma) = \left[\frac{\sin(K\sigma)}{K\sigma} \right]^2 = \text{Si}^2(K\sigma)$$

The plot of this function is shown also in Figure[1.2]. Although it goes more slowly to zero than $\text{Si}(K\sigma)$ the secondary maximum is further from central maximum and is much less pronounced. Although a better profile of an absorption band is obtained in this way the effective resolution of the spectrum is roughly halved when compared with the raw unapodised spectrum, as will be shown later. For the programme written for the interferometer used in connection with this thesis a novel apodising function has been used; novel in the sense that it has not been used before in interferometry but is quite well known in other applications. The function used is

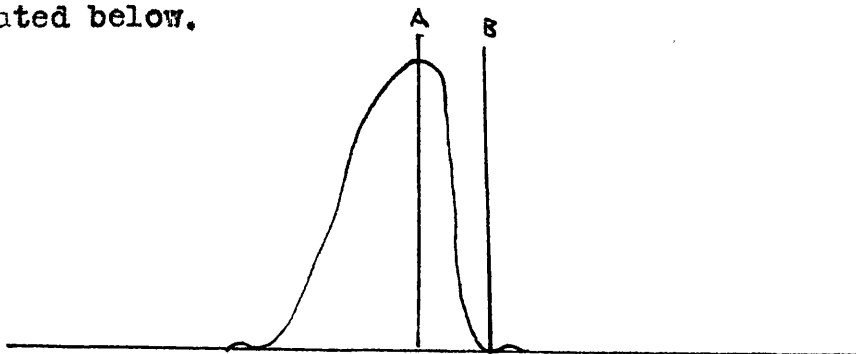
$$F(\Delta) = \frac{\sin(\Delta/L)}{(\Delta/L)} \quad \text{for } -L \leq \Delta \leq L$$

$$F(\Delta) = 0 \quad \text{for } |\Delta| > |L|$$

This implies one is using a mainly rectangular function as instrumental function. Theory predicts that this system should have a higher resolution than systems using a triangular function as apodiser. This has not been checked by testing various apodisers but the spectra obtained have

been quite satisfactory. The programme itself and its features will be described in the next section.

There is no obvious analogue of the slits of a conventional spectrometer in an interferometer. It might appear, therefore, that the resolution of an interferometer was merely a function of design and there was no variable parameter with which to vary this resolution. In fact the resolution of a particular spectrum is proportional to the maximum path difference taken. This can be shown by assuming that the Rayleigh criterion for resolution of two monochromatic bands is satisfactory. This criterion requires, that for two bands to be resolved, the central maximum of the one band must not fall over the minimum of the second band. This is illustrated below.



To be resolved from the above band, the maximum of a second band must not fall between the lines A and B.

A monochromatic band, as mentioned earlier, is convoluted to an observed band that has the shape of the instrumental function. Consider a raw unapodised spectrum from an interferometer. It was shown above that a finite maximum path length implied an instrumental function of form $\frac{\sin(K\sigma)}{K\sigma}$. For a monochromatic absorption $B(\sigma)$ the exact form of the observed band is

$$B'(\sigma) = \frac{\sin [2\pi(\Delta\sigma)L]}{2\pi(\Delta\sigma)L}$$

where L as before is maximum path difference taken. The spectral resolution of $B'(\sigma)$ can be obtained by finding where $B'(\sigma)$ first goes zero, i.e. the higher the resolution the narrower the instrumental function. Putting $B'(\sigma) = 0$ requires $2\pi(\Delta\sigma)L = \pi$ or $\Delta\sigma = \frac{1}{2L}$. Thus the resolution is proportional to maximum path difference.

For an apodised spectrum with a triangular apodising function the exact form of $B'(\sigma)$ is

$$B'(\sigma) = \left[\frac{\sin[\pi(\Delta\sigma)L]}{\pi(\Delta\sigma)L} \right]^2$$

and the same arguments as before yield $\Delta\sigma = \frac{1}{L}$. The resolution of a spectrum is roughly halved therefore if it is apodised with a triangular function.

The fundamental advantage of interferometry was first stated by Fellgett⁷ in 1950. He showed that using a single channel detector to measure all the spectral elements simultaneously is analogous to spectrographic methods of detection and has great advantage over direct methods; he called such forms of spectroscopy multiplex spectroscopy. Suppose that there are N spectral elements to be measured in a time T . With a slit spectrometer each element is scanned for a time T/N . With an interferometer each element is scanned for the whole time T . For instruments whose noise is not increased by the arrival of several spectral elements simultaneously it is well known that the accuracy of the measurements vary as the square root of the total time for the measurement. For the slit spectrometer this accuracy A_1 , say, is $(T/N)^{1/2}$ while for the interferometer the accuracy A_2 is $T^{1/2}$. The ratio A_2/A_1 is thus $N^{1/2}$ which implies that the interferometer has a distinct advantage over the conventional spectrometer which is greater the larger the spectral range considered. This advantage is commonly stated in three different but equivalent ways : -

(1) For a given time of measurement the signal to noise ratio of the interferometer is $N^{1/2}$ times better than with a conventional instrument.

(2) To achieve a given signal to noise ratio the time required with the interferometer is only $1/N$ that of the conventional instrument.

(3) For the same time and signal to noise ratio there is a greater resolution (undefined) with the interferometer as compared with the conventional instrument.

1.4 Programme

It was mentioned earlier that the cosine was an even function and that this implied that the interferogram function $I(\Delta)$ should also be even, i.e. $I(\Delta) = I(-\Delta)$. Thus all the information about the spectrum is contained in one half of the interferogram. Another implication of the fact that both cosine and interferogram are even functions is that the function $I(\Delta)$ can be represented by a series of cosines only. For these two reasons it is common to compute numerically what is called a 'single-sided cosine Fourier transform'. Only one half of the interferogram is used to calculate the cosine Fourier coefficients. A programme was available for this written by Dr J. R. Thompson of the Mathematics Department. This programme has been extensively used but for several reasons has not always been satisfactory; this is not the fault of the programme because this calculates exactly what it is asked to calculate. Deviation from the symmetrical interferogram can be caused in two ways. The most common way occurs in the process of digitising; at 8 micron intervals of Δ the value of $I(\Delta)$ is digitised onto paper tape and it is essential for there to be a reading on tape at zero path difference when $\Delta = 0$. If there is no reading on the tape that corresponds to this then a phase error is automatically given to the

digitally sampled interferogram, and it no longer is an even function even if it is in fact even as far as the instrumental output is concerned. The other possible reason for loss of the even function occurs when the optics are not correctly aligned; in this case an unsymmetrical interferogram results and even if there is a reading on tape corresponding to $\Delta = 0$ the actual interferogram is not even. When either of the above faults occur in the interferogram, actual or measured, a certain amount of information is lost in the sine part of the Fourier transform, which takes care of the uneven part of the function. Computed spectra from unsymmetrical interferograms show a marked 'skewness' and the intensities of the bands are considerably distorted. To overcome these difficulties a programme has been written that computes both the sine and cosine Fourier transforms of the interferogram; the actual spectrum required is derived from the individual transform by taking the sum of the squares of these. If at $\sigma \text{ cm}^{-1}$ the sine and cosine transforms are $S(\sigma)$ and $C(\sigma)$ respectively, then the proper spectral intensity is given by $B(\sigma)$ where

$$B^2(\sigma) = C^2(\sigma) + S^2(\sigma)$$

It should be noticed that if the interferogram is even then

then $S(\sigma) = 0$ and the above relation reduces to

$$B(\sigma) = C(\sigma)$$

To perform this type of calculation both sides of the interferogram are required and is generally called a "double-sided sine squared plus cosine squared" transform. There are a number of set-backs with this method, and these will be dealt with in a later section.

The programme has been written in both Elliott 803 and Atlas (Harwell) Algol. The Elliott programme utilises a Creed teleprinter as a plotter while the Atlas version is written to take use of the facility of an off-line graph plotter. The number of occasions sines and cosines are used in the calculations would make the programme prohibitively long if these were calculated each time as required even in a low resolution study. A computer normally sums a convenient infinite series each time a trigonometrical function is required. To save this waiting of time, all the sines and cosines that are possibly required are calculated before the programme proper begins and placed in the store. Suppose that there are $2N+1$ points in the interferogram corresponding to values of $I(\Delta)$ (actually proportional to Δ) with Δ varying integrally from $-N$ through zero to N . All possible cosines required can be included

in the expression $\cos(2\pi Z/N)$ where Z also can vary integrally between 0 and $2N$. These $(2N+1)$ cosines (and hence sines) are quickly calculated and stored as two arrays. The first stage proper in the calculation is to make the average value of $I(\Delta)$ zero by an unusual weighting process. The value of P defined by the relation

$$P = \left[\frac{1}{4} I(N) + \frac{1}{4} I(-N) + \frac{1}{2} \sum_{\Delta = -N+1}^{N-1} I(\Delta) \right] / N$$

is subtracted from each value $I(\Delta)$ to give a new set of numbers $I'(\Delta)$ say. The cosine and sine components are now separated by taking suitable linear combinations of $I'(\Delta)$ and $I'(-\Delta)$. From the array $I'(\Delta)$, $\Delta = -N \dots N$, the two arrays $C(\Delta)$ and $S(\Delta)$, $\Delta = 0, 1, \dots, N$, are set up as shown in equation

$$\begin{aligned} C(\Delta) &= \frac{1}{2} [I'(-\Delta) + I'(\Delta)] \\ S(\Delta) &= \frac{1}{2} [I'(\Delta) - I'(-\Delta)] \end{aligned}$$

These two functions are even and odd respectively and cosine and sine Fourier transforms suffice for each function without loss of information. At this stage the apodisation is introduced; a typical term $C(\Delta)$ is multiplied by $\sin(\pi Z/N)/(2 \cdot Z/N)$ to give a new array of terms $C'(\Delta)$. The first and last terms are given half weight in the Fourier transforms that follow. Considering

just the cosine transform, the $C'(\Delta)$ array produces another array $C \cdot F(K)$, $K = 0, 1 \dots N$, of Fourier coefficients defined by

$$C \cdot F(K) = \sum_{\Delta=0}^N C'(\Delta) \cos(K\Delta\pi/N)$$

It will be noticed that in a 500 point double sided transform approximately 65,000 cosines will be required although there will be at most only 1,000 different ones used. This accounts for the setting up of the cosine array.

Each of the $(N+1)$ Fourier coefficients is calculated in turn using a conventional double loop in the programme. Provision is made to ensure that $K\Delta\pi/N$ is less than 2π by subtracting units of 2π from it until this condition is satisfied. This is required because only cosines for angles less than 2π exist in the array. A similar procedure is used to calculate the sine-Fourier coefficients, and the true absorption intensity is given by the square root of the sums of the squares of corresponding sine and cosine Fourier coefficients. Standard procedures are used for the plotting of the spectrum depending on whether the 803 teleprinter or Atlas graph plotter is used.

Both programmes are given in the appendix to this chapter. The first one written for the Elliott requires the A 104 Algol compiler while the second programme uses the compilers as shown at the top of the programme.

1.5 Description of Interferometer.

The interferometer used in the work connected with this thesis was a prototype FS-520 manufactured by Research and Industrial Instruments Company. A block diagram is shown in Figure [1.3]. Many faults were encountered with the instrument and can be variously described as belonging to the following categories; (a) mechanical, (b) electronic, (c) vacuum, (d) optical and (e) computing troubles. These will be discussed in detail in the next section.

The optics of the system are very simple and can be very briefly described. Referring to Figure [1.3], radiation from the source (S) is collimated by the concave mirror (A) and reflected towards the beam splitter by the plane mirror (B). The beam splitter divides the radiation into two beams both of which are reflected by plane mirrors, one of which is fixed (D) while the other can be moved on an axis perpendicular to itself (C). The recombined beam is condensed by the concave mirror (E) and brought to an intermediate focus in the cell housing by the convex mirror (F). The sample is normally placed in the cell housing at this focus. After passage through the sample the beam is brought to a final focus by the Cassegrainian system of mirrors (G) and (M), this final focus falling on

the window of the detector.

The mirror (C) is moved along the optical axis by the drive unit; this is basically a LAPPED piston and cylinder system. The piston on one end carries the plane mirror (C) and at the other end the one half of a Moire grating. The rate at which the path difference changes is twice that of the mirror movement rate. The Moire system consists of the grating mentioned above along with a fixed grating in a separate casting held about 50 microns from the moving one. The system is designed to ensure that relative rotation of one grating with respect to the other is impossible. Light from the Moire lamp is collimated and shadows of the fringes produced after passage of the light through the gratings is focused on a photocell. At 4 microns intervals of mirror movement the intensity of radiation on the photocell is sufficient to trigger off the mechanism that records digitally the intensity of radiation falling on the Golay detector. The signal detected by the Golay is also displayed visually on a strip chart recorder. A typical interferogram is shown in Figure [1.4].

The cell housing is fastened to one side of the main tank; both of which are evacuable independently by a rotary

vacuum pump. The source is a high pressure mercury lamp, water cooled, and chopped at 12.5 cycles per second; the detector used is a Golay detector with a diamond window.

1.6 Faults encountered with the FS-520 Interferometer.

As mentioned previously the kinds of 'teething' problems associated with the FS-520 can be placed in the following general categories; a) mechanical, b) electronic, c) vacuum, d) optical, and e) computing troubles. These will each be briefly discussed.

(a) The mechanical troubles occurred mainly when the older type of drive was fitted. This drive consisted of a stainless steel cable which connected the gear box to the piston. The movement of the piston was not always perfect, and irregular punching occurred at times. This is not very serious at relatively slow drive speeds because the punching interval is a function of distance rather than time. A few spectra however, that were recorded immediately before the cable snapped were quite meaningless, but this was not realised until it was known that the cable had in fact broken. Occasionally when the present drive appears to be sticking slightly, movement of the piston at maximum speed backwards and forwards along the length of the drive two or three times, to re-distribute the lubricant, generally produces a smooth drive again.

(b) The electronic troubles encountered generally manifested themselves as unusual features on the

interferogram. The most common fault was for a spike to appear on the monitored interferogram each time a data point was being punched. Sometimes the value punched on the tape corresponded to a position of the pen recorder actually on a spike. This resulted in a noisy interferogram and a consequently noisy spectrum. On a number of occasions this fault corrected itself but at other times earthing various parts of the electronics was required to remedy this. Another annoying feature that occurred occasionally was for an overall good interferogram to have a series of regular bumps on it. This was an infuriating but generally only temporary fault. It was thought to be due to a dirty thermostat or the like being used by somebody elsewhere in the department.

(c) and (d) Initially, a great deal of trouble was encountered in obtaining a good vacuum in the cell housing. Cleaning and regreasing the O-rings on the ports had no effect; the fault was found eventually to be a poor connection between the Golay and the sample chamber. Even when the sample chamber was properly evacuated it was still thought that it was inadequate and that water vapour bands were creeping onto the spectrum. This was in fact an optical fault and not a vacuum one. The bands that had

been attributed to water vapour were the well known channel spectra that are equally well known in conventional spectroscopy. Channel spectra arise from interference of the optical beam between the two faces of a parallel thin sheet. If the thickness of the sheet is α cm, and the separation of the bands of the channel spectrum is λ cm^{-1} then the two are related by $2\alpha\lambda = 1$. The most common causes of the channel spectra in interferometry are (a) the black polythene filter used to remove radiation above 450 cm^{-1} and (b) the quartz envelope of the mercury source. The source in the FS-520 is nowadays specially roughened on the surface to avoid this fault but the black polythene (whose thickness corresponded to that predicted by the channel spectrum) was quite smooth. After squeezing this in a vice the channel spectra disappeared.

One of the most important optical problems was the construction of an adequate beam splitter. The beam splitter is really the weak link of an interferometer, the rest of the instrument being entirely dependent on its correct functioning. Any uneven strain in the melinex film is reflected in a poor interferogram with very low minimum to maximum peak values, and no certain method can be given for making a good beam splitter. It is also

difficult to align the beam splitter correctly in its cradle which is situated on the base of the interferometer. The most common mishap with the optics is for there to be a total loss of alignment of one of the two plane mirrors. It is possible for the system to be so badly misaligned that zero path difference (z.p.d.) cannot be found on the recorder. The procedure for finding z.p.d. is as follows. The chopper is switched off and the gear box is set in neutral allowing the drive to be turned by hand. The moveable mirror is adjusted until the beam splitter is roughly equi distant between both mirrors. The moveable mirror is now adjusted very slowly until 'fringes' are visible on a piece of paper situated in front of the sample chamber. When this is achieved the micrometers which control the axes of the fixed mirror are adjusted until the 'fringes' are evenly spaced across the paper. The optics should now be correctly aligned. Quite often this is not the case and further adjustment is required. The recommended technique for this is to run through z.p.d. changing the micrometer settings each time until a satisfactory symmetrical interferogram is obtained. This method generally works but is very tedious and a better way has been developed. This consists of running the drive at the slowest speed and stopping it actually on z.p.d.

The micrometers are then adjusted for maximum energy; by moving off z.p.d. and back again and adjusting the micrometers once again the correct alignment is quickly found.

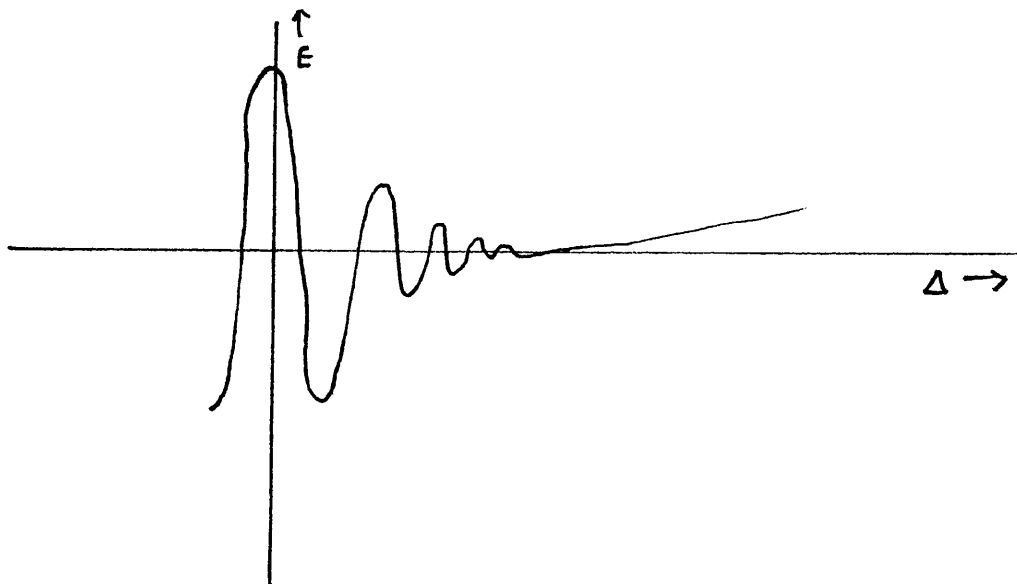
(e) The computing troubles were in fact faults that were not spotted until the spectrum in question had been computed. The most serious fault which fortunately only occurred occasionally, was the effect of dropping a digit from the data tape. If this occurs when the interferogram is near completion a 'spike' is effectively placed on the interferogram. The programme would transform this to a cosine curve and this would be superimposed on the rest of the spectrum. The spectrum would appear as if a channel spectrum was being produced. This is quite useful in finding where the dropped digit is. The thickness of the imaginary sheet which was causing the interference corresponds to the distance from z.p.d. that the dropped digit occurred. The relative amplitude of the 'channel spectrum' would indicate the magnitude of the digit dropped by the A/D converter. If the spectrum was swamped by the interference bands then it is quite likely that the dropped digit was one that indicated the hundreds of the data point. Consequently this data tape would be editable. The effect of two dropped digits would be more complicated

and probably incapable of correction.

There are a number of mundane things which can go wrong, and these are worth mentioning because they often have the same symptoms as more serious faults.

The Moire lamp has an average lifetime of about nine months. The lamp usually goes out during a run and this is manifested by the cessation of punching. It is possible to check whether the light has gone out (or is something more serious) by noting if the p.v. cell is 'triggering' on an oscilloscope. Replacement of the lamp is a simple matter and generally the exact location of the lamp is not critical.

One of three things can have happened during a run if the base line slowly creeps towards higher energy as shown below.



The most common thing is for the source not to have been switched on long enough before use. It is necessary to have been warming up for at least twenty minutes. Usually if the source has been on long enough then this wandering base line can be attributed to the sample chamber not being evacuated for long enough a period before the run was started. At least ten minutes evacuation is required (with a double stage rotary pump) to obtain a reasonable vacuum. If neither of the above things are responsible for the sloping base line then the most probable cause is too thin a mull; during the run the sample slips down the plate slowly with consequent increase in energy at the detector. If the background slopes towards the energy decrease direction then this is an indication that the interferometer has a leak somewhere. It might be thought that this could equally be caused by the source going out. However, apart from the fact that the source can be seen from outside the interferometer, the energy level would decrease far more steeply than in the above cases. The source does in fact have a finite life of about eighteen months. Although they lose their hard ultraviolet emission properties they retain their far infrared emitting properties entirely until they actually die. Replacement of the source is such a tedious operation that it is worth while noting that even if the

source 'apparently dies' during a run it still may be usable. During the last few weeks of its life the source will often arc again when it has been left to cool after such an 'apparent death'.

1.7 Interferometry versus slit spectroscopy.

The theoretical advantages of interferometry over slit spectrometers are not always realised. Even so, it is a better method of measurement in many circumstances and the Fellgett advantage does appear to manifest itself.

Energy is at a premium in the far infrared and this fact coupled with the fact that most of the resolved radiation in a conventional spectrometer falls on the jaws of the slits means that much smaller amounts of sample are required in an interferometer. Since the resolution of the interferometer is merely a function of mirror travel a spectrum between 40 and 440 cm^{-1} to a resolution of 1 cm^{-1} can be obtained in about 30 minutes; a comparable spectrum from a grating spectrometer would take far longer. A very strong point in favour of the FS-520 interferometer is easy accessibility of the sample area. This can be approached quite easily from four sides and use of sophisticated sample cells is very simple. The sample area is particularly convenient for the normal solid, liquid or gas cell.

In normal operation the interferometer is evacuated thus eliminating the very troublesome water vapour spectrum. With a double beam conventional spectrometer it is necessary to purge the instrument with dry air; theoretically this is

not essential but the amount of energy available after water vapour has absorbed is very small. Even with dry air purging the PE 225 poor spectra are quite often obtained below 300 cm^{-1}

The size of the FS-520 is comparable with most conventional spectrometers. In the near future however, the interferometers available commercially will have a distinct size advantage. R.I.I.C. are making an FS-720 interferometer which will stand on a small table. An added advantage of the smaller interferometer will be the ease of replacement of the beam splitter. The range of frequencies studied is critically dependent on the thickness of the beam splitter. It is standard with the FS-520 to cover the range $40\text{-}400 \text{ cm}^{-1}$ with a 25 micron beam splitter made of melinex. If a 50 micron melinex was used instead the range $20\text{-}200 \text{ cm}^{-1}$ would be covered. With the FS-520 changing the beam splitter is a tedious job because the exact tension of the melinex is critical and quite difficult to obtain. The mirrors also have to be re-aligned although this is not quite so awkward. This difficulty will not exist in the smaller interferometer since it will only take a matter of minutes to change the beam splitter.

The biggest disadvantage of interferometric spectroscopy is the time delay between experiment and

reception of results since one has to wait for a computer to calculate the spectrum. The cost of calculation of this spectrum can also cost around £2 to obtain a resolution of 1 cm^{-1} between 100 and 400 cm^{-1} . Both the time lag and the heavy cost of computation will be avoided when the interferometer with bench analogue computer becomes generally available.

The second fault to be found with the interferometer concerns the background of the instrument. A typical background run is shown in Figure [1.5]. Besides the general inconvenient shape of the background there are major absorptions at 382 and 436 cm^{-1} due to melinex and at 73 and 142 cm^{-1} due to polythene. The background tends to be slightly variable (probably due to imperfect interferograms) and to really establish the existence of weak features in a spectrum may require several interferograms of the same compound to be computed. It is possible to remove the background of the instrument, thus making it effectively a double-beam system, by "ratioing" the spectrum in question against a typical background spectrum; this may be conveniently performed by the computer. This process of "ratioing" out the background is particularly difficult with the FS-520 because the fine gain control has a discrete set of gains

rather than a continuous gain control; it is difficult therefore to obtain both interferogram of sample and background on the same milli-volt level as is required for optimum "ratioing". Perry¹⁴ has shown that although a double-sided computation has a larger signal to noise ratio than a single-sided run the double sided computations are more reproducible especially at low frequencies.

It is generally true that with a conventional spectrometer one always gets some sort of spectrum from a compound even if it is a poor spectrum. This is not true of interferometry for apart from the faults mentioned above there are a number of things that can go wrong with the interferogram that can produce false absorptions or completely ruin a spectrum. For instance, quite often the baseline of the interferogram slopes quite steeply from the horizontal ruining the resulting spectrum. This fault and the many others not mentioned however probably merely indicate the state of the art at present. These now elusive faults which can and do now appear in a typical run will probably be well documented in a few years, as more chemists become familiar with this instrument.

1.8 APPENDIX

A) ELLIOTT PROGRAM.

```

DOUBLE SIDED FOURIER TRANSFORM'
BEGIN
  INTEGER N'  READ N'
  BEGIN
    REAL Q,SUM,SUM1'
    ARRAY F(-N:N),S(0:N),U,V(0:N),COSAR,SINAR(0:2*N)'
    INTEGER Z,Y,J,P,K,INDEX'
    SWITCH X:=L,L1'
    FOR Z:=0 STEP 1 UNTIL (N DIV 2) DO
      COSAR(Z):=COS(3.14159265*Z/N)'
    FOR Z:=0 STEP 1 UNTIL (N DIV 2) DO
      BEGIN
        COSAR(N DIV 2+Z):=-COSAR(N DIV 2-Z)'
        COSAR(N+Z):=-COSAR(Z)'
        COSAR(3*N DIV 2+Z):=COSAR(N DIV 2-Z)'
        SINAR(Z):=COSAR(N DIV 2-Z)'
      END'
    FOR Z:=(N DIV 2+1) STEP 1 UNTIL 2*N DO
      SINAR(Z):=COSAR(Z-N DIV 2)'
    READ Z'
    FOR Y:=1 STEP 1 UNTIL Z DO
      BEGIN
        FOR Q:=-N STEP 1 UNTIL N DO
          READ F(Q)'
          Q:=0'
          Q:=(F(-N)+F(N))/2'
          FOR J:=1-N STEP 1 UNTIL N-1 DO
            Q:=Q+F(J)'
            Q:=Q/(2*N)'
          FOR P:=-N STEP 1 UNTIL N DO
            F(P):=F(P)-Q'
          FOR P:=1 STEP 1 UNTIL N DO
            BEGIN
              S(0):=3.14159265*P/N'
              U(P):=(F(P)+F(-P))*SINAR(P)/(2*S(0))'
              V(P):=(F(P)-F(-P))*SINAR(P)/(2*S(0))'
            END'
          END'
        END'
      END'
    END'
  END'

```

```

UCO:=FCO/2'
VCO:=0'
UCN:=UCN/2'
VCN:=VCN/2'
FOR K:=0 STEP 1 UNTIL N DO
BEGIN
  SUM:=SUM1:=0'
  INDEX:=-K'
  FOR J:=0 STEP 1 UNTIL N DO
  BEGIN
    INDEX:=INDEX +K'
    L1: IF INDEX LESS (2*N) THEN GOTO L
    ELSE INDEX :=INDEX-(2*N)'
    GOTO L1'
    L: SUM:=UCJ)*COSAR(INDEX)+SUM'
    SUM1:=VCJ)*SINAR(INDEX)+SUM1'
  END'
  F(K):=SUM*2/N'
  S(K):=SUM1*2/N'
  F(K):=SQRT(F(K)**2+S(K)**2)'
END'
SUM:=SUM1:=F(CO)'
FOR K:=1 STEP 1 UNTIL N DO
IF SUM GR F(K) THEN SUM:=F(K) ELSE IF SUM1
LESS F(K) THEN SUM1:=F(K) ELSE INDEX:=0'
FOR K:=0 STEP 1 UNTIL N DO
BEGIN
  PRINT K'
  F(K):=F(K)-SUM+0.000001'
  F(K):=ENTIER(F(K)*60/SUM1)'
  FOR J:=0 STEP 1 UNTIL F(K) DO
  PRINT ££S??'
  PRINT SAMELINE,£+?'
END'
PRINT ££R100??'
END'
END'
END'

```

B) ATLAS PROGRAM.

JOB VZO11 MORRIS FOURIER TRANSFORMS

INPUT 1 INTERFEROGRAMS

OUTPUT 0 LINEPRINTER 200 LINES

OUTPUT 12 LINEPRINTER 200 LINES

OUTPUT 13 LINEPRINTER 200 LINES

TAPE IBM 14 MORRIS COMMON(P)/PLEASE LABEL MORRIS, LEICESTER, 1966

COMPUTING 2 MINUTES

STORE 50 BLOCKS

COMPILER ALGOL

INPUT ICT 7-HOLE TAPE WITH GRAPH I/O PROCEDURES;

begin

integer N,N1,N2,N3,N4,N5,N6,N7; select input(1);

N1:=read;

N2:=read;

N3:=read;

N4:=read;

N5:=read;

N6:=read;

N7:=read;

N:=(N1-1)÷2);

begin

real SUM,SUM1,Q;

array F[-N:N],S,U,V[0:N],COSAR,SINAR[0:2*N];

integer Z,Y,J,P,K,INDEX;

switch X:=L,L1;

for Z:=0 step 1 until (N÷2) do

COSAR[Z]:=cos(3.14159265*Z/N);

for Z:=0 step 1 until (N÷2) do

begin

COSAR[N÷2+Z]:=-COSAR[N÷2-Z];

COSAR[N+Z]:=-COSAR[Z];

COSAR[3*N÷2+Z]:=COSAR[N÷2-Z];

SINAR[Z]:=COSAR[N÷2-Z];

end;

for Z:=(N÷2+1) step 1 until 2*N do

SINAR [Z]:=COSAR[Z-N÷2];

for Y:=1 step 1 until N6-1 do

begin

graph papertrow;

graph identification(←JOB VZO11 MORRIS→);

for J:=-N step 1 until N do

F[J]:=read;

Q:=(F[N]+F[-N])/2;

for J:=1-N step 1 until N-1 do

Q:=Q+F[J];

Q:=Q/(2*N);

for P:=-N step 1 until N do

F[P]:=F[P]-Q;

for P:=1 step 1 until N do

```

begin
    S[0]:=3.14159265*P/N;
    U[P]:=(F[P]+F[-P])*SINAR[P]/(2*S[0]);
    V[P]:=(F[P]-F[-P])*SINAR[P]/(2*S[0]);
end;

U[0]:=F[0]/2;
V[0]:=0;
U[N]:=U[N]/2;
V[N]:=V[N]/2;
for K:=0 step 1 until N do
begin
    SUM:=SUM1:=0;
    INDEX:=-K;
    for J:=0 step 1 until N do
begin
    INDEX:=INDEX+K;
    L1:if INDEX<(2*N) then go to L
    else INDEX:=INDEX-(2*N);
    go to L1;
    L:SUM:=U[J]*COSAR[INDEX]+SUM;
    SUM1:=V[J]*SINAR[INDEX]+SUM1;
end;
end;

F[K]:=SUM*2/N;
S[K]:=SUM1*2/N;
F[K]:=sqrt(F[K]exp2+S[K]exp2);
end;

SUM:=SUM1:=F[0];
for K:=1 step 1 until N do
if SUM >F[K] then SUM:=F[K] else if
SUM1 <F[K] then SUM1:=F[K] else
INDEX:=0;
graph header(0,N/10,0,(SUM1+.0002)/12.5,(K));
for K:=0 step 1 until N do
graph data(K,F[K]);
end;
end;
graph end;

end
***Z

```

FIGURE 1.1

Relative emission from a black body.

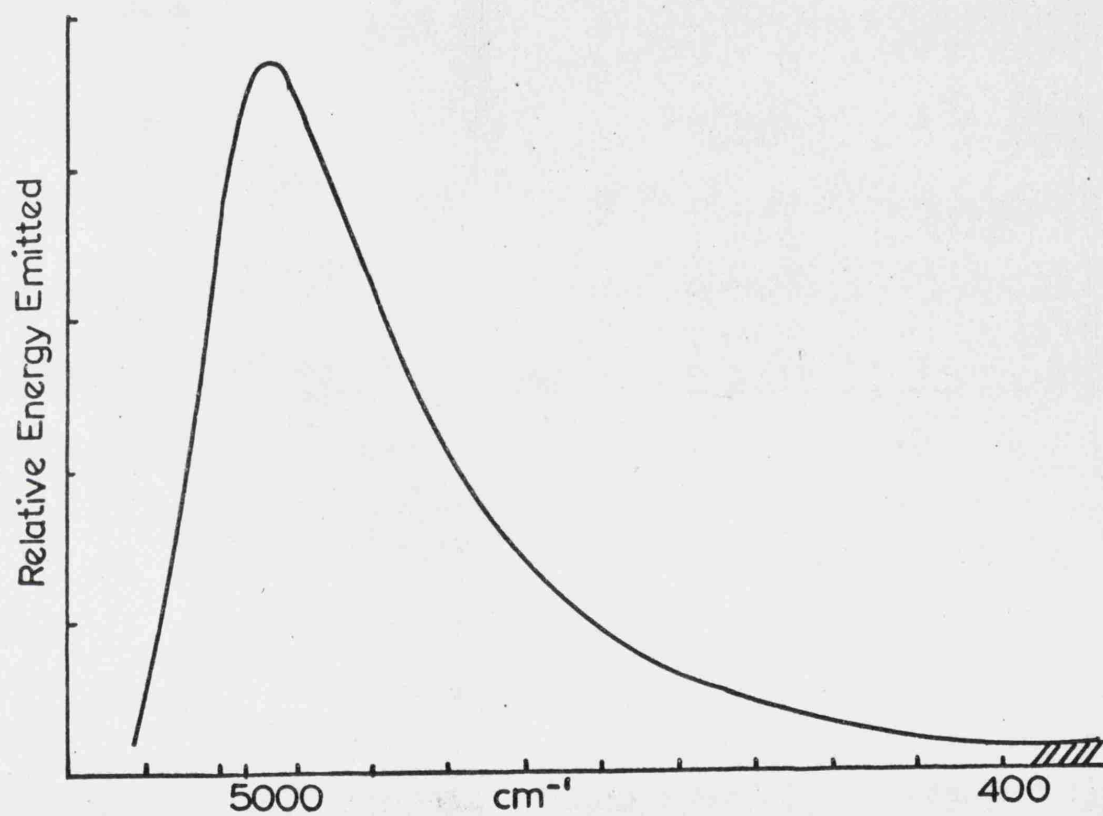
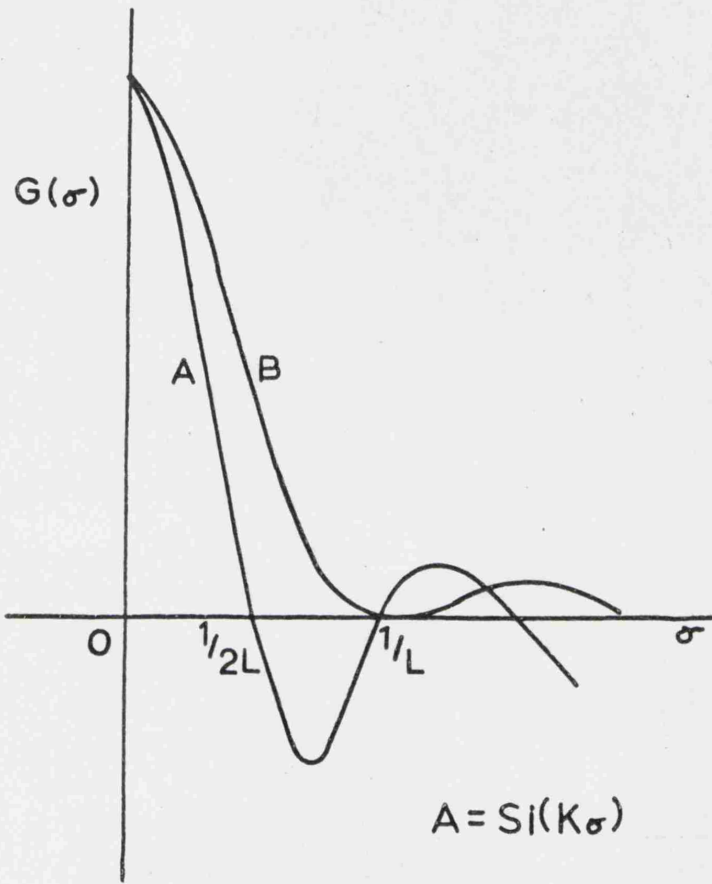


FIGURE 1.2

Instrumental functions.



$$A = \text{Si}(K\sigma)$$

$$B = \text{Si}^2(K\sigma)$$

FIGURE 1.3

Block diagram of an FS-520 interferometer.

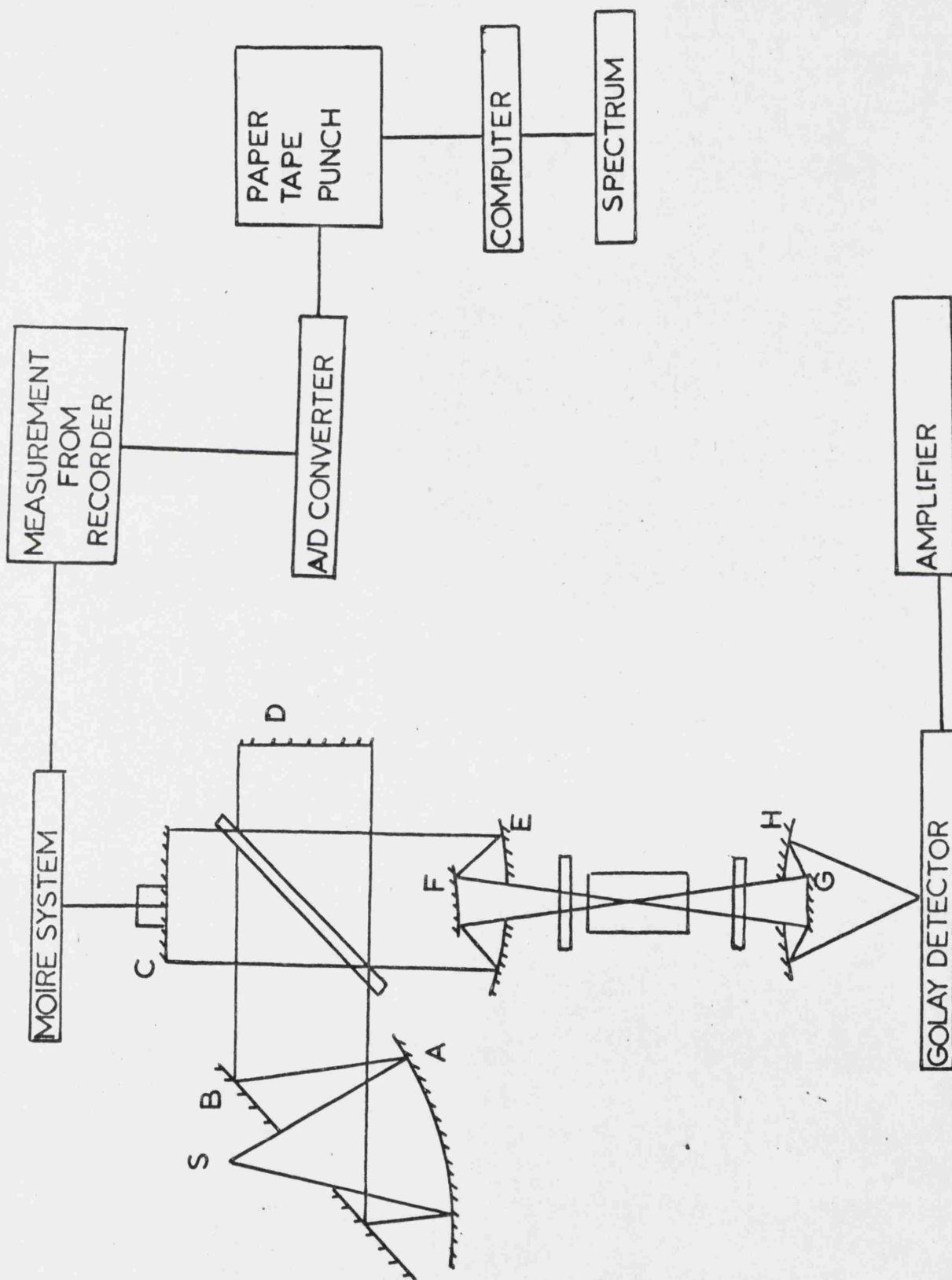


FIGURE 1.4

Typical interferogram.

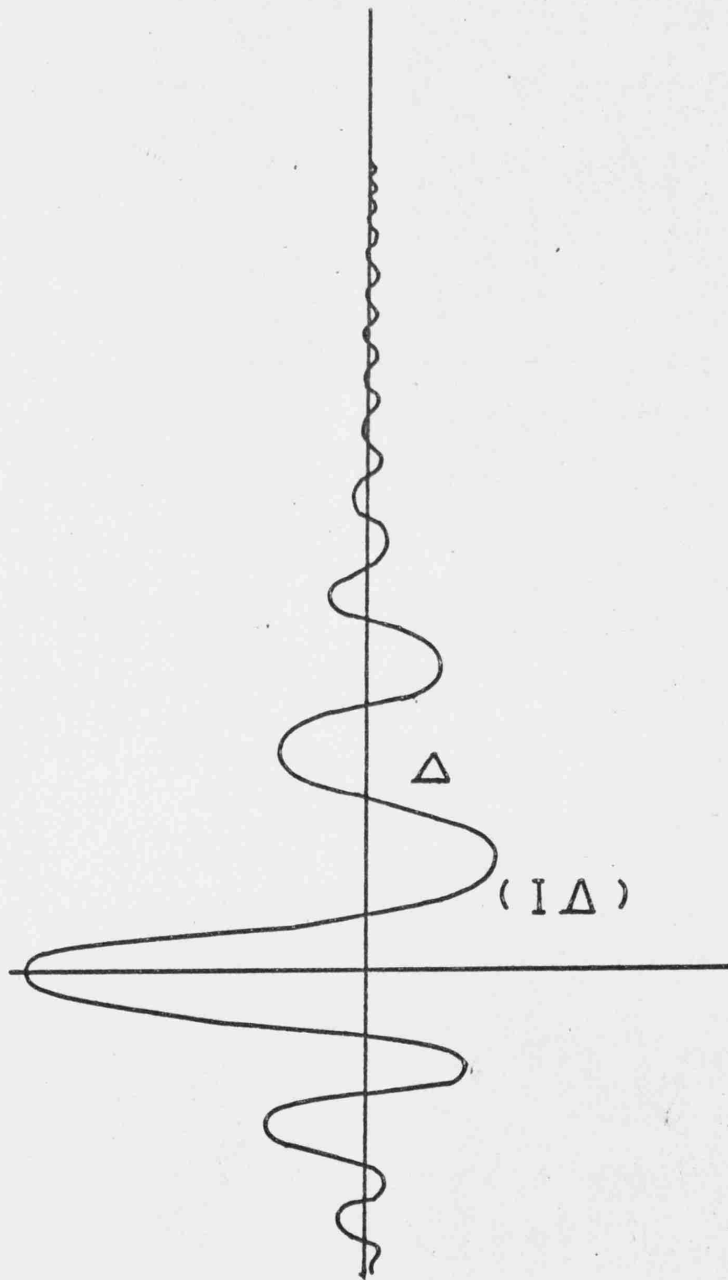
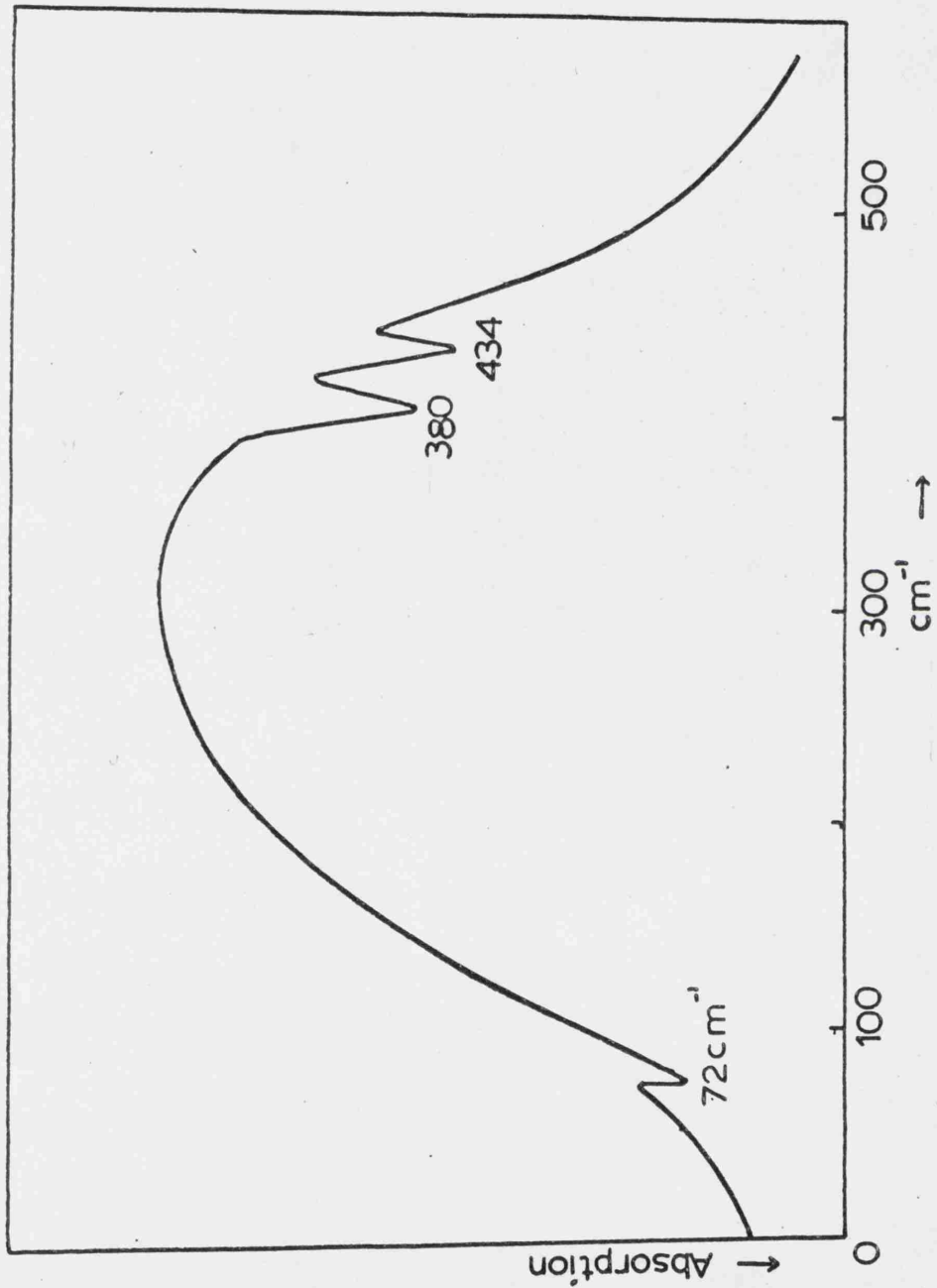


FIGURE 1.5

Typical interferometric background spectrum.



CHAPTER TWO

SLIT SPECTROMETRY

CHAPTER 2 - SLIT SPECTROMETRY2.1 Introduction.

The backbone of this thesis has been concerned with interferometry and the information obtained from it. By no means, however, have all the results quoted in this thesis been obtained interferometrically. This department is equipped with a number of conventional slit spectrometers. The author has used besides the interferometer, a Perkin-Elmer PE-225, a Perkin-Elmer LR-1 (Raman), a Unicam SP-100 and a single beam evacuated far infrared spectrometer¹⁵ (475-175 cm^{-1}). The last two instruments are mentioned for the sake of completeness since only a handful of spectra have been run on these. However, it is pertinent to discuss the performances of the other two instruments. The PE-225, a well established instrument, need only be mentioned briefly, but the LR-1 being a new instrument deserves a fairly detailed description.

2.2 The Perkin-Elmer PE-225.

This is a double beam spectrometer covering the spectral region $5000-200\text{ cm}^{-1}$ in the four separate ranges $5000-2000$, $2500-1000$, $1000-400$ and $410-200\text{ cm}^{-1}$. Unlike the SP 100, which is in this case filled with dry nitrogen, the PE-225 is continually flushed by dry air. With this particular instrument the drying process is not very successful and quite often water vapour bands creep onto the spectrum below 310 cm^{-1} . Another part of the spectrum that is not covered very well is $460-410\text{ cm}^{-1}$. It is quite likely that weak or even some medium bands are missed if they occur in this region. For instance some metal-nitrogen stretching frequencies in amines of the type $[\text{M}(\text{NH}_3)_4][\text{M}'\text{X}_4]$ ($\text{X} = \text{halogen}$) that should occur near 420 cm^{-1} have not been observed.

Above 400 cm^{-1} solids have been run in nujol suspensions supported on KBr plates. Below 400 cm^{-1} the same suspension was supported on polythene plates. The nujol was the 'degassed' variety supplied by Mr. J.B.Cornell¹⁶.

The temperature in the beam is near 70°C and this is obviously unsatisfactory for thermally unstable compounds. There is an air blower which blows cold (wet) air onto the sample and cools it to 65°C . This is still warm enough to

decompose some samples. For this reason a cold cell was designed for use with the PE-225. The coolant is liquid nitrogen and therefore above 400 cm^{-1} AgCl plates are used. The author used the cold cell on a few occasions but did not detect substantial differences in the spectra compared with the normal run. Besides retarding decomposition of sample the cold cell in theory should sharpen up the bands especially those below 300 cm^{-1} . The transition normally referred to in vibrational spectroscopy is the one from the ground state level to the first excited state. However, at room temperature this first excited state is substantially occupied at low frequencies and thus the transition from this state and the second excited state will also be observable. This transition in theory should be indistinguishable from the normal one but because the potential energy curve is not exactly harmonic the transition will in fact occur at a slightly different position. This will be manifested by a broadening of the band studied.

According to the Boltzmann distribution law the ratio of the population of the first excited state (N_1) relative to the ground state (N_0) is given by :-

$$N_1/N_0 = e^{-hc\omega/KT} = e^{-1.44\omega/T}$$

where h , c , K , e and T have the usual significance, ω is

the frequency of the band considered. Thus the higher the frequency considered the smaller will be the percentage of molecules in this first excited state, and the less significant will be this broadening. Table [2.1] shows the relative population of this level at various frequencies at the three temperatures (a) -196°C , (b) 25°C and (c) 75°C . It is apparent that at low temperatures and even at low frequencies the first excited state is extensively depopulated compared with room temperature and that a substantial sharpening of the bands should be apparent. However, this was in fact hardly ever realised in practice. Figure [2.1] shows the plot of relative population versus frequency for the three temperatures mentioned above.

2.3 The Perkin-Elmer LR-1.

For the last year of the work with which this thesis has been concerned, a Perkin-Elmer model LR-1 Laser-Excited Raman Spectrometer has been available. Using a He/Ne 9mw laser which emits at $6328\overset{\circ}{\text{A}}$ ($15,802\text{ cm}^{-1}$) it is claimed that this instrument could obtain spectra of compounds that are transparent in the red region of the spectrum. This is not precisely true with either solids or liquids. Aqueous H_2TeBr_6 , a red solution, gave a very good Raman spectrum while solutions of ReF_6Cl in CFCl_3 apparently having the same red colour gave practically no signal. $(\text{Et}_4\text{N})\text{TeI}_4$ and K_2PtCl_4 are both red crystalline solids but only the former compound gave a spectrum. Presumably the visible spectrum of a compound should be taken to obtain a first indication of the possibility of obtaining its Raman spectrum.

The use of laser excitation results in a substantial reduction in the size of a Raman spectrometer when compared with the normal mercury arc instruments. The LR-1 is basically constructed from Perkin-Elmer building block components and only the sample area is of new design. The laser radiation, plane polarised, enters the sample area horizontally, is reflected by a plane mirror downwards into the sample cell and makes several traverses through the sample. The optics of the sample area are demountable and

depend on whether the sample is solid or liquid. After passage through these optics the Raman radiation enters the entrance slit of a double pass monochromator. While in the monochromator it is both dispersed and chopped (at 13 c.p.s. before emergence at the exit slit. This radiation is detected by^a photomultiplier before amplification and demonstration of a 0-10 mv. strip chart recorder.

The frequency shifts from the exciting line are measured in Drum Numbers (DN). Zero DN corresponds to 4000 cm^{-1} while 2400 DN is equivalent to zero cm^{-1} (i.e. the exciting line). There is no simple relation between DN and wavenumber shifts although over limited ranges the relation tends to be linear. It is rather inconvenient that the spectrum produced is neither linear in wavelength or wave number. Below 800 cm^{-1} the instrument was calibrated with the known Raman bands of carbon tetrachloride, dichloroethane, tetrachloroethylene and benzene.

As mentioned previously, the laser emits primarily at 6328\AA but if not aligned properly when the micro cell is being used then there is also marked emission at 6402\AA indicated by an apparent strong band at 2320 DN (180 cm^{-1}). Also at all times non laser transitions are produced (due to the atomic spectrum of Ne) but are normally removed

by a spike filter. The most serious bands below $\Delta\nu = 900 \text{ cm}^{-1}$ occur at the following frequency shifts with the given intensity :- 134 cm^{-1} (2345 DN)_w, 181 cm^{-1} (2325 DN)_{vw}, 198 cm^{-1} (2318 DN)_{vw}, 286 cm^{-1} (2281 DN)_w, 386 cm^{-1} (2238 DN)_{vw} broad, 437 cm^{-1} (2216 DN)_s, 495 cm^{-1} (2185 DN)_{vs} broad, 640 cm^{-1} (2121 DN)_m, and 830 cm^{-1} (2034 DN)_w. The very strong broad band at 2185 is not in fact due to a non laser transition but is one of the 'ghosts' of the instrument. Although the monochromator is designed to prevent stray light from reaching the detector it is found that some of the scattered excited radiation does get through to the photomultiplier when the monochromator is set at 2185 DN. Apparently at this setting the exciting line passes through the chopper in a reverse direction and is then scattered from various surfaces before reaching the exit slit. There is obviously room for improvement here with this instrument.

The above spurious bands are not normally observed because a spike filter which transmits 80% of radiation at 6328\AA removes most of the other radiation before the beam reaches the sample. If the sample scatters badly however, some of the features may be observed. Besides the spike filter there are two other optional filters which can be used to (a) remove the ghost, and (b) bring

down the background near the exciting line more steeply than usual.

The colour filter (F_2) which has the transmission curve shown in Figure [2.2] removes the exciting line and quite substantially removes the radiation that is quite close to it (in frequency). Since the exciting line is responsible for the ghost this filter effectively removes this ghost and is meant to be used in the region 2260 DN to 0 DN. The background in the region of 2260-2160 DN with and without this filter is illustrated in Figure [2.3].

The interference filter (F_1) is used to bring down the level of the background off the exciting line more steeply than normal. It has the transmission shown in Figure [2.4], and the resultant background curve is also shown in this figure.

From the transmission curve it is apparent that this filter is designed to remove the exciting line, but not substantially affect Raman shifts quite close to it.

At 2260 DN both filters transmit the same amount and the instrument has the facility of an 'auto-mode'. When used in this fashion F_1 is operable until 2260 DN when F_2 automatically cuts in as F_1 cuts out. In the manual with

the instrument it is suggested that the normal operation involves using this 'auto-mode' facility, but this is debatable. In the opinion of the author better results are generally obtained without the use of filters, especially below 300 cm^{-1} . However, for solid samples the state-of-the-art is such that both methods must be used as a matter of course in order to obtain the maximum information possible. When used without filters the typical background is shown in Figure [2.5].

Certainly the filter F_1 is useless in the study of low frequency shifts ($< 150\text{ cm}^{-1}$). When used in the 'auto-mode' K_2TeBr_6 only showed the stretching modes of the anion around 200 cm^{-1} ; without filters quite strong bands were observed down to 70 cm^{-1} . The conclusion from this result is that most of the low frequency Raman radiation is also removed (or reduced in intensity) by the interference filter. The other major snag when the instrument is used in the 'auto-mode' is that the relative intensities of those bands observed are meaningless. This is well illustrated with $(\text{NH}_4)_2\text{TeCl}_6$. When used in 'auto-mode' the spectrum shown in Figure [2.6] was obtained. However, when run without filters, spectral intensities were completely altered (this is also shown in Figure [2.6]).

The Cary 81-laser instrument spectrum of this compound also shows the three bands of equal intensity.

The packing requirements of the solid sample holder are completely different for both of the above methods of use. When used without filters it is essential that as little as possible of the exciting radiation gets through the sample to the monochromator. The more that does get through, the worse is the spectrum obtained. The holder is filled by dropping sample into it until the exit slit of the holder is just covered. None or very little tamping of the sample is required. For use in the 'auto-mode' the sample preparation depends on the ease of excitation of the sample. For the first trial run the sample is placed in the holder and tamped quite heavily. Just enough sample is placed in the holder so that the top part of the exit slit is not covered. If no excitation of the sample occurs then only enough sample must be placed in the holder to half cover the exit slit. A pointed spatula is then put into the exit slit and the sample altered in distribution until there is a 'gully' for the laser-beam to be reflected straight off the sample. This reflectance method sometimes produces results where the above method fails. It is worth mentioning here that particular difficulty was

experienced in exciting white samples with the laser. This is very unexpected because there can be no electronic absorption of the laser frequency by colourless compounds. The same trouble has apparently been found with the Cary-81 when the He/Ne laser attachment is used¹⁷. The sample holder provided is useless when air unstable compounds are to be investigated. However, it has proved possible to obtain Raman spectra of some solids by the novel method of placing the solid, in its ampoule, merely beneath the laser beam! By adjusting the height of the ampoule correctly, a satisfactory spectrum could sometimes be achieved. This method can only be used in the 'auto-mode' but using it, a very good spectrum of $(\text{NEt}_4)[\text{NbCl}_6]$ was obtained.

With liquids and solutions the laser was generally more successful in excitation of the sample. The 3 ml. liquid cell holder supplied was both easy to use and align properly. In many cases it was not found necessary even to filter solution before use. This is a marked improvement on non-laser instruments where any scattering material tends to ruin the spectrum. In marked contrast to colourless solids, colourless liquids provided no difficulty in excitation and very good spectra were obtained. The one notable exception to this was found

with liquid water; the broad weak feature near 170 cm^{-1} could not be properly located. Quite good spectra were obtained irrespective of whether they were run in the 'auto-mode' or with the filters out. For unstable liquids or those which might corrode the cell (which cost £120) it was found possible to improvise with a home made cell and still obtain reasonable spectra. This glass cell has the shape shown in Figure [2.7]. The point marked X is optically flattened so that none of the laser beam is lost by reflection. The dumping mirror and optics designed for use with the liquid microcell are used in conjunction with the cell so that the maximum number of traverses of the sample could be obtained. The cell is fixed in position by a piece of plasticine. For liquids which are thermally unstable or for a low temperature study, a particularly successful cold cell was designed by Dr. D.M. Adams. ~~This is illustrated in Figure [2.2].~~ One of the above home-made cells is used. There are two difficulties involved in using this system. Perhaps the most important is due to the fact that the Raman radiation has to pass through two separate glass windows. It is very hard to arrange for both pieces of glass to be normal to the radiation and some loss of signal is inevitable. At first sight it might appear that the second difficulty was more

significant; it is tricky to align the cell properly with the sample holder lid closed. However, by leaving the lid open and closing the blinds in the room a perfectly good spectrum could be obtained in the dark. Apart from these difficulties the cold cell operated perfectly. Spectra of solids obtained by freezing liquids could not be obtained, presumably because of too much scatter.

It was found particularly simple to obtain depolarisation ratios for liquids. A demountable Ahrens prism is quite quickly fitted between the sample and monochromator. Merely by altering the alignment of this prism from horizontal to vertical and taking the direct ratio of these two readings from the recorder is the depolarisation ratio P measured. It is important to note that this ratio refers to measurement with plane polarised light. It is usual to quote values P' with respect to unpolarised light. Generally P does not equal P' but they can be shown to be related by :-

$$P' = \frac{2P}{1 + P}$$

A band is said to be polarised whenever the depolarisation ratio is less than $6/7$. This value is determined by

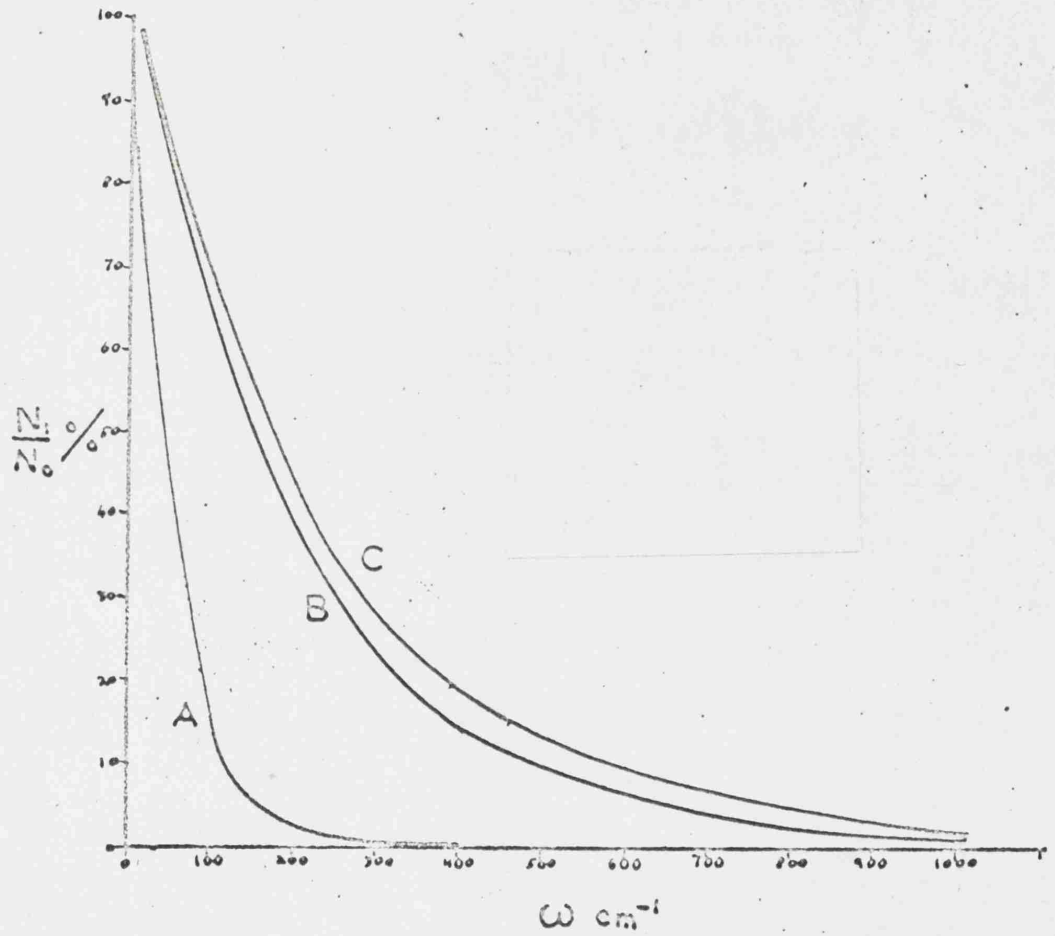
quantum mechanical considerations and refers to measurements with unpolarised light. The above relation leads to an equivalent value of $3/4$ when dealing with plane polarised light. The use of the polariser is well illustrated with H_2TeCl_6 . The region $400-200\text{ cm}^{-1}$ is shown in Figure [2.8]. The continuous line shows the spectrum obtained without the polariser in, while the dotted line is that obtained with it in. Thus there are seen to be two bands in this region with the higher one polarised.

Two practical considerations should be mentioned before this section is closed. The first one is concerned with how close to the exciting line Raman shifts can be observed. It might be thought that with a highly monochromatic coherent exciting line that shifts of only 10 cm^{-1} might be observed, but Perkin-Elmer only claim that shifts of greater than 30 cm^{-1} are detectable. In practice no bands at shifts less than 65 cm^{-1} have so far been observed. The second point involves the resolution of the LR-I. The monochromator is adjusted for best resolution using an argon lamp. This has an emission at $667.7\overset{\circ}{\text{A}}$ while the neon in the laser has an emission at $667.8\overset{\circ}{\text{A}}$. This is observable when the spike filter is not being used. The two emissions are separated by just 1 DN at 2030 DN.

The argon band corresponds to a frequency of $14,977 \text{ cm}^{-1}$ while the neon one to $14,974 \text{ cm}^{-1}$ thus supplying two sharp bands with only 3 cm^{-1} separation. These bands should be clearly resolved when conditions are optimum. The practical test for resolution involves study of the 459 cm^{-1} band in C Cl_4 ; this is the A_1 symmetric breathing mode of the tetrahedron and is very strong. The chlorine isotope effect is such that there is a 2.5 cm^{-1} separation of two bands in this mode. It is of course far more difficult to resolve such a system compared to the above ideal case of Ar/Ne. While the Ar/Ne test worked perfectly, the C Cl_4 test was never obtained to any real satisfaction. Although signs of splitting were indicated, these splittings were impossible to measure.

FIGURE 2.1

Boltzmann Distribution Curves.



Boltzmann Distribution Curve

for :-

A -196°C , B 25°C , C 75°C .

FIGURE 2.2

Transmission characteristic of the colour filter (F_2).

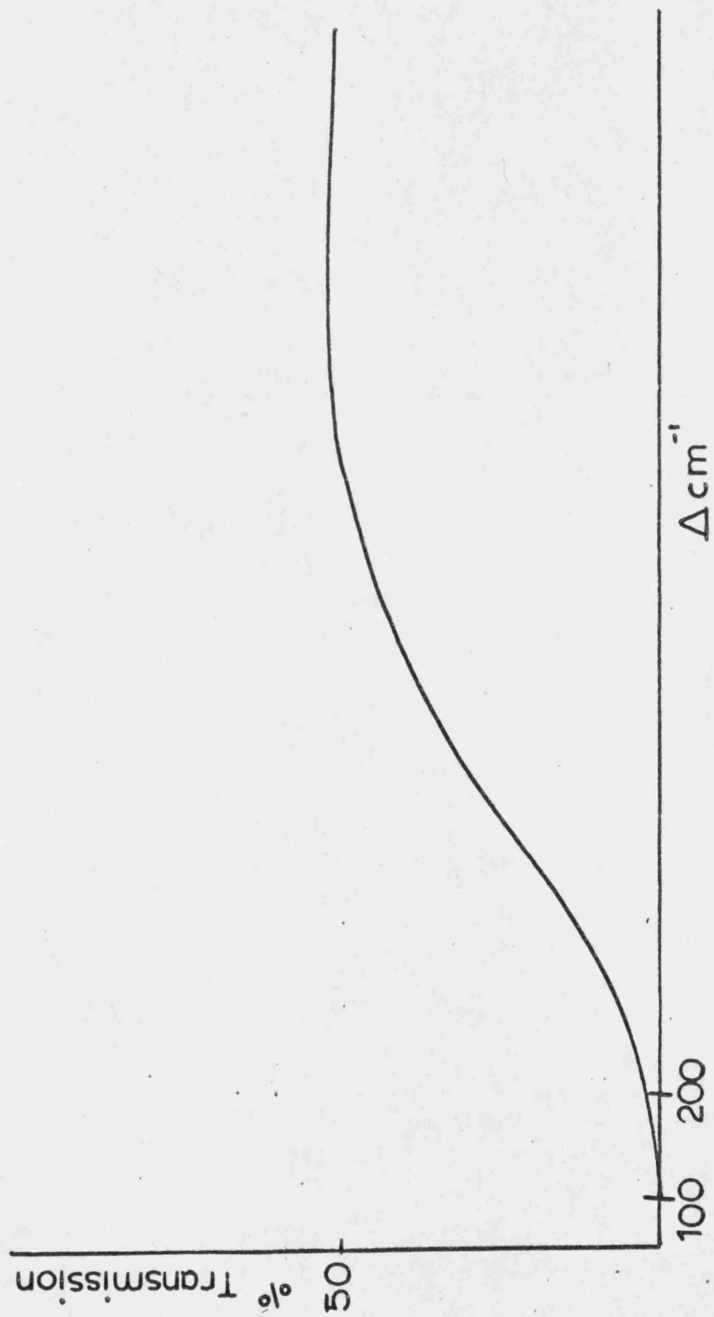


FIGURE 2.3

Background of LR-1 in the region of 2200DN both with and without colour filter in.

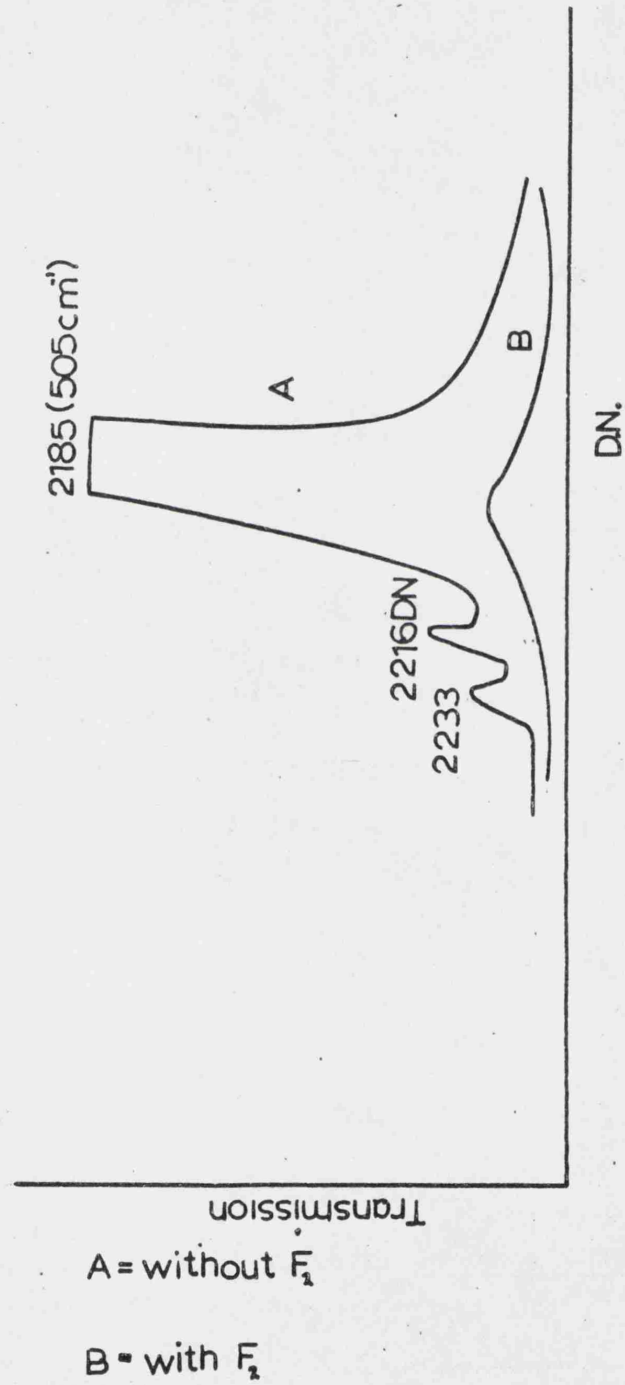
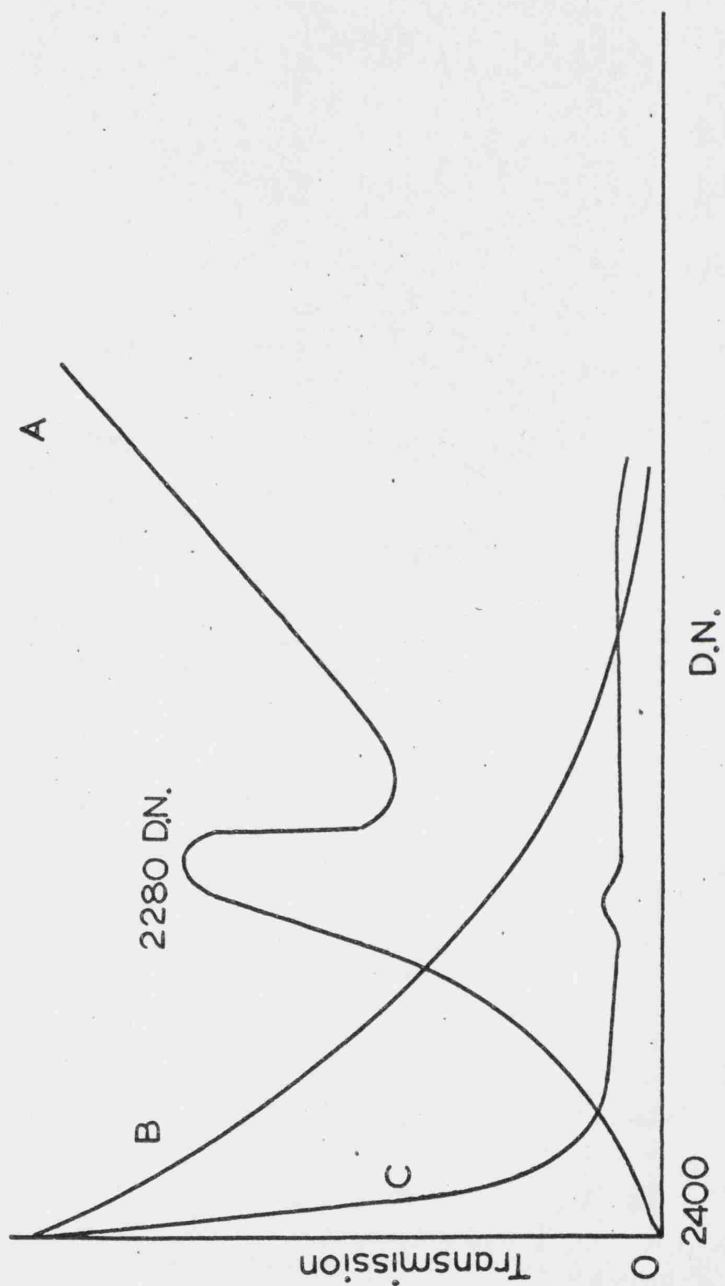


FIGURE 2.4

Transmission characteristic of interference filter (F_1),
and resultant background spectrum near exciting line.



- A = transmission characteristic
- B = background without F_1
- C = background with F_1

FIGURE 2.5

Background spectrum when filters not in use.

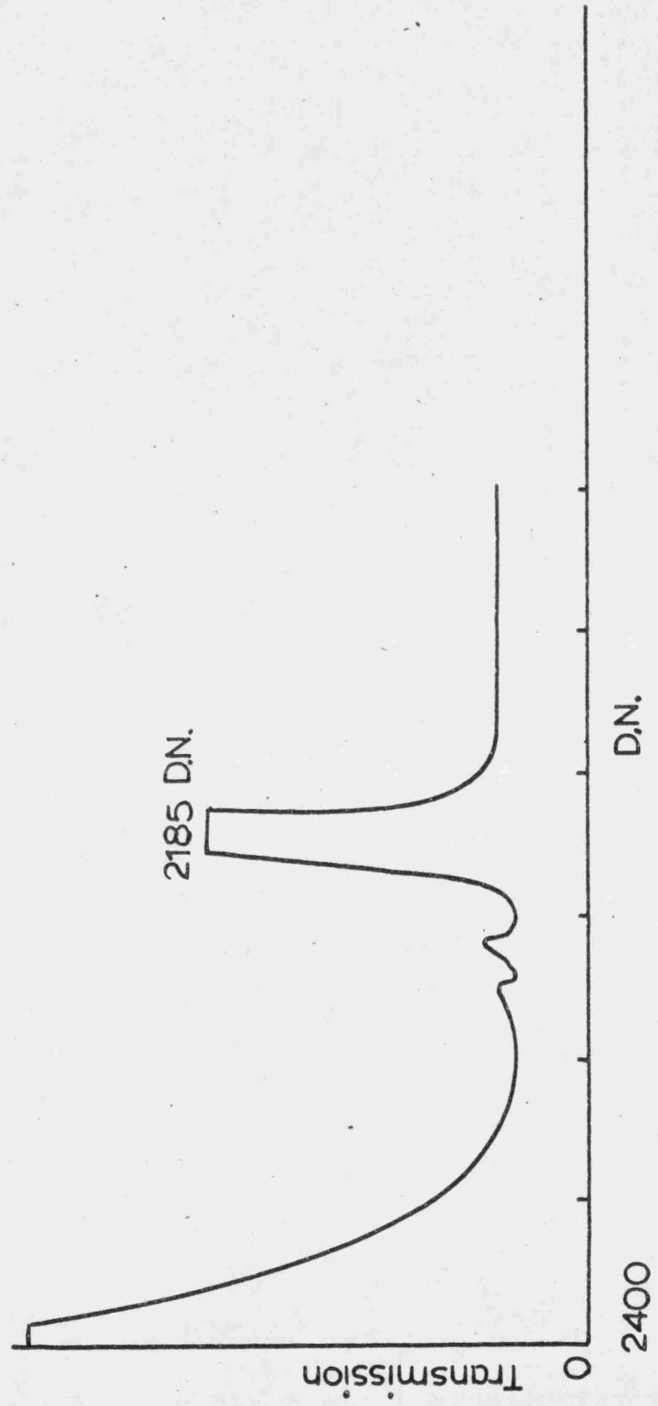
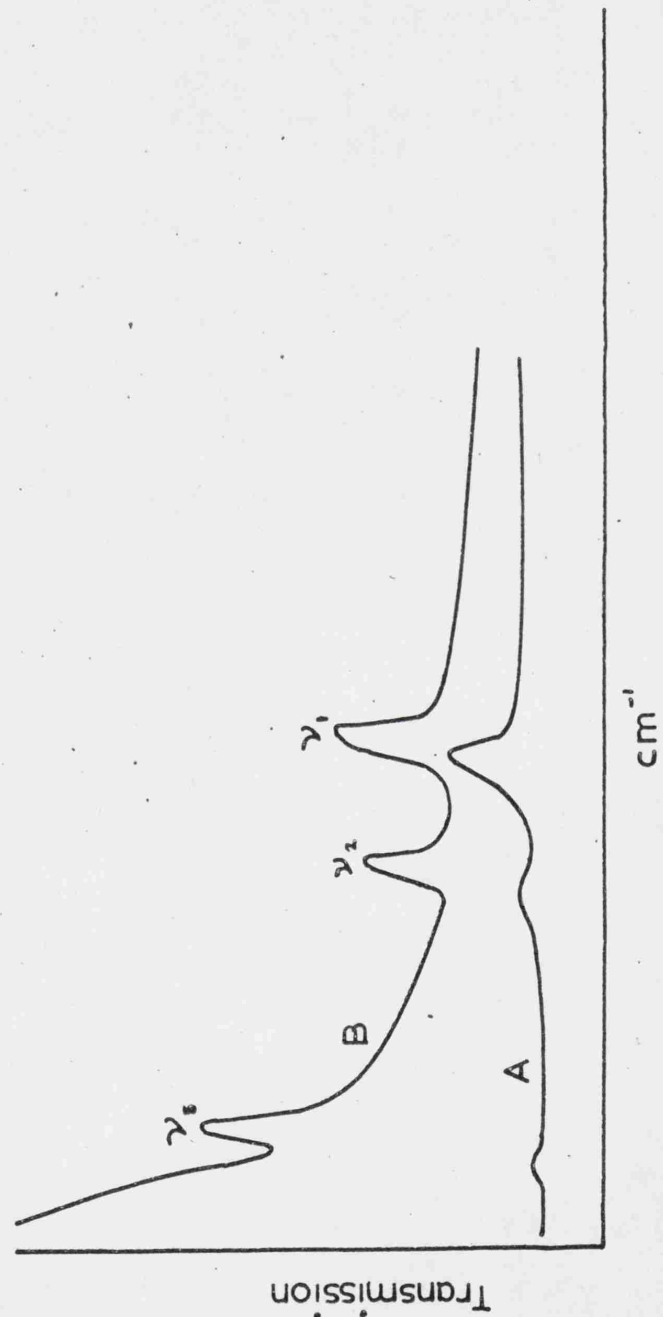


FIGURE 2.6

Raman spectrum of ammonium hexachlorotellurate.



A = with filters

B = without filters

FIGURE 2.7

Sealed Raman cell for air-sensitive liquid samples.

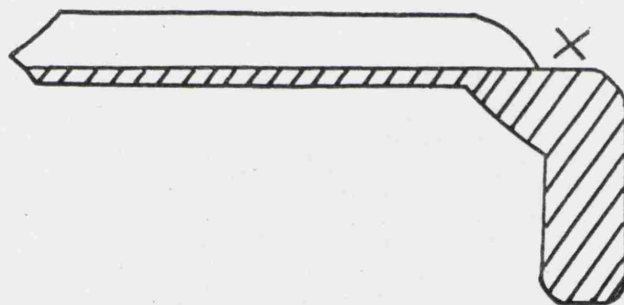
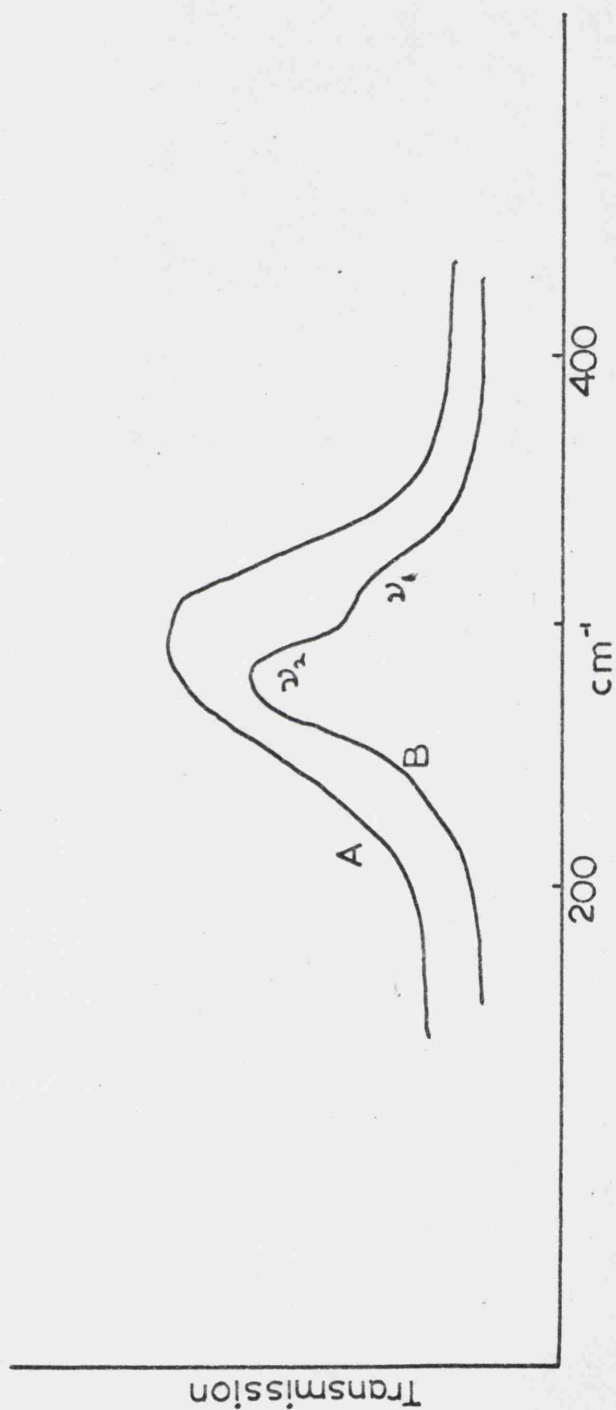


FIGURE 2.8

Raman spectrum of hexachlorotelluric acid.



A=Without polarizer in (//)
B=With polarizer in (⊥)

TABLE 2.1

Dependence of 1st excited state population on temperature and frequency.

(cm^{-1})	T($^{\circ}\text{K}$)	$100 \frac{N_1}{N_0}$
100	350	66.3
100	300	61.9
100	77	15.4
200	350	43.9
200	300	38.3
200	77	2.4
400	350	19.3
400	300	14.7
400	77	.06
1000	350	1.6
1000	300	0.8
1000	77	⊗
3000	350	⊗
3000	300	⊗
3000	77	⊗

350°K is the temperature of the beam of the PE-225,
300°K is room temperature and 77°K the temperature
of the cold cell.

⊗ less than .0001

CHAPTER THREE

OCTAHEDRAL ANIONS

CHAPTER THREE - OCTAHEDRAL ANIONS3.1 Introduction

The vibrational spectra of hexahalogenometallates are well understood. Only below 130 cm^{-1} is the interpretation of the infrared spectra in any possible doubt. The first reported infrared spectrum of an $[\text{MCl}_6]^{n-}$ anion was by Adams¹⁸. He investigated the spectra of the compounds $\text{K}_2[\text{MCl}_6]$ ($\text{M} = \text{Ir, Os, Pt, Pd}$) between 400 and 170 cm^{-1} and concluded the absorption near 300 cm^{-1} was due to a metal chlorine stretching frequency and that below 200 cm^{-1} to a bending mode. For the stretching mode the chlorine isotope effect was observable and usually the $\text{M}-\text{Cl}^{37}$ stretching vibration was resolved. Since this first work, many papers have been published which have included spectra of $[\text{MX}_6]^{n-}$ anions,^{12, 18-31} Many of the investigations only searched to 200 cm^{-1} , and thus much work is still left to perform before complete spectra are obtained.

All the above infrared work was concerned with solids; on the other hand practically all Raman investigations of such systems have been limited to solution measurements. Although Raman spectra of octahedral anions have been available since 1934 it was only recently that acceptable data was obtained. For example, the first investigation of

$[\text{SnBr}_6]^{2-}$ ions in solution concluded that this ion had D_{4h} symmetry. Also, the possibility of obtaining Raman spectra from deeply coloured solid compounds has only arisen since the discovery of the laser. Woodward was able to study some coloured solutions by use of the Helium discharge lamp, but this was not powerful enough to excite coloured solids. Since the first work of Woodward³³ on $[\text{SnCl}_6]^{2-}$ only a limited number of other systems have been investigated.³⁴⁻³⁷ No coloured solid samples have so far been investigated and the only white solids investigated so far are $(\text{Et}_4\text{N})_2[\text{SnCl}_6]$ $(\text{Et}_4\text{N})[\text{AsCl}_6]$ and $\text{Cs}_2[\text{GeCl}_6]$. Thus the Raman studies described in this chapter represent the first comprehensive study of solid complex halides.

The first force constant calculation on octahedral halides used a modified Urey-Bradley force field²⁴. Quite good agreement was found between calculated and observed frequencies for the neutral metal hexafluorides where ν_6 , the inactive mode, was also known from combination bands. Calculations on hexachloro and bromometallates using the same force field were also performed, and reasonable force constants obtained. The only drawback with the calculations on the chloro- and bromo species was that the infrared and Raman data used referred to different physical states of the

sample. This trouble did not occur for the fluorides because the full vibrational spectrum was observed from the infrared spectrum of the vapour. Since, as will be shown later, the Raman frequencies of the chlorometallates in solution never quite compare exactly with those of a solid salt, the calculated force constants for these systems will be slightly in error. For the first time, observations of the complete vibrational spectrum of samples in the one state have now enabled accurate calculations of force constants of these chloro and bromo species. Also in this chapter the dependence of frequencies of the anion and associated force constants with variation of cation has been investigated. It has been previously noticed that ν_3 , the infrared active stretching mode of the octahedron, does decrease as the cation is increased in size.^{21,30} Where observable, the lattice mode variation, ν_L , of the cation has also been correlated with cation weight.

If maximum information is to be obtained from such an investigation then judicious choice of system for study is required. As far as the Raman requirements are concerned, the sample must generally be both air stable and either yellow or orange-red in colour. From the non-transition metals the pair of anions $[\text{SnCl}_6]^{2-}$ and $[\text{PbCl}_6]^{2-}$ were obvious ones to choose. The ideal transition element to

study was Pt as $[\text{PtCl}_6]^{2-}$ and $[\text{PtBr}_6]^{2-}$ are yellow and red respectively; in fact only $[\text{PtCl}_6]^{2-}$ was studied in detail. This anion is of special interest because of the unusual feature in its solution Raman spectrum; ν_2 was observed to be more intense than ν_1 . With the understanding obtained from study of the Sn, Pb and Pt anions, where no electronic distortions are expected to occur, it was thought likely that investigation of the $[\text{TeX}_6]^{2-}$ (X = Cl, Br, I) anions might prove fruitful. The chloride is yellow, bromide orange and iodide black.

Besides the above anions being investigated in detail, other octahedral anions were studied less fully where it was thought useful information might be obtained.

3.2 Force Constants

Consider a molecule that is labelled in some co-ordinate system by co-ordinates of the type q_1 . The potential energy of the system will be dependent on the changes in the q_1 's and for small displacements is given

by

$$2V = 2V_0 + 2 \sum_{i=1}^{3N} \left(\frac{\partial V}{\partial q_i} \right)_0 \cdot q_i + \sum_{i,j=1}^{3N} \left(\frac{\partial^2 V}{\partial q_i \partial q_j} \right)_0 q_i q_j \quad (1)$$

$$+ \text{higher terms}$$

$$= 2V_0 + 2 \sum_{i=1}^{3N} f_i q_i + \sum_{i,j=1}^{3N} f_{ij} q_i q_j \quad (2)$$

$$+ \text{higher terms}$$

The coefficients f_i and f_{ij} are the force constants. The expression for V can be simplified by a number of assumptions. If the energy at equilibrium is taken as zero then one can put $V_0=0$. Also when all q_1 's are zero then the molecule is in equilibrium position and the energy of the system is a minimum. This leads one to the relation:-

$$\left(\frac{\partial V}{\partial q_i} \right)_0 (=f_i) = 0 \quad \text{for } i = 1, 2, \dots, 3N. \quad (3)$$

The last point to remember is that for very small vibrations the terms higher than quadratic can be neglected.

Remembering these above points the expression for V is much

simpler :-

$$2V = \sum_{i,j=1}^{3N} f_{ij} q_i q_j \quad (4)$$

[Note $f_{ij} = f_{ji}$]

The form of V in (4) is the basic assumption of the general valence force field [G.V.F.F.]. There is a force constant for every pair of co-ordinates in the molecule considered.

If instead of considering changes in the position of the atoms in the molecule one considers the changes in the internal co-ordinates the form of V is further simplified to

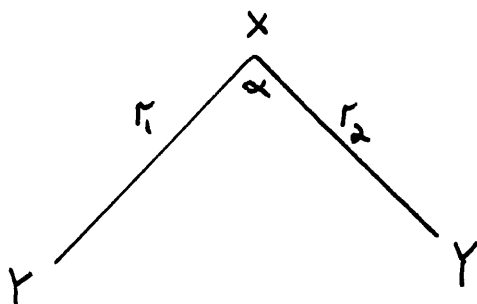
$$2V = \sum_{i,j=1}^{3N-6} f_{ij} q_i q_j \quad (5)$$

q_i is now considered to be the change in some internal co-ordinate from its equilibrium value. As stated above the G.V.F.F. allows for stretching and bending force constants as well as interaction force constants between every pair of stretching and bending force constant.

If this interaction was totally neglected, one would be left with the simple valence force field (S.V.F.F.). This allows stretching and bending force constants only³⁹⁻⁴⁰.

Both the G.V.F.F. and the S.V.F.F. are inadequate for some

chemical applications. From an N atom system ($3N-6$) frequencies at most can be obtained but the G.V.F.F. postulates a far greater number of force constants. This means that there will be many different sets of values of these force constants that will satisfy the observed frequencies. The choice of the correct set can sometimes be helped by use of isotopic substitution which is assumed to change the frequencies but not the potential field. Usually however, this method is impracticable and the G.V.F.F. has to be abandoned in favour of a simpler field. The S.V.F.F. is usually too simple to be useful; generally there are far less force constants than frequencies and one has to be satisfied with a "best-fit". The above difficulties can be illustrated by a bent XY_2 system. The internal co-ordinates are shown in the figure below



The G.V.F.F. expression for the potential energy is given by equation [6] while the S.V.F.F. representation is shown in equation [7].

$$2V = f_{11} (\Delta r_1)^2 + f_{11} (\Delta r_2)^2 + f_{33} r^2 (\Delta \alpha)^2 + 2f_{12} (\Delta r_1) (\Delta r_2) + 2 f_{13} r (\Delta r_1) (\Delta \alpha) + 2f_{13} r (\Delta r_2) (\Delta \alpha) \quad [6]$$

$$2V = f_{11} (\Delta r_1)^2 + f_{11} (\Delta r_2)^2 + f_{33} r^2 (\Delta \alpha)^2 \quad [7]$$

The G.F.V.V. requires therefore, four force constants while the S.V.F.F. only two. An XY_2 molecule has three fundamental vibrations which shows that the G.V.F.F. is too complicated while the S.V.F.F. too simple. With some complicated molecules the discrepancies between the numbers of force constants and frequencies becomes large.

The most useful type of force field would be one in which there were the same number of force constants as frequencies and where a large percentage of these constants were physically meaningful. Perhaps the best compromise involves the assumption of the Urey-Bradley field (U.B.F.F.)⁴¹; this is equivalent to the S.V.F.F. but also includes repulsive force constants between non bonded atoms. The advantage of this field over the G.V.F.F. is two-fold. The most important one is the number of force constants is far less than in G.V.F.F. and do tend to have more obvious physical meaning. The second advantage is that it is

easier to transfer U.B.F.F. constants from one molecule to another. One disadvantage of U.B.F.F. occurs with highly symmetric molecules. For such molecules symmetry properties tend to reduce the number of different force constants from a reasonable number to an inadequately small number. It is perhaps not exactly true to say that the U.B.F.F. is a hybrid between G.V.F.F. and S.V.F.F. because the interaction constants in U.B.F.F. are repulsive while in G.V.F.F. they are attractive. Nevertheless it is a useful way to imagine it.

The construction of the potential energy F-matrix assuming a U.B.F.F. will now be given. The most general statement of the U.B.F.F. is

$$\begin{aligned}
 V = & \frac{1}{2} \sum_i [K_i + \sum_{j(\neq i)} (t_{ij}^2 F_{ij}^1 + s_{ij}^2 F_{ij}^2)] (\Delta r_i)^2 \\
 + & \frac{1}{2} \sum_{i < j} [H_{ij} - s_{ij} s_{ji} F_{ij}^1 + t_{ij} t_{ji} F_{ij}^1] (r_{ij} \Delta \alpha_{ij})^2 \\
 + & \sum_{i < j} [-t_{ij} t_{ji} F_{ij}^1 + s_{ij} s_{ji} F_{ij}^1] (\Delta r_i) (\Delta r_j) \\
 + & \sum_{i \neq j} [t_{ij} s_{ji} F_{ij}^1 + t_{ji} s_{ij} F_{ij}^1] (r_j/r_i)^{1/2} (\Delta r_i) (\Delta r_{ij} \Delta \alpha_{ij})
 \end{aligned}$$

where

$$s_{ij} = (r_i - r_j \cos \alpha_{ij}) / q_{ij} \quad [9]$$

$$s_{ji} = (r_j - r_i \cos \alpha_{ij}) / q_{ij} \quad [10]$$

$$t_{ij} = (r_j \sin \alpha_{ij}) / q_{ij} \quad [11]$$

$$t_{ji} = (r_i \sin \alpha_{ij}) / q_{ij} \quad [12]$$

$$q_{ij}^2 = r_i^2 + r_j^2 - 2r_i r_j \cos(\alpha_{ij}) \quad [13]$$

$$\text{with } r_{ij} = r_i r_j \quad [14]$$

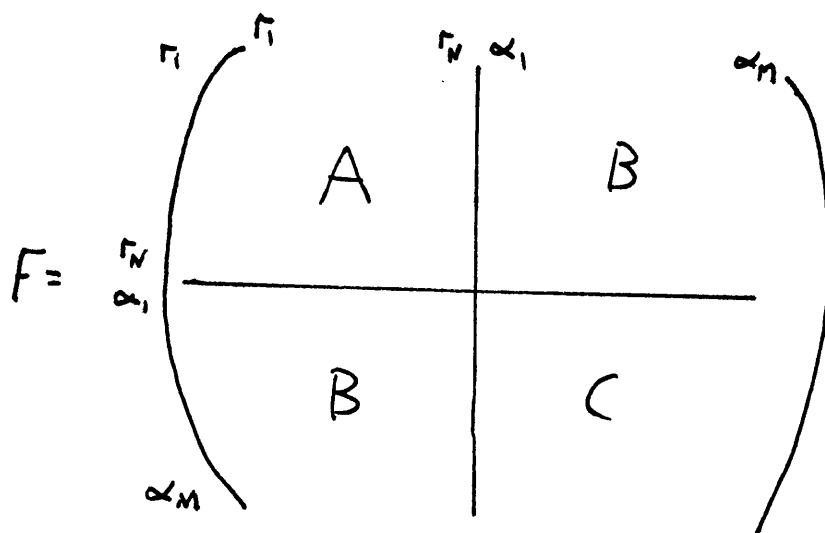
K_1 and H_{ij} represent stretching and bending force constants respectively with F_{ij} being the repulsive constant; F_{ij}^1 is normally taken as being $^{-1/10} F_{ij}$.

For the purpose here it is convenient to represent [8]

as

$$\begin{aligned} V = & \frac{1}{2} \sum [a_i] (\Delta r_i)^2 + \frac{1}{2} \sum [b_{ij}] (r_{ij} \Delta \alpha_{ij})^2 \\ & + \sum [c_i] (\Delta r_i) (\Delta r_j) + \sum [d_{ij}] (\Delta r_i) (r_{ij} \Delta \alpha_{ij}) \end{aligned} \quad [15]$$

The G.V.F.F. Matrix F will be a square array of terms shown in equation [16].



Only internal coordinates which are bond stretches or angle bends are considered. To arrange for all elements of F to have the same dimensions it is customary to multiply all elements in block B by r and all in C by r^2 . Thus the terms $r_x \alpha_{yz}$ and $a_{wx} \alpha_{yz}$ in blocks B and C respectively become $r r_x \alpha_{yz}$ and $r^2 a_{wx} \alpha_{yz}$. It is not necessary to do this, but it is useful in that it enables one to follow what is happening more easily. The relation between F and the potential energy is quite close. Consider the row vector of the internal coordinates $(r_1 \dots r_N, \alpha_1 \dots \alpha_M) = P$. The matrix expression PP^1 is a (1×1) matrix (i.e. a pure number) and is in fact the potential energy of the system considered.

The simple empirical rules for obtaining the form of the U.B.F.F. can now be stated. Consider each of the three blocks of the matrix F in turn.

Block A

In this block there are two types of term, the $(\Delta r_1)^2$ ones and those of form $(\Delta r_1)(\Delta r_j)$. Those terms involving the $(\Delta r_1)^2$ lie on the diagonal of matrix A, and the coefficients are given simply by a_1 . The off-diagonal terms which involve $(\Delta r_1)(\Delta r_j)$ have as coefficient C_1 .

Block B

The elements of this matrix involve terms of the general form $(\Delta r_1)(\Delta \alpha_{jK})$ but not all are represented in the U.B.F.F. Only those terms which have j or K equal to 1 are included; thus if neither j or K are equal to 1, the coefficient is zero. For the terms where one or other of j or K is equal to 1 the coefficient is given by $d_1(j,K)$ where (j,K) is that value of j or K NOT equal to 1. This rule is best explained by an illustration. In the fragment of the potential energy matrix below the values of the coefficients are shown.

	α_{12}	α_{13}	α_{34}
r_1	d_{12}	d_{13}	0
r_2	d_{21}	0	0
r_3	0	d_{31}	d_{34}

Block C

The G.V.F.F. allows for the most general type of term in this block, i.e. $(\Delta\alpha_{ij})(\Delta\alpha_{kl})$ but the U.B.F.F. only includes terms of the form $(\Delta^2\alpha_{ij})$. Thus all non diagonal terms are zero while those which lie on the diagonal have coefficient b_{ij} .

There is one condition to the above rule which takes priority over them. If the pair of internal coordinates considered in a particular term do not have a common atom then the values of the coefficient is zero and not that as given before.

The actual value of the coefficients a,b,c,d. are found by inspection on equating equation [15] with equation [8].

The above method of determining the form of the force constants has been given in some detail because all too often authors, in their papers, indicate that the coefficients of the U.B.F.F. were obtained by comparison with the general field, but do not indicate exactly how this was achieved. Just the opposite is true where symmetrization of the F-matrix is considered. This is done in exactly the same manner as the G-matrix, is very well documented³⁸, and need not be dwelt upon here.

For an octahedral molecule MX_6 the conventional internal coordinates taken are shown in Figure [3.1].

The necessary symmetry coordinates are :-

$$\begin{aligned}
 S_1 (A_{1g}) &= (1/\sqrt{6})(r_1 + r_2 + r_3 + r_4 + r_5 + r_6) \\
 S_2 (E_g) &= (1/\sqrt{12})(2r_5 + 2r_6 - r_1 - r_2 - r_3 - r_4) \\
 S_3 (F_{1u}) &= (1/\sqrt{2})(r_5 - r_6) \\
 S_4 (F_{1u}) &= (1/\sqrt{8})(r)(\alpha_{51} + \alpha_{52} + \alpha_{53} + \alpha_{54} - \alpha_{61} - \alpha_{62} - \alpha_{63} - \alpha_{64}) \\
 S_5 (F_{2g}) &= (1/2)(r)(\alpha_{12} - \alpha_{23} + \alpha_{34} - \alpha_{41}) \\
 S_6 (F_{2u}) &= (1/\sqrt{8})(r)(\alpha_{51} - \alpha_{52} + \alpha_{53} - \alpha_{54} - \alpha_{61} + \alpha_{62} - \alpha_{63} + \alpha_{64})
 \end{aligned}$$

Using the coefficients of these coordinates as the elements of the U-matrix, and remembering the equivalence of bonds and angles in an MX_6 molecule, the resulting elements of the F-matrix after symmetrization (UFU^t) on the U.B.F.F. are found to be :-

$$\begin{aligned}
 (A_{1g}), F_{11} &= K + 4F \\
 (E_g), F_{22} &= K + F + 3F^1 \\
 (F_{1u}), F_{33} &= K + 2(F + F^1), F_{34} = F + F^1, F_{44} = H + \frac{1}{2}(F + F^1) \\
 (F_{2g}), F_{55} &= H + \frac{1}{2}(F + F^1) \\
 (F_{2u}), F_{66} &= H + \frac{1}{2}(F + F^1)
 \end{aligned}$$

These elements can be further simplified by using the standard assumption that $F^1 = -F/10$. K, H and F represent

the M-X stretching, X-M-X bending and X --- X repulsive force constants respectively. In the normal coordinate analyses that follow the modified Urey-Bradley force field (M.U.B.F.F.) was used. This follows the treatment of Hiraishi²⁴. Here two further interaction force constants are envisaged. One of them, A, represents interaction between adjacent bonds while the other, B, allows for interaction between any two angles of the octahedron that are not coplanar. Using this modified system Hiraishi has shown that the elements of F-matrix are now :-

$$\begin{aligned}
 F_{11} &= K + A + 4F, & F_{22} &= K + A + 0.7F, & F_{33} &= K - A + 1.8F, \\
 F_{34} &= 0.9F, & F_{44} &= H + 2B + 0.55F, & F_{55} &= H + 0.55F \\
 \text{and } F_{66} &= H + 0.55F - 2B.
 \end{aligned}$$

With this field five force constants can be found to give an exact fit to the five observed frequencies, although only K, the stretching force constant, is chemically meaningful.

3.3 Hexahalogenoplatinates.

Raman spectra of $[\text{PtCl}_6]^{2-}$ and $[\text{PtBr}_6]^{2-}$ have been observed in aqueous solution by Woodward and Creighton¹⁹ using a helium discharge lamp. Spectra have not been reported before for the solids.

Only the infrared spectra of the potassium,^{12,18,24} caesium,²⁶ ammonium,²⁴ and tetraethylammonium²⁰ chloroplatinates have been reported previously and only below 200 cm^{-1} for the potassium salt.

The compounds $M_2^I[\text{PtCl}_6]$, ($M^I = \text{K, Rb, Cs, Tl, NH}_4$) are known to crystallize with the face centred cubic structure. As well as elemental analysis, all the above compounds were characterised by their X-ray powder photographs, and indexed on a face centred cubic basis. The lattice constant for the thallium salt does not appear in the literature and is $a = 9.75\text{\AA}$. The powder photographs of the salts with $M^I = \text{Ag, Me}_4\text{N, Et}_4\text{N, Bu}_4\text{N, Ph}_4\text{As}$ and Ph_2I were also taken. The silver salt was indexable as face centred cubic with $a = 9.93\text{\AA}$. This is perhaps larger than would be expected since the ionic radius of Ag^+ is 1.26\AA compared to K^+ for which the ionic radius is 1.33\AA ; K_2PtCl_6 has an a -value of only 9.77\AA . The methyl-ammonium salt was indexable on the basis of a slightly distorted face centred cubic structure. For $(h^2+k^2+l^2)$ values of greater than 27 some forbidden

reflections were observed. The lattice parameter for this salt was 12.66\AA ; 2.4\AA larger than that of the caesium analogue. The distortion from the cubic structure is probably a reflection of the packing requirements of the methyl group in the lattice, i.e. the structure is still basically face centred cubic. This is supported by the powder photograph of the tetraethylammonium salt which is also indexable on a cubic basis ($a = 14.07\text{\AA}$) but has forbidden lines appearing for $(h^2 + k^2 + l^2)$ values as low as 21. The photographs of the tetra-n-butylammonium and tetraphenylarsonium salts were proportionately more complicated. Whether this reflects merely a more pronounced distortion of cubic structure or a complete change of structure (say anti-rutile) is not certain. However, the spectra of these salts could be assigned on the assumption that they were isomorphous with the other chloroplatinates. The powder photograph of the diphenyliodonium salt was even more complicated than the tetraphenylarsonium salt and this is taken as good evidence that a new structure is adopted. The photograph was not indexed but was very similar to that of the corresponding bromide.

A regular octahedral species has ν_1 (A_{1g}), ν_2 (E_g) and ν_3 (F_{2g}) Raman active; ν_3 (F_{1u}) and ν_4 (F_{1u}) infrared active; ν_5 (F_{2u}) is inactive. These normal vibrations are

depicted in Figure [3.2]. The absorption frequencies for the chloro and bromo platinates studied are listed in Table [3.1] with assignments. Woodward and Creighton³⁵ found for $[\text{PtCl}_6]^{2-}$ and $[\text{PtBr}_6]^{2-}$ that ν_1 and ν_2 are closer together than for non-transition metal octahedral halides, and that the intensities are in the unusual order $\nu_2 > \nu_1$. The proximity of the two stretching vibrations is confirmed for the solid salts but the relative intensities are more variable. For the potassium and caesium salts ν_1 and ν_2 are of comparable intensity. Half bandwidths are ca. 15 cm^{-1} . ν_3 the Raman active band is unusually strong being the most intense feature of the spectrum for potassium, caesium and tetraethylammonium salts. The spectrum of K_2PtCl_6 is shown in Figure [2.3]. For the organic cations difficulty was experienced in exciting the samples. Whether this is a feature of the physical state of these samples or a dilution effect is not certain. The same difficulty was found with the other halometallates, discussed later.

In the infrared spectrum ν_4 is always intense and sharp (ca. 10 cm^{-1} half-bandwidth) but ν_3 varies considerably with change of cation and is at least twice the width of ν_4 , except for the ammonium salt for which the half band-width values are ν_3 , 30 cm^{-1} and ν_4 , 40 cm^{-1} . ν_3 is always asymmetric on the low-frequency side, probably

due to absorption of $[\text{PtCl}_6]^{2-}$ ions with varying proportions of ^{37}Cl . Half bandwidths increase in the order Tl (15 cm^{-1}); NH_4 , Rb, Co (ca. 20 cm^{-1}); K, Ag, NMe_4 , NBu_4^n , AsPh_4 , (ca. 30 cm^{-1}); NEt_4 (55 cm^{-1}). The general features of these four classes are depicted in Figure [3·4]. The silver salt is unusual in having ν_4 at 215 cm^{-1} , 20 cm^{-1} higher than any other ν_4 ; ν_3 however is at a quite reasonable frequency.

Using diphenyliodonium as cation causes a change in structure from that of K_2PtCl_6 , reflected in a relaxation of the selection rules. The diphenyliodonium cation is presumably bent being formally analogous to H_2O in structure, i.e. two ligands and two lone pairs coordinated to the central atom in a tetrahedral manner, with the lone pairs forcing the ligands closer together than required by T_d symmetry. Diphenyliodonium chloride has two regions of absorption between 410 and 200 cm^{-1} ; a doublet of medium intensity centred on 260 cm^{-1} while a weaker feature appears at 403 cm^{-1} . For the hexachloroplatinate ν_3 is split and a weak-medium band appears at 338 cm^{-1} , coincident with the Raman value for ν_1 . ν_2 might also be present but would be overlaid by the split ν_3 . ν_4 and ν_5 are also clearly split, and a strong band appears at 86 cm^{-1} which is assigned to the infrared active component of ν_6 (vide infra). Taking average values for the split bands ν_6 is

calculated to be at 91 cm^{-1} , in good agreement with the experimental value. These results are consistent with the complex anion having C_{3v} site-symmetry, as in the hexagonal K_3MnF_6 structure³⁰. They are not consistent with a layer structure of the bis(p-toluidinium)hexachlororhenate(IV) type⁴², which requires C_1 site-symmetry for the complex anion. The correlation table for MX_6 molecules is given below.

	ν_1	ν_2	ν_3	ν_4	ν_5	ν_6
O_h	A_{1g}	E_g	F_{1u}	F_{1u}	F_{2g}	F_{2u}
C_{32}	A_1	E	$A_1 + E$	$A_1 + E$	$A_1 + E$	$A_2 + E$
C_1	A_g	$2A_g$	$3A_u$	$3A_u$	$3A_g$	$3A_u$

With C_{3v} symmetry $A_1 + E_2$ are infrared active while A_u is infrared active in C_1 symmetry. ν_6 [as in $(Ph_2I)_2PtCl_6$] was not observed in the Raman spectrum, but this is not conclusive as the performance of the instrument with solids at very low shifts is not very good; also, the difficulty of excitation of samples with organic cations has already been mentioned. In contrast to the chloride $(Ph_2I)_2 [PtBr_6]$ shows only a single sharp ν (Pt-Br) band in the infrared spectrum. This is surprising in view of the fact that the powder photograph was similar to that of the chloride.

Although K_2PtBr_6 , a tomato red solid, gave a good Raman spectrum, the Ph_2I salt was too brown to give one.

Most of the compounds used have further absorption at very low frequencies. These bands, whose origin has been discussed previously,^{12,21} could be either ν_6 or lattice modes associated with the cations. If they were due to ν_6 the change of selection rules implied would require spectra of the complexity of that observed for $(Ph_2I)_2[PtCl_6]$, and this is not found. Their dependence upon cation mass, as shown in Figure [3.5], argues strongly for their assignment as translational lattice modes. On mass considerations alone, Ph_2I^+ would be expected to translate ca. 55 cm^{-1} ; this strengthens the assignment of the 86 cm^{-1} band to ν_6 . The change in site symmetry from O_h to C_{3v} would not be expected to have a profound effect on the position of the lattice mode. This statement can be supported by a comparison of the lattice modes in the unrelated systems M_2PtCl_4 ⁴³ and M_2PtCl_6 [$M = K, Rb, Cs$]; the bands attributed to the lattice modes are listed below (in cm^{-1}).

	$M_2 [PtCl_4]$	$M_2 [PtCl_6]$
K	106	106
Rb	82	84
Cs	80	73

Although several force constant calculations have been made for complex halides, none has been made with Raman and infrared data which related to the same state. Comparison of the Raman frequencies of $[\text{PtCl}_6]^{2-}$ obtained in aqueous solution¹⁹ with the solid state value shows that no one cation fits the solution values and that, consequently, force constants calculated using data from different states are slightly in error. Force constants calculated here have used a modified Urey-Bradley force field (MUBFF) mentioned previously. Abramowitz and Levin⁴⁴ have recently made a comparison between force constants obtained using this field and those obtained with the general field; they concluded that the MUBFF yields values for the principal force constants in good agreement with those obtained from the general force field. Using a computer initial values of the force constants were refined until an exact fit was obtained with the observed values of ν_1 to ν_5 . ν_6 was then calculated. Force constants are listed in table [3.2] and ν_6 is included in table [3.1].

For $M_2[\text{PtCl}_6]$ there is an approximate linear decrease in K , the stretching force constant, with increase in ionic size from Ag^+ to Cs^+ , after which a limiting value of 1.73 to 1.74 millidynes/ \AA is reached for the large

organic cations. This is related to the general lowering of the three stretching frequencies in the same sequence, shown most clearly by ν_3 . The plot of K versus ionic size is shown in Figure [3.6]; the radius of the alkyl-ammonium ions were taken as these indicated by calculations on limiting mobilities by Stokes' law⁴⁵.

The orange compound $K_2PtCl_4Br_2$, formed by reaction of bromine with potassium chloroplatinite⁴⁶, has the spectra given in table [3.3]. It could be cis- or trans- $K_2[PtCl_4Br_2]$, or a 2:1 mixture of $K_2[PtCl_6]$ and $K_2[PtBr_6]$. The correlation between O_h and both D_{4h} and C_{2v} is given below.

	ν_1	ν_2	ν_3	ν_4	ν_5	ν_6
O_h	A_{1g}	E_g	F_{1u}	F_{1u}	F_{2g}	F_{2u}
D_{4h}	A_{1g}	$A_{1g}+B_{1g}$	$A_{2u}+E_u$	$A_{2u}+E_u$	$B_{2g}+E_g$	$B_{2u}+E_u$
C_{2v}	A_1	A_1+A_2	$A_1+B_1+B_2$	$A_1+B_1+B_2$	$A_1+B_1+B_2$	$A_2+B_1+B_2$

For D_{4h} symmetry (trans formulation) $A_{2u}+E_u$ are infrared active while A_{1g}, B_{1g}, B_{2g} and E_g are Raman active. For C_{2v} (cis formulation) all bands are Raman active and only A_2 is infrared inactive. The relative simplicity of the spectra rules out the cis but is consistent with the trans formulation, although it is necessary to assume that the site-symmetry of the anions is lowered sufficiently to allow

$\nu(\text{Pt-Cl}_4)$, E_u , to be split and $\nu(\text{Pt-Br})$, A_{1g} , to be infrared active. The spectra might also be interpreted as the sum of contributions from $[\text{PtCl}_6]^{2-}$ and $[\text{PtBr}_6]^{2-}$, but the bands are shifted considerably from the positions for the two separate potassium salts. To confirm the identity of the compound, the X-ray powder photograph was taken. This was indexable on a face-centred cubic basis assuming $a = 9.90\text{\AA}$. The observed and calculated values of $\sin^2\theta$ are shown in table [3.4]. The compound thus is not a mixture of chloro- and bromoplatinates. It is strange that it packs in a cubic lattice but this is consistent with the interpretation that $\text{trans-}[\text{PtCl}_4\text{Cl}_2]$ anions are packed randomly in crystal. This also explains the lowering of the site symmetry postulated in the interpretation of the spectra. The lattice parameter (9.90\AA) may be compared with those of the chloroplatinate (9.76\AA) and the bromoplatinate (10.30\AA).

A fair approximation to the modes and assignments of the spectra of trans-}[\text{K}_2\text{PtCl}_4\text{Br}_2] can be obtained by calculating the expected modes for the separate PtCl_4 and PtBr_2 moieties. This is done below.

	Infrared	Raman
PtCl ₄ (D _{4h})	1 stretch, 2 bends	2 stretches, 1 bend
PtBr ₂ (D _{∞h})	1 stretch, 1 bend	1 stretch
PtCl ₄ +PtBr ₂	2 stretches, 3 bends	3 stretches, 1 bend

This should be compared with the requirements calculated using correlation tables which are 2 stretches and 3 bends in the infrared and 3 stretches and 2 bends in the Raman. There is thus one Raman active bend not predicted by treating the two D_{4h} and D_{∞h} residues separately. This bend is probably therefore, associated with both chlorine and bromine bending. However, since it is certainly below 150 cm⁻¹ it has been assigned as mainly ν (Pt-Br). The strong band in the infrared at 92 cm⁻¹ attributed to ν (Pt-Br), E_u, probably also has a lattice mode contribution from the potassium ions included in it.

3.4 Hexachloro-stannates and plumbates

Raman spectra of aqueous solutions of $[\text{SnCl}_6]^{2-}$ and of $[\text{PbCl}_6]^{2-}$ have been reported by Woodward and Anderson³³, and Creighton and Woodward³⁴ respectively. Using He/Ne laser excitations we have now extended these observations to series of the solid complex chlorides $M_2^I [\text{MCl}_6]$ ($M = \text{Sn, Pb}$). These compounds have the cubic $K_2 [\text{PtCl}_6]$ structure for $M^I = \text{K, Rb, Cs, NH}_4$,⁴⁷ and X-ray powder photographs for $M^I = \text{NMe}_4$ and NEt_4 can also be indexed on a cubic structure. The NMe_4 salts were indexable with $a = 12.60\text{\AA}$ ($M = \text{Sn}$) and $a = 12.71$ ($M = \text{Pb}$) but as with the platinum analogues some forbidden lines were observed for high hkl values; even more distorted were the NEt_4 salts indexed with $a = 14.00\text{\AA}$ ($M = \text{Sn}$) and $a = 14.11\text{\AA}$ ($M = \text{Pb}$). Correspondingly $(\text{NBu}_4^{\text{n}})_2 [\text{SnCl}_6]$ had an even more complicated powder photograph as did both Ph_4As salts. The Ph_2I compounds had photograph more complex than the Ph_4As salts and this is taken again as good evidence that they adopt a different structure from that of $K_2 [\text{PtCl}_6]$.

The infrared active stretching frequency, ν_3 , has been observed for $(\text{NH}_4)_2 [\text{SnCl}_6]^{24,25}$ and $M_2^I [\text{MCl}_6]$, ($M^I = \text{K, Rb, Cs, NEt}_4$), ($M = \text{Sn, Pb}$),^{20,30} but the only lower frequency bands known are those for $K_2 \text{SnCl}_6$ and $(\text{NH}_4)_2 \text{SnCl}_6$ given by

Greenwood and Straughan²⁸. A series of these complexes have now been studied to 60 cm^{-1} . The bands observed with obvious assignments are given in tables [3.5] and [3.6].

The yellow hexachloroplumbates yielded good Raman spectra in which ν_1 was considerably stronger than ν_2 . Some difficulty was experienced with the white tin complexes and only ν_1 was found in several cases, even though the samples were microcrystalline. Surprisingly, difficulty has been encountered in exciting Raman spectra of many other white or colourless inorganic solids with the 6328\AA ; better spectra might be obtained with conventional mercury sources. The same difficulty has been noticed by other workers¹⁷. With the platinum, tin and lead complexes, $M_2^I [MCl_6]$, poorer spectra were obtained when $M^I =$ organic cation than when an inorganic cation was used. Results reported here for the solids compare well with the solution values and the assignments follow clearly.

In the infrared spectra ν_3 and ν_4 are unambiguously assigned in every case; the shapes and half-band widths ($\Delta\nu_{1/2}$) vary considerably with M^I . For the ammonium salt ν_4 is very broad (ca. 75 cm^{-1} half bandwidth) and is wider than ν_3 ($\Delta\nu_{1/2}$ ca. 60 cm^{-1}), and for $K_2 [SnCl_6]$ both ν_3 ($\Delta\nu_{1/2}$ ca. 100 cm^{-1}) and ν_4 ($\Delta\nu_{1/2}$ ca. 60 cm^{-1}) are very broad. Otherwise, ν_3 is $30\text{-}50\text{ cm}^{-1}$ and ν_4 $25\text{-}30\text{ cm}^{-1}$ half

bandwidth. The compounds $(NR_4)_2[SnCl_6]$, (R = Et, Bu) and $(Et_4N)_2[PbCl_6]$ have ν_3 clearly split; it is distorted in most other cases. These factors made the bands difficult to measure accurately. Agreement between the values reported here and those already published is good, making general allowance for these factors. The band centre frequency has generally been reported here, not the band maximum frequency, in the cases of asymmetric bands.

As for $(Ph_2I)_2[PtCl_6]$, the diphenyliodonium salts have complex spectra which indicate a pronounced lowering of site-symmetry. In both cases ν_3 is resolved into two components, accompanied by a weaker band co-incident with the Raman value for ν_1 . ν_4 for the tin salt splits and a band appears at 89 cm^{-1} which is assigned to normally inactive ν_6 . It is too high to be a lattice mode (vide infra) and it is close to the position calculated for ν_6 for $Cs_2[SnCl_6]$. In $(Ph_2I)_2[PbCl_6]$, ν_4 is asymmetric but not split.

Cation-dependent lattice modes were found for both series of anions and decrease in a fairly regular manner with increase in cation mass. The band at 110 cm^{-1} reported by Greenwood and Straughan²⁸ was not found, but a strong absorption at 83 cm^{-1} was observed, more consistent with previous values of lattice modes for potassium in

complex halides¹².

Since the infrared active lattice modes are of F_{1u} symmetry they can interact with ν_4 . It is unlikely that this is significant in the present series, except for the ammonium salts. $(NH_4)_2 [MCl_6]$ ($M = Sn, Pb, Pt$) have ν_L at 122, 106 and 134 cm^{-1} respectively; in each case ν_4 is the highest observed for the complex anion. Thus it is quite possible that in the unperturbed spectra of the ammonium salts ν_4 and ν_L would be much closer together. There is in any case a slight decrease in ν_4 with decrease in ν_L for the hexachlorostannates, but it is unlikely that this is primarily attributable to interaction between ν_4 and ν_L , as the stretching modes also show the same trend with expansion of the lattice.

No force constants have been calculated for $[SnCl_6]^{2-}$ and $[PbCl_6]^{2-}$ using infrared and Raman data taken from the same state. This has now been done using the MUBFF. Calculated force constants are shown in table [3.7]. The vibrational frequencies for the lead complex ions are substantially lower than for those for tin. This lowering is accompanied by a decrease in bond stretching force constant, K , showing that the changes are only partly due to mass effects; there is a genuine decrease in M-Cl bond strength from tin to lead. K shows a general decrease with

increase in lattice size, except for the highly distorted diphenyliodonium salt; for the tin complexes the change is very slight.

3.5 Hexahalogenotellurates

The hexahalogenotellurate anions $[\text{TeX}_6]^{3-}$ ($X = \text{Cl}, \text{Br}, \text{I}$) are of particular structural interest. Gillespie and Nyholm⁴⁸, suggested that they should be distorted from octahedral by the effect of the lone pair of electrons: however, several crystal structure determinations⁴⁹⁻⁵² have failed to show any significant distortion. Furthermore the solid complexes $M_2^I[\text{TeX}_6]$, ($M^I = \text{K}, \text{Rb}, \text{Cs}, \text{NH}_4$), ($X = \text{Cl}, \text{Br}$), have been shown to have the K_2PtCl_6 structure^{50,52,53}. X-ray powder photographs have been taken of $M_2^I[\text{TeX}_6]$, ($X = \text{Cl}, \text{Br}$) ($M^I = \text{NMe}_4, \text{NEt}_4, \text{AsPh}_4$) and $(\text{Ph}_2\text{I})_2\text{TeCl}_6$. Both $M^I = \text{NMe}_4$ and NEt_4 are indexable on a slightly distorted face centred cubic basis; $M^I = \text{NMe}_4$ $a = 12.90\text{\AA}$, $X = \text{Cl}$, $a = 13.32\text{\AA}$, $X = \text{Br}$; $M^I = \text{NEt}_4$, $a = 14.14\text{\AA}$, $X = \text{Cl}$, $a = 15.09$ $X = \text{Br}$. The $(\text{Et}_4\text{N})_2\text{TeBr}_6$ X-ray photograph showed that this compound was more distorted than the other Et_4N salts since forbidden lines appeared for $(h^2 + k^2 + l^2)$ values as low as 18. Both the Ph_4As and Ph_2I salts had comparably complicated photographs; whether the Ph_4As and Ph_2I salts have the same structure (presumably different from K_2PtCl_6) or different ones is not certain. It is possible that the same situation occurs here as with the Pt, Sn and Pb series where the Ph_4As salt tends to be merely distorted from $\text{K}_2[\text{PtCl}_6]$ while the Ph_2I

salt appears to adopt a new structure.

Greenwood and Straughan²⁸ recently summarised the situation and reported far-infrared spectra of seven hexahalogenotellurates, concluding that there is no distortion of the individual octahedra due to the lone pair of electrons. Partial or complete Raman and infrared data for twenty-one hexahalogenotellurates are now reported; the interpretation of this data has been aided by our studies of the series $[\text{MCl}_6]^{2-}$, (M = Sn, Pb, Pt), for which there are no electronic complications. No Raman work has been reported previously for these compounds because their intense colours preclude excitation of the spectra with the usual mercury arc. Using a He/Ne laser, spectra have been obtained of the yellow chlorides and orange bromides, but results could not be obtained from the black iodides. The frequencies observed are shown in tables [3.8] and [3.9] for the chlorides and bromides plus iodides respectively; assignments are also included.

The Raman spectra of the free acids H_2TeX_6 (X = Cl, Br) in solution, show the three lines expected for regular octahedral ions. In both cases the highest frequency line is polarised and is therefore ν_1 (A_{1g}). The Raman spectra of the solid salts show three similar bands; there is no sign

of any splitting, consistent with undistorted $[\text{TeX}_6]^{2-}$ octahedra. Half-bandwidths, $\Delta\nu_{1/2}$, are comparable with those found for hexahalogenoplatinates and plumbates under similar instrumental conditions. With the larger organic cations less complete spectra were obtained due to increased difficulty in exciting the spectra.

The far-infrared spectra are more complex than the Raman spectra, but the most striking feature is the extraordinary breadth of ν_3 (F_{1u}). For the hexachlorotellurates $\Delta\nu_{1/2}$ can be as great as 180 cm^{-1} . It is unlikely that this breadth can be accounted for solely by "crystal effects" as was suggested by Greenwood and Straughan²⁸. In order to understand the effect better the behaviour of ν_3 and ν_4 in $[\text{MCl}_6]^{2-}$ ($M = \text{Pt}, \text{Sn}, \text{Pb}$) has been studied previously. It was found that ν_3 is always broader than ν_4 , except for ammonium salts in which ν_4 is broadened unusually, reaching $\Delta\nu_{1/2}$ values of $40\text{-}80 \text{ cm}^{-1}$. The largest value of ν_3 found was for $\text{K}_2[\text{SnCl}_6]$ ($\Delta\nu_{1/2}$ ca. 100 cm^{-1}), but values of $40\text{-}80 \text{ cm}^{-1}$ were most common. Tetraalkylammonium cations, particularly NEt_4^+ , tend to produce resolvable or near resolvable splitting in ν_3 .

The same pattern of behaviour is found for $[\text{TeCl}_6]^{2-}$ salts, but ν_3 is broader than in the $[\text{MCl}_6]^{2-}$ salts. It is also more intense relative to ν_4 , which shows no abnormal

broadening. Thus potassium, ammonium and pyridinium $[\text{TeCl}_6]^{2-}$ salts have $\Delta\nu_{1/2}$ ca. 180 cm^{-1} ; the other cations yield $\Delta\nu_{1/2}$ ca. 80 cm^{-1} , and there is generally some asymmetry, which is first resolvable for $(\text{NMe}_4)_2 [\text{TeCl}_6]$.

$(\text{Ph}_2\text{I})_2 [\text{TeCl}_6]$ shows complex splitting of ν_3 which can be interpreted as for the platinum analogue. Thus $288(\text{m-s}) \text{ cm}^{-1}$ corresponds to the Raman value for ν_1 , $258(\text{m-s}) \text{ cm}^{-1}$ is close to ν_2 (the exact value is difficult to determine as this peak overlies absorption close to the cation), and ν_3 is split into a triplet. Very similar results are obtained with tetraphenylarsonium as cation. Both these hexachlorotellurates have spectra consistent with C_{3v} site-symmetry for the complex ion.

The bromides and iodides show ν_3 bands which are broad compared with the other $[\text{MX}_6]^{2-}$ anions, but much narrower than for $[\text{TeCl}_6]^{2-}$. Among the bromides only the pyridinium salt showed any splitting. $(\text{Et}_4\text{N})_2 [\text{TeI}_6]$ has ν_3 clearly split and for $(\text{Py H})_2 [\text{TeI}_6]$ it is asymmetric on the high frequency side, but it was not resolvable as reported by Greenwood and Straughan²⁸. There are other discrepancies between this work and theirs; ν_3 found 12 cm^{-1} higher for $(\text{NMe}_4)_2 [\text{TeCl}_6]$; and an additional band was observed at $79 \text{ cm}^{-1} (\text{s})$.

The splittings found in ν_3 are not different in kind from those shown by other anions $[\text{MX}_6]^{2-}$ where the cation is varied and it is concluded that, for $[\text{TeX}_6]^{2-}$, the lone pair is not primarily responsible for the splitting. Consistent with this conclusion no splitting was observed in the Raman lines.

The decrease in $\Delta\nu_{1/2}$ for ν_3 in $[\text{TeX}_6]^{2-}$ as chloride is replaced by bromide and then iodide seems to be a general feature of metal-halogen vibrations. It is equally clear in series such as $[\text{PtX}_6]^{2-}$, (X = F, Cl, Br, I), and suggests a correlation between $\Delta\nu_{1/2}$ and degree of covalency or polarity of the bonds. It is likely, however, that the exceptional widths of ν_3 for $[\text{TeX}_6]^{2-}$ is related to the partial distribution of the lone pair. The presence of a stereochemically active lone pair has no broadening effect; bandwidths are normal for TeX_4 , (X = Cl, Br, I)⁵⁴⁻⁵⁷. Urch⁵⁸ suggests that the lone pair in $[\text{TeX}_6]^{2-}$ may be in an A_1g antibonding molecular orbital and as such will effectively reduce the electronegativity of tellurium. Compatible with this, ν_3 for $[\text{TeCl}_6]^{2-}$ is very low compared with $[\text{SnCl}_6]^{2-}$ and the bond stretching force constants for the potassium salts are 0.92 and 1.07 millidynes/Å respectively. Only ν_3 shows this abnormal broadening and it is the only antisymmetric mode of vibration, one which requires the

metal atom to move. The initially A_{1g}^x orbital containing the lone pair will then no longer be of g -symmetry and will be able to mix in with other bonding orbitals thereby achieving some transient directional effect and providing a mechanism for the broadening.

Below 150 cm^{-1} the infrared spectra are complicated. In contrast to other ions of the $[MX_6]^{2-}$ type, ν_4 is not as readily identified for $[\text{TeX}_6]^{2-}$. For the chlorides, absorption is found below 100 cm^{-1} but there are no strong, sharp bands ca. 140 cm^{-1} where ν_4 would be expected (cf. ν_5), except for the Ph_4As^+ salt. It is concluded that ν_4 is abnormally weak in this series.

ν_4 and the cation lattice mode, ν_L , are of the same symmetry species and will interact. If they are quite widely separated in frequency it is reasonable to make assignments to them, as in series $[\text{MCl}_6]^{2-}$, ($\text{M} = \text{Sn}, \text{Pb}, \text{Pt}$). For bromo and iodotellurates it is doubtful if such assignments would be meaningful and therefore they have not been definitely made here.

The results of some force constant calculations, using the MUBFF are shown in tables [3.10] and [3.11] where various values of ν_4 and ν_5 have been assumed. The general trend of values is consistent with those for other series.

$[\text{TeCl}_6]^{2-}$ and $[\text{TeBr}_6]^{2-}$ have closely similar values of K , in contrast to other ions $[\text{MX}_6]^{2-}$, ($X = \text{Cl}, \text{Br}$; $M = \text{Pt}, \text{Sn}$)⁵⁴, for which the ratio $K(\text{M-Br})/K(\text{M-Cl})$ is usually 0.79-0.85. Thus this ratio for the halotellurates varies between 0.87 and 0.94. This can also be understood in terms of Urch's description⁵⁸ of the bonding in ions such as $[\text{TeX}_6]^{2-}$ and would seem to be good evidence in its favour.

The compound analysing as $\text{H}_2\text{TeBr}_6 \cdot 2\text{H}_2\text{O}$ was prepared according to Ripon⁵⁹. The chloro analogue could not be made in a pure state. It was thought that the structure of this might be $(\text{H}_3\text{O})_2[\text{TeBr}_6]$. The H_3O^+ ion could be present in such a compound in one of three ways. If hydrogen bonding was significant then the H_3O^+ would be rigidly held in the lattice and the spectra of $[\text{H}_3\text{O}]_2[\text{TeBr}_6]$ might be interpreted as similar to $(\text{Ph}_2\text{I})_2\text{TeBr}_6$. On the other hand, if hydrogen bonding was absent then free rotation of H_3O^+ would be expected; depending on the nature of rotation the H_3O^+ ion would appear to have either spherical or conical symmetry. A structure including a conical cation would again be analogous to $(\text{Ph}_2\text{I})_2[\text{TeBr}_6]$ but one with a spherical cation would be expected to adopt to $\text{K}_2[\text{PtCl}_6]$ structure (as does $(\text{NH}_4)_2[\text{TeBr}_6]$).

The X-ray powder photograph was taken of the compound and was found not to be isostructural with $\text{K}_2[\text{PtCl}_6]$; on

the other hand the photograph was not as complicated as would have been expected if it had been isostructural with $(\text{Ph}_2\text{I})_2 [\text{PtCl}_6]$.

The infrared spectrum was measured to 200 cm^{-1} and the sample gave a good Raman spectrum. The observed frequencies are shown in table [3.12]. The band at 190 cm^{-1} in the infrared may or may not be a true band since the performance of the PE-225 below 200 cm^{-1} is doubtful; also in the Raman spectrum the bands observed at 185 and 137 cm^{-1} are both in well known spurious positions for the LR-1. The interpretation of the spectra will be discussed with both possibilities in mind.

Neglecting the bands at 190 , 185 and 137 cm^{-1} first, then the best interpretation of the spectra is on an octahedral basis with the H_2O^+ ion causing a lowering of symmetry to C_{3v} . In the solid salts of $[\text{TeBr}_6]^{2-}$ ν_1 , ν_2 and ν_3 were around 175 , 150 and 190 cm^{-1} respectively; ν_3 is considerably higher than ν_1 whereas in all other cases of $[\text{MX}_6]^{2-}$ $\nu_1 > \nu_3$. If $[\text{TeBr}_6]^{2-}$ is present then it is necessary to postulate a rise in frequency of the stretches of about 50 cm^{-1} compared to the other solid salts. Thus in the Raman spectrum the bands at 226 and 210 cm^{-1} are assigned to ν_1 and ν_2 respectively. The band at 122 cm^{-1} is attributed to ν_3 and that at 85 cm^{-1} to a lattice mode.

The strong broad (but not split) band in the infrared at 238 cm^{-1} is assigned to ν_3 while the strong absorptions at 222 cm^{-1} with a shoulder at 210 cm^{-1} are assigned to ν_1 and ν_2 respectively.

If $\text{H}_2\text{TeBr}_6 \cdot 2\text{H}_2\text{O}$ does not contain discrete $[\text{TeBr}_6]^{2-}$ anions then the lattice is likely to contain either $[\text{TeBr}_3]^+$ or TeBr_4 . For these species to be present it would be necessary to postulate structures $[\text{TeBr}_3^+][\text{H}_3\text{O}^+]_2[\text{Br}^-]_3$ and $[\text{TeBr}_4][\text{H}_3\text{O}^+]_2[\text{Br}^-]_2$ respectively. The former lattice would contain pyramidal TeBr_3^+ (C_{3v}) ions while the structure of TeBr_4 in the lattice would be expected to be similar to that of SF_4 (C_{2v}). The correlation between C_{3v} and C_{2v} for the above species is given below.

	ν_1	ν_2	ν_3	ν_4
T (MX_4)	A_1	E	F_2	F_2
C_{3v} (MX_3)	A_1	A_1	E	E
C_{2v} (MX_4)	A_1	$A_1 + A_2$	$A_1 + B_1 + B_2$	$A_1 + B_1 + B_2$

Another possible structure that would require $[\text{TeBr}_3]^+$ would be $[\text{TeBr}_3]^+[\text{HBr}_2]^-[\text{Br}]^-[\text{H}_3\text{O}]^+ \cdot \text{H}_2\text{O}$, but this was rejected because no absorption between 1550 and 700 cm^{-1} was observed, which is where $[\text{HBr}_2]^-$ might normally be expected to absorb.

Taking the C_{3v} postulate first, reasonable agreement can be obtained by comparing the data here with that of Adams and Lock⁵⁴ who postulate a $TeBr_3^+Br^-$ structure for solid $TeBr_4$. Thus in the infrared the assignments are 238(A) and 222(E) both ν (Te-Br) while the medium band near 190 cm^{-1} is associated with the bromide ion⁵⁴. In the Raman shifts are assigned thus :- 226(A) and 210(E) both ν (Te-Br) and 122 cm^{-1} (A) and 85(E) δ (Te-Br). This assignment assumes thus that the two Raman bands at 185 and 137 cm^{-1} are spurious but gives an explanation for the infrared band near 190 cm^{-1} .

An explanation of the spectra on the basis of the presence of $TeBr_4$ would require the three bands in doubt to be real. Four stretching vibrations are required in both the Raman and infrared spectra. Four bands (viz. 238, 222, 210, 190 cm^{-1}) can be found in the infrared but only three are observed in the Raman. Five bending modes are expected also in the Raman whereas only three were observed. On balance the presence of $TeBr_3^+$ species being present in the compound $H_2TeBr_6 \cdot 2H_2O$ is postulated by the author. Low frequency infrared data or X-ray evidence is really necessary to decide which of the possibilities is correct.

3.6 1st row transition hexachlorometallates and related systems.

1st row transition hexachlorometallates have only recently been prepared; Piper *et al.*⁶⁰ have characterised the species $[\text{Co}^{\text{III}}(\text{pn})_3][\text{M}^{\text{III}}\text{Cl}_6]$, ($\text{M} = \text{Cr}, \text{Mn}, \text{Fe}$; $\text{pn} = 1,2\text{-propanediamine}$). $[\text{M}^{\text{II}}\text{Cl}_6]^{4-}$ ($\text{M} = \text{Mn}, \text{Fe}$) ions have been postulated in the ores chloromanganokalite⁶¹ (K_4MnCl_6) and rinneite⁶² ($\text{K}_3\text{NaFeCl}_6$) respectively, but not properly confirmed. Besides the above compounds, Piper also made $[\text{Co}(\text{NH}_3)_6][\text{FeCl}_6]$, and $[\text{Co}(\text{pn})_3][\text{InCl}_6]$.

The spectra of these $[\text{MCl}_6]^{3-}$ species were taken in the infrared; to help assignments the cation spectra were also observed in $[\text{Co}(\text{NH}_3)_6]\text{Cl}_3$ and $[\text{Co}(\text{pn})_3]\text{Cl}_3$. The related system of compounds $\text{K}_2[\text{MnCl}_6]$, $\text{K}_3[\text{IrCl}_6]$, $(\text{NEt}_4)_3[\text{IrCl}_6]$ and $[\text{Co}(\text{NH}_3)_6][\text{IrCl}_6]$ were also prepared and their spectra taken. Assignments of anion bands are given in table [3.13].

$[\text{Co}(\text{pn})_3]\text{Cl}_3$ has infrared absorption at 376sh, 366s, 335s, 277br, 226br,w and 105vs. This last band at 105 cm^{-1} is almost certainly a lattice mode of the chloride ion since this band disappears in the other complexes studied. In all cases the cation and anion spectra overlap to some extent but the cation absorption in the complexes is close to that in free $[\text{Co}(\text{pn})_3]\text{Cl}_3$.

$K_2[MnCl_6]$ has the $K_2[PtCl_6]$ structure⁶³; the assignments of ν_3 at 358 cm^{-1} and ν_4 at 200 cm^{-1} are obvious. The band observed at 102 cm^{-1} is almost certainly K^+ lattice mode. $K_2[MnCl_6]$ can only have the electronic structure t_{2g}^3 . The compounds $[Co(pn)_3][MCl_6]$, ($M = Cr, Mn, Fe, In$) have been shown to be isostructural but the exact structures not found. The transition metal anion complexes have also all been shown to be high spin; thus the electronic configurations of $[MCl_6]^{3-}$ are t_{2g}^3 ($M = Cr$), $t_{2g}^3 e_g^1$ ($M = Mn$) and $t_{2g}^3 e_g^2$ ($M = Fe$). Values of ν_3 are sensitive to the arrangement of electrons in the d-orbitals and the oxidation state of the metal. The presence of two electrons in the e_g antibonding orbital in the iron complex causes a drastic lowering of $\nu(M-Cl)$ compared with the chromium complex; $\nu(Cr-Cl)$ is observed at 315 cm^{-1} while the iron analogue has $\nu(Fe-Cl)$ 67 cm^{-1} lower. This is directly comparable with the complexes trans- $[M^{III}Cl_2D_2]Cl_2$ ⁶⁴ where D is a chelating diarsine. Where $M = Co$ (electronic configuration t_{2g}^3) $\nu(M-Cl)$ is at 384 cm^{-1} but introduction of an electron into the e_g level ($M = Ni$) causes $\nu(M-Cl)$ to drop to 238 cm^{-1} . $[MnCl_6]^{3-}$ is expected to suffer John-Teller distortion, probably to give four short and two long bonds. In accordance with this, a single $\nu(Mn-Cl)$ band (at 342 cm^{-1})

is found higher than the analogous ν (Cr-Cl band and comparable with ν_3 in $K_2[MnCl_6]$ (not expected to suffer distortion) allowing for the different cation. ν_3 in $K_2[MnCl_6]$ would be expected to be higher than ' ν_3 ' in $[MnCl_6]^{3-}$ because of the increased oxidation state of the manganese. The single band ν (Mn-Cl) in $[MnCl_6]^{3-}$ is therefore probably more correctly assigned to the E_u stretching mode of the D_{4h} $[MnCl_4]$ group; if the long bonds are lengthened to the extent found for (say) CrF_2 , one would expect this to give rise to a discrete (lower) stretching frequency. Thus the assignment of the band at 184 cm^{-1} as ν_4 is in some doubt. This almost certainly however, is a bending mode whether it be associated with the $[MnCl_4]$ group or $[MnCl_6]^{3-}$ octahedron. It is possible that a stretch of the long Mn-Cl bond is overlaid by a cation band. ν (In-Cl) is as low as that of ν (Fe-Cl); this can be rationalised by taking into account (a) the increase in mass and (b) the absence of any ligand field stabilization energy for indium.

The spectra of $[Co(NH_3)_6][MCl_6]$, ($M = Fe, Ir$), were similar to those of the above series. The probably structure of these complexes, considering the comparable size of the ions, is that of NaCl or CsCl. It seems likely that for the iridium complex ν_4 for the cation (δ (Co-N)) is at 320 cm^{-1}

and ν_3 for the anion is at 302 cm^{-1} ; both bands are sharp and no splittings are observed. In contrast both these bands (and ν_4 for the anion) are split for the iron complex, suggesting a lower site symmetry. Thus ν_3 for the cation while centred at 290 cm^{-1} is composed of a main strong band at 248 cm^{-1} with shoulders either side at 272 and 227 cm^{-1} . Similarly ν_4 consists of a strong band at 181 cm^{-1} with a shoulder at 160 cm^{-1} . The comparison of $\nu(\text{Ir-Cl})$ and $\nu(\text{Fe-Cl})$ in these complexes shows dramatically the effect of the presence of electrons in the eg level in the Fe complex; $[\text{IrCl}_6]^{3-}$ is a high field, low spin complex with configuration t_{2g}^6 . A Raman signal was obtained also from the iron complex; a strong band at 283 cm^{-1} is attributed to ν_1 for the anion while a weaker feature at 313 cm^{-1} is left unassigned. Both spectra show well developed sharp bands at lower frequencies, but these are unlikely to be due to the inactive ν_6 . They are possibly associated with the reststrahlen frequencies of the complex ions; consistent with this these bands are lower in the iridium complex which has a higher formula weight for the anion than the iron complex.

The sharp bands associated with $[\text{Co}(\text{NH}_3)_6][\text{IrCl}_6]$ are in sharp contrast to those of $\text{K}_3[\text{IrCl}_6]$. $\text{K}_2[\text{IrCl}_6]$ is reported to have both ν_3 and ν_4 sharp but the analogous

bands in K_3IrCl_6 are described as broad unsymmetrical features¹². Under higher resolution ν_3 and ν_4 in this latter complex is now seen to be composed of several components; a more extreme form of this is shown by $(Et_4N)_3[IrCl_6]$ in which ν_3 and ν_4 are both split and complex absorption is found below 100 cm^{-1} , probably due to ν_6 and ν_L . Thus in the ν_3 region there is a strong band at 305 cm^{-1} with a shoulder at 317 cm^{-1} and a separate component at 336 cm^{-1} . In the bending region a doublet is observed at 171 and 188 cm^{-1} (strong) and another band is situated at 221 cm^{-1} . A crystal structure determination of K_3IrCl_6 would be interesting to find out what is the actual site symmetry of the $[IrCl_6]$ group. The structures are, probably, related to the crystal structure which in certain modifications can obviously have a low enough site symmetry⁴⁷ to explain the infrared splittings observed.

3.7 Hexachlorocerates.

$(\text{Me}_4\text{N})_2 [\text{CeCl}_6]$ is reported to have the K_2PtCl_6 structure⁶⁵ while a recent crystal structure determination of $\text{Cs}_2 [\text{CeCl}_6]$ ⁶⁶ has shown to crystallise in the $\text{K}_2 [\text{GeF}_6]$ structure. The preparation of caesium complex has not been published yet but the methylanamonium salt is quite easily prepared.⁶⁵ The tetraethylammonium and diphenyliodonium salts of $[\text{CeCl}_6]^{2-}$ have been prepared by analogous methods; it is likely that the Et_4N^+ salt will be isostructural with the Me_4N^+ salt while the Ph_2I^+ salt will probably suffer some distortion. No vibrational spectra of $[\text{CeCl}_6]^{2-}$ or any other lanthanide analogue has been previously reported.

$(\text{Et}_4\text{N})_2 [\text{CeCl}_6]$, although yellow, did not yield a Raman spectra but ν_3 and ν_4 were both strong in the infrared with ν_3 at 268 cm^{-1} and ν_4 at 117 cm^{-1} . $(\text{Ph}_2\text{I})_2 [\text{CeCl}_6]$ gave only a poor Raman spectrum but ν_1 , ν_2 and ν_5 were found; ν_1 and ν_2 were at 295 and 265 cm^{-1} respectively while ν_5 (very weak) appeared at 120 cm^{-1} . The infrared spectrum was consistent with a lowering of site-symmetry of the $[\text{CeCl}_6]^{2-}$, probably to C_{3v} . Four bands were observed between 300 and 255 cm^{-1} . Two strong features at 277 and 265 cm^{-1} both had clear shoulders on them; the band at

277 cm^{-1} had a shoulder at 294 cm^{-1} while the 265 cm^{-1} had one at 258 cm^{-1} . This lowest band (258 cm^{-1}) can be attributed to cation absorption. The most convincing assignment of the bands at 277 and 265 cm^{-1} is that they represent ν_3 , split by the low site symmetry. An alternative assignment would be to equate the 277 cm^{-1} band with ν_3 and the 265 cm^{-1} with ν_2 ; either assignment implies a lowering of site-symmetry from that of $\text{K}_2[\text{PtCl}_6]$. The absorption at 294 cm^{-1} is obviously the Raman active frequency ν_1 . ν_4 was also clearly split with a strong band at 114 cm^{-1} and a shoulder at 120 cm^{-1} . One strange feature of the spectrum was a medium-strong band at 217 cm^{-1} ; this is unlikely to be an impurity band since the compound had satisfactory analysis figures. Using values of ν_1 to ν_5 of 294, 265, 267, 117 and 120 cm^{-1} respectively the MUBFF force constants were calculated. They were (in millidynes/ \AA) K, 1.14; F, 0.11; H, 0.02; A, 0.26; B, 0.01.

3.8 General Conclusions

For the octahedral hexahalometallates studied correlations between M-Cl bond stretching force constants and cation size, and between lattice modes and cation mass have been investigated. Correlations between these parameters have definitely been established.

The complexes $(\text{Ph}_2\text{I})_2[\text{MCl}_6]$, ($\text{M} = \text{Pt}, \text{Sn}, \text{Pb}, \text{Te}, \text{Ce}$) have vibrational spectra consistent with C_{3v} site symmetry of the anion. This is probably caused by the unsymmetrical cation Ph_2I . No splittings, however, were observed for the complex $(\text{Ph}_2\text{I})_2[\text{PtBr}_6]$.

For the first time Raman data on $[\text{TeX}_6]^{2-}$, ($\text{X} = \text{Cl}, \text{Br}$) and $[\text{CeCl}_6]^{3-}$ have been reported. The spectra of the tellurium compounds show that the lone pair on tellurium does not occupy a stereochemical position. The first infrared data on $[\text{CeCl}_6]^{3-}$ and $[\text{MCl}_6]^{3-}$, ($\text{M} = \text{Cr}, \text{Mn}, \text{Fe}$) has also been reported. The spectra of the first row transition hexachlorometallates are rationalised in terms of the Jahn-Teller effect and the electronic structure of the transition metal.

For solid $\text{K}_2[\text{PtCl}_6]$ the anomalous intensities of ν_1 and ν_2 observed in solution spectra were not found. The proximity of the bands however was confirmed. The suggestion by Woodward and Creighton³⁵ that the low δ -value

$(\delta = (\nu_1 - \nu_2) / \nu_1)$ is due in some way to the presence of six non bonding electrons on Pt is probably wrong. For $[\text{SeCl}_6]^{2-}$ $\delta = 0.21$,⁶⁷ but for $[\text{TeCl}_6]^{2-}$ (and $[\text{TeBr}_6]^{2-}$) δ has been found to be 0.08. Woodward and Creighton have correlated δ -values of around 0.25 with ions that do not have lone pairs, and values of less than 0.1 with those of species with lone pairs. Since $[\text{SeCl}_6]^{2-}$ and $[\text{TeBr}_6]^{2-}$ have the same electron configuration they would, on Woodward's theory, be expected to have the same δ -value. The same kind of discrepancy occurs with $[\text{TlCl}_6]^{3-}$. ($\delta = .06$)⁸¹ and $[\text{InCl}_6]^{3-}$, ($\delta = .36$)³⁷.

The stretching force constant for $[\text{MCl}_6]^{2-}$ decreases in the order $\text{Pt} > \text{Ce} > \text{Sn} > \text{Te} > \text{Pb}$. This order probably reflects to some extent the order also of bond strengths of the metal-chlorine bonds.

3.9 Experimental

$K_2 [PtCl_6]$ and $K_2 [PtBr_6]$ were obtained from Johnson Matthey and Co. Limited and used without further purification. $M_2 [PtCl_6]$ ($M = Rb, Co, NH_4, NMe_4, NEt_4, NBu_4, AsPh_4, IPh_2$) were prepared by mixing warm aqueous solutions of MCl and $K_2 [PtCl_6]$, cooling before filtering the precipitate and recrystallising from dilute HCl . $(Ph_2I)_2 [PtBr_6]$ was made in analogous manner. For $M = Tl$ and Ag the complexes were made by mixing $M[NO_3]$ and $K_2 [PtCl_6]$.

$K_2 [PtBr_2Cl_4]$ was prepared by adding the calculated amount of bromine to alcoholic $K_2 [PtCl_4]$, refrigerating overnight, and collecting the product.

$M_2 [SnCl_6]$, ($M = K, NH_4, Rb, Cs, NMe_4, NEt_4, NBu_4, AsPh_4, IPh_2$), were made by mixing solutions of MCl in 1:1 HCl and $H_2 SnCl_6$. The Pb analogues were made in a similar manner; $H_2 PbCl_6$ was made first by dissolving PbO_2 in 11N HCl at $0^\circ C$ and filtering the excess PbO_2 . $K_2 PbCl_6$ could not be made by this method.

$H_2 [TeCl_6]$ and $H_2 [TeBr_6]$ were prepared in solution by dissolving TeO_2 in the relevant concentrated acid. The salts $M_2 [TeX_6]$ ($X = Cl, Br, I$; $M = Cs, NMe_4, NEt_4, PyH, AsPh_4, IPh_2$) were made by adding aqueous solutions of MX to free acid⁶⁸. For $M = K, Rb$ or NH_4 concentration of the resulting

solution was necessary before crystallisation occurred.

$[\text{Co}(\text{pn})_3][\text{MCl}_6]$, ($\text{M} = \text{Cr}, \text{Mn}, \text{Fe}$) and $[\text{Co}(\text{NH}_3)_6][\text{MCl}_6]$, ($\text{M} = \text{Fe}, \text{In}$) were prepared according to the method of Piper⁶⁰. $(\text{NEt}_4)_3[\text{IrCl}_6]$ and $[\text{Co}(\text{NH}_3)_6][\text{IrCl}_6]$ were prepared by mixing $(\text{NEt}_4)\text{Cl}$ and $[\text{Co}(\text{NH}_3)_6]\text{Cl}_3$ respectively in water to an aqueous solution of $\text{K}_3[\text{IrCl}_6]$.

$(\text{NEt}_4)_2[\text{CeCl}_6]$ and $(\text{Ph}_2\text{I})_2[\text{CeCl}_6]$ were made in a similar fashion to the published method for the preparation of $(\text{NMe}_4)_2[\text{CeCl}_6]$.⁶⁵

Representative analyses :-

$\text{Cs}_2[\text{PtCl}_6]$, calculated, Cl 31.6%; found, Cl 31.5%

$(\text{Ph}_2\text{I})_2[\text{PtCl}_6]$, calculated, C 35.5%, H 25%, Cl, 26.2%
found, C 35.7%, H 3.1%, Cl, 26.2%

$(\text{NEt}_4)_2[\text{PtCl}_6]$, calculated, C 28.8%, H 6%, Cl 31.9%;
found, C 29.0%, H 6%, Cl 31.7%.

$(\text{Ph}_2\text{I})_2[\text{PtBr}_6]$, calculated, C 23.5%, H 1.9%, Br 39%;
found, C 23.49%, H 1.89%, Br = 38.6%,

$\text{K}_2[\text{PtCl}_4\text{Br}_2]$, calculated, Br 27.8%, Cl 24.6%;
found, Br 27.6%, Cl 24.3%.

$\text{Rb}_2[\text{SnCl}_6]$ calculated, Cl 42.4%; found, Cl 42.2%

$(\text{Ph}_4\text{As})_2[\text{SnCl}_6]$ expected, C 52.6%, H 3.7%, Cl 19.4%,
found, C 52.6%, H 3.4%, Cl 19.7%.

$(\text{NEt}_4)_2[\text{SnCl}_6]$, calculated, C 32.1%, H 6.7%, Cl 36%,
found, C 32.1%, H 7.1%, Cl 35.7%.

$\text{Cs}_2 [\text{TeCl}_6]$, expected, Cl 35.1%; found, Cl 35.1%
 $(\text{Ph}_2\text{I})_2 [\text{TeCl}_6]$, expected, C 38.7%, H 2.7%, Cl 28.6%;
 found, C 38.9%, H 2.7%, Cl 28.9%.
 $(\text{NEt}_4)_2 [\text{TeCl}_6]$, expected, C 31.9%, H 6.7%, Cl 35.4%;
 found, C 32.2%, H 6.1%, Cl 35.5%.
 $\text{Rb}_2 [\text{TeBr}_6]$, calculated, Br 61.5%; found Br 61.8%.
 $(\text{NMe}_4)_2 [\text{TeBr}_6]$, calc. C 12.7%, H 3.2%, Br 63.2%;
 found, C 12.9%, H 3.5%, Br 63%.
 $[\text{Co}(\text{NH}_3)_6][\text{FeCl}_6]$, calc. N 20.1%, Cl 50.9%;
 found, N 19.5%, Cl 49.6%.
 $(\text{Ph}_2\text{I})_2 [\text{CeCl}_6]$, calc. C 31.5%, H 2.6%, Cl 23.5%;
 found, C 31.49%, H = 2.4%, Cl = 23.7%.

Spectra were recorded on the following instruments:-

- (a) Perkin-Elmer PE-225, (b) R.I.I.C. FS-520,
 (c) FTC-100/FS-620, (d) Perkin-Elmer LR-I.

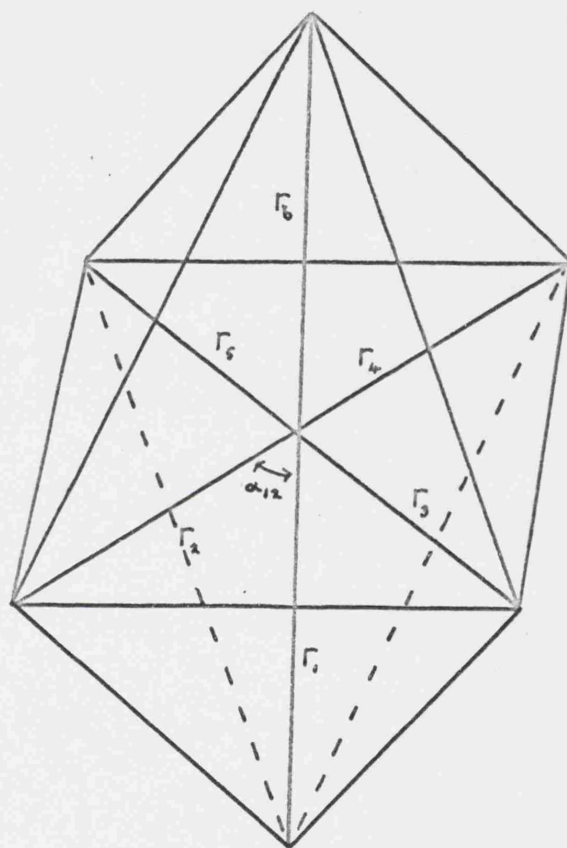
Where applicable, transforms were computed to a resolution of 5 cm^{-1} .

Normal co-ordinate analyses were calculated on an Elliott 803 computer, using a programme written by Mr. R. G. Churchill.

X-ray powder photographs were taken with a Deyhe camera using K radiation. Dr. D. R. Russell helped in interpreting some of the powder photographs.

FIGURE 3.1

Internal coordinates for an octahedral MX_6 molecule



α_{ij} defined as angle between
internal coordinates r_i and r_j

FIGURE 3.2

Normal modes of an octahedral MX_6 molecule

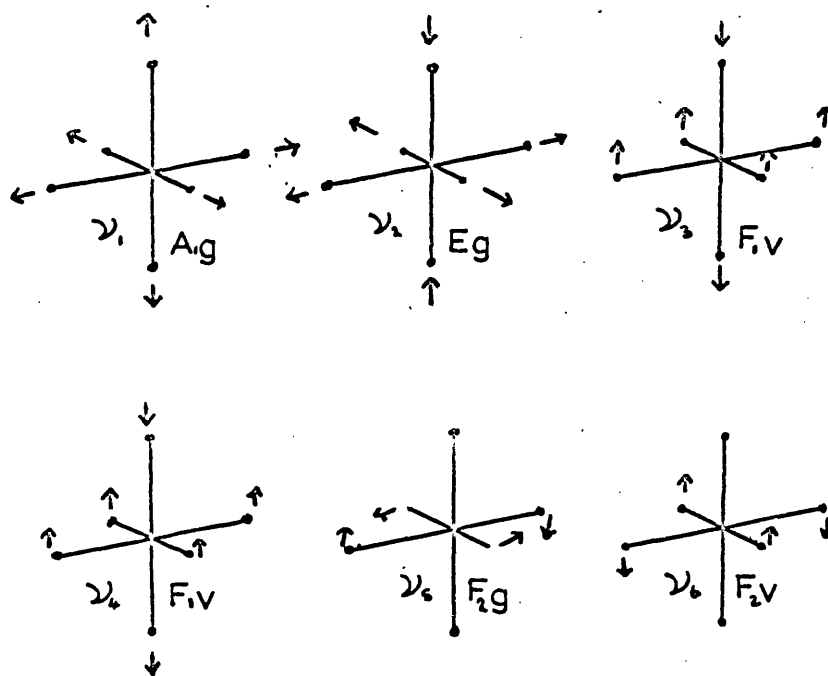


FIGURE 3.3

Raman spectrum of solid potassium hexachloroplatinate.

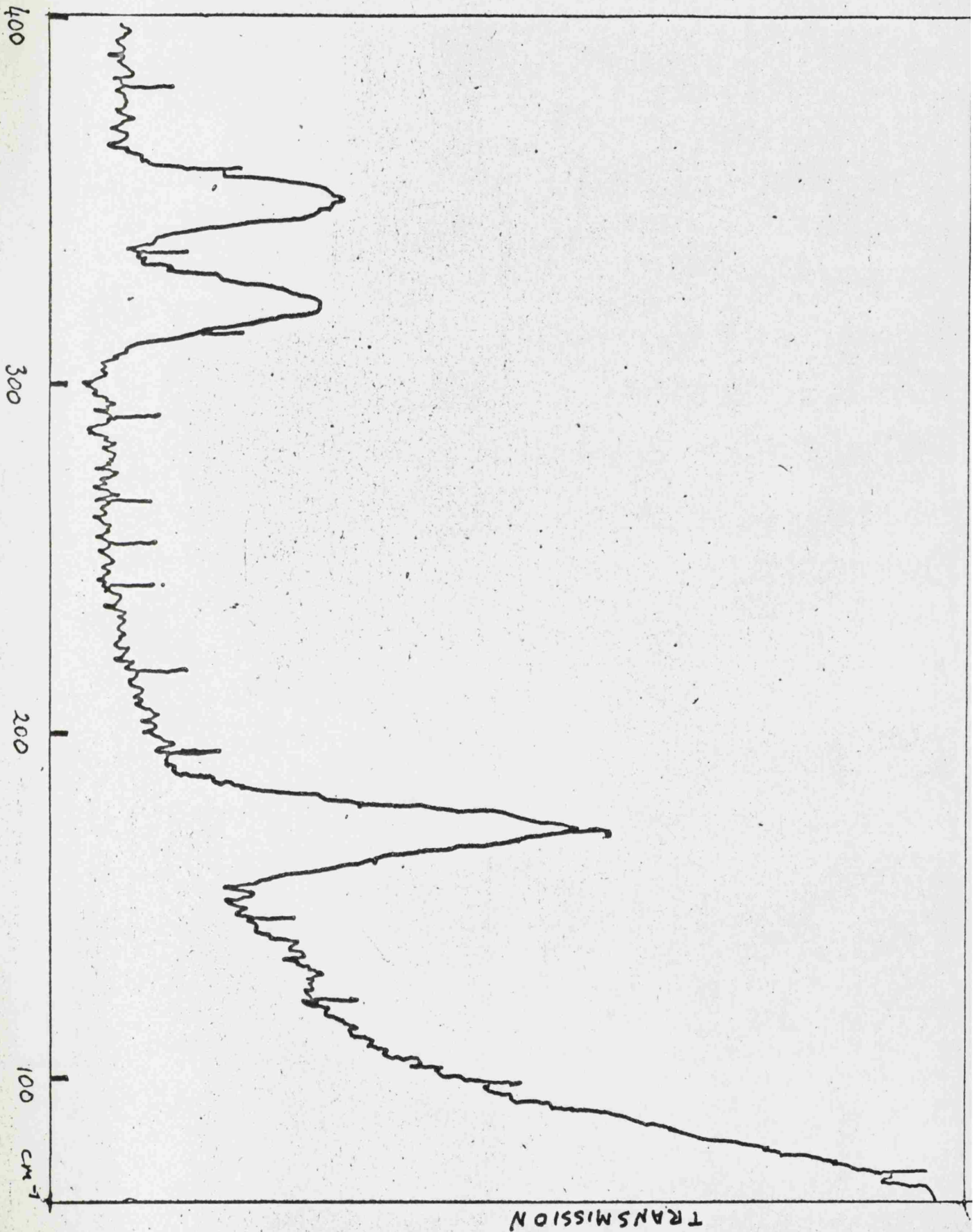
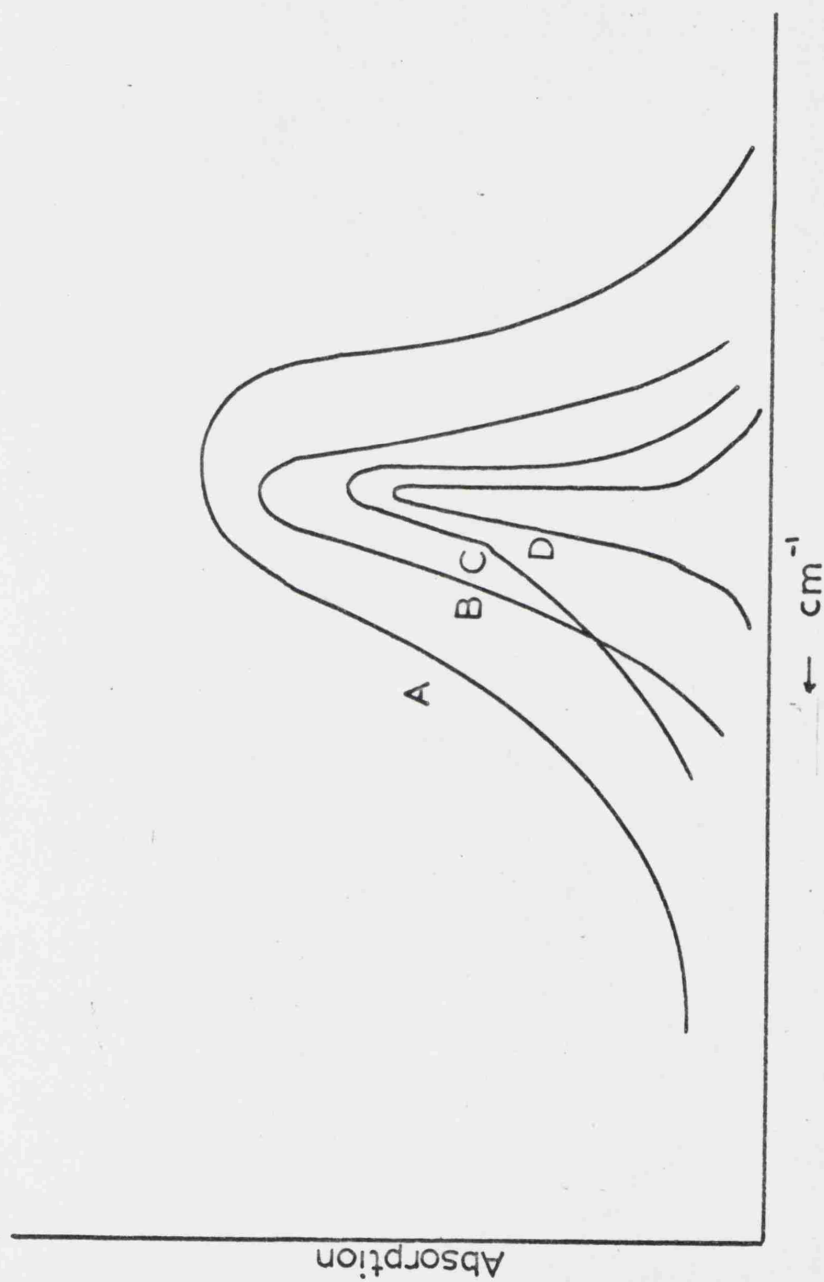


FIGURE 3.4

The four types of band-shape of ν_3 encountered with solid hexachloroplatinates.



- A = NEt_4
- B = $\text{K, Ag, NMe}_4, \text{NBu}_4, \text{AsPh}_4$
- C = NH, Rb, Cs
- D = TL

FIGURE 3.5

Dependence of cation lattice-mode frequency upon cation mass of some hexachloroplatinates.

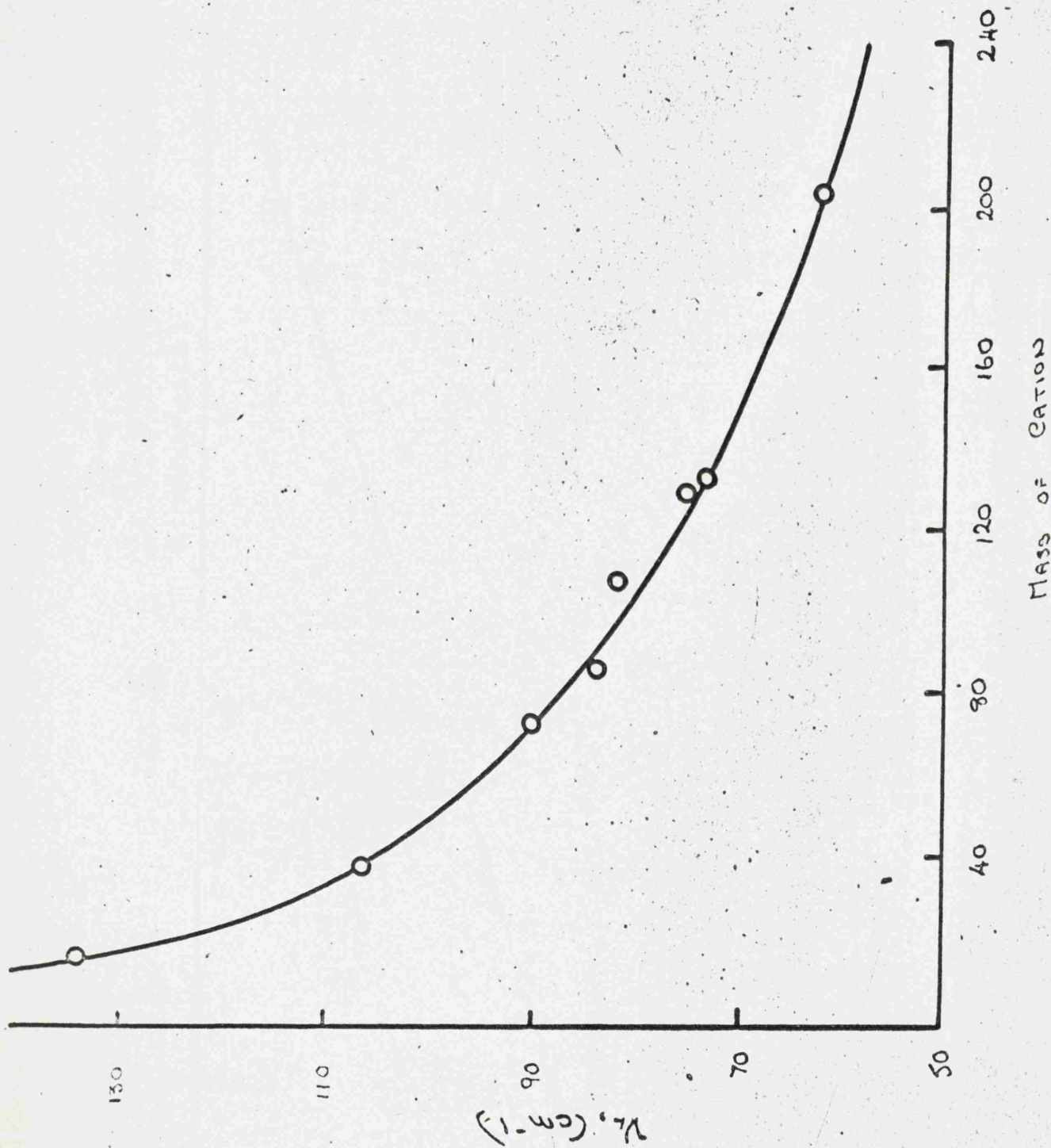


FIGURE 3.6

Plot of bond-stretching force constant, (K), versus cationic radius, r^+ , for some hexachloroplatinates.

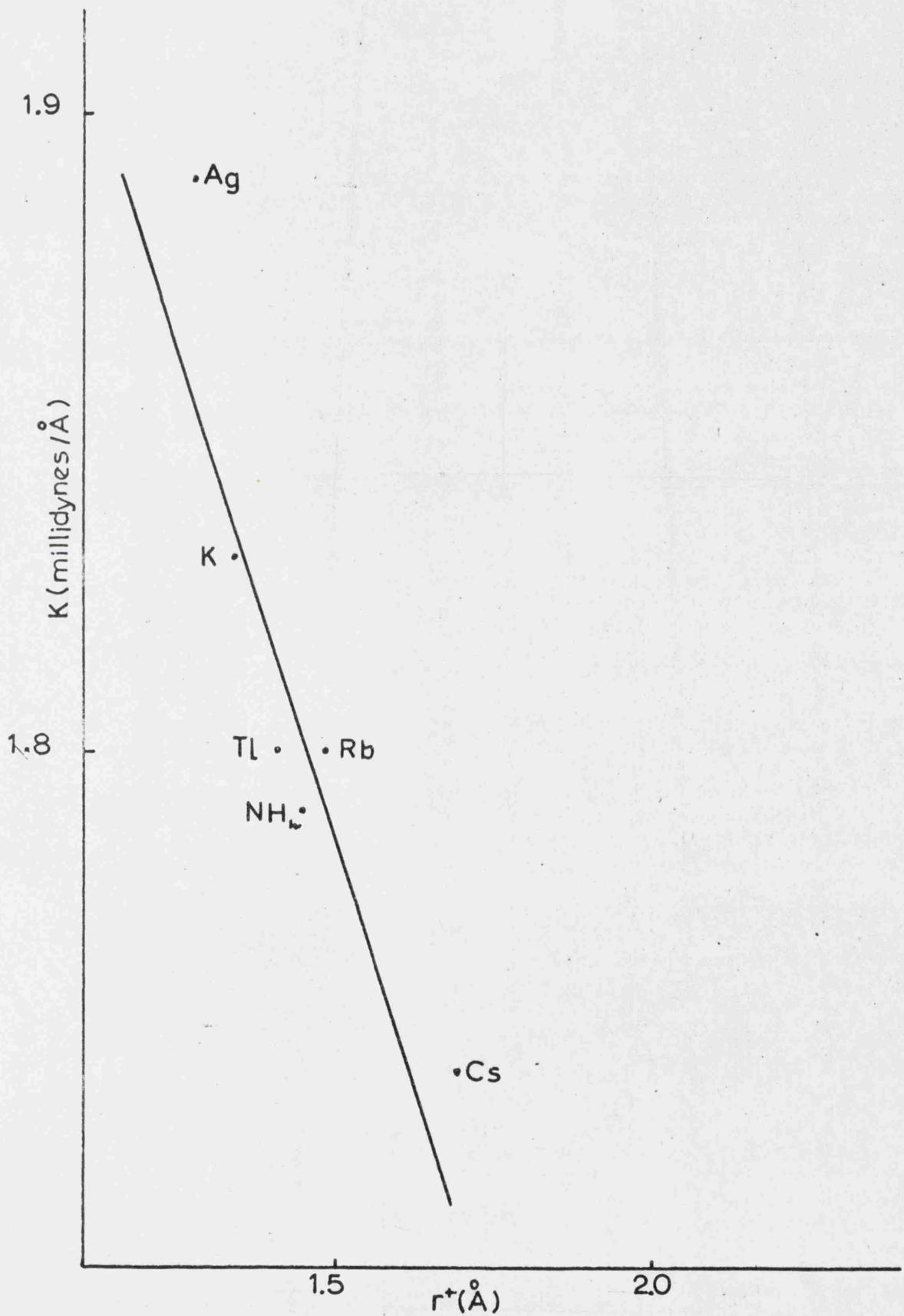


Table 3.1

Frequencies (cm^{-1}) of $M_2^I[\text{PtCl}_6]$ and $M_2^I[\text{PtBr}_6]$
in the solid state.

$[\text{PtCl}_6]^{2-}$	ν_1	ν_2	ν_3	ν_4	ν_5	$[\nu_6]^\dagger$	$\nu_L(\text{IR})$
K	350	320	341	186	171	82	106(vs,br)
Rb	342	316	337	185	173	87	84(vs)
Cs	337	312	332	186	172	83	73(vs)
Tl	353	319	339	182	167	79	62(vs)
Ag	340	328	337	215	186	53	82
NH_4	345	316	338	193	177	84	134(vs) 97
NMe_4	339	315	326	182	166	77	90(vs)
NEt_4	340	315	325	181	160	65	75(s,br)
n-NBu_4	335	315	325	181	177	99	-
AsPh_4	337	313	327	187	167	70	-
IPh_2	335 [§]	314	323 306	180 164	180 165	91 [*]	-
Aqueous Solution	344	320	-	-	162	-	
$[\text{PtBr}_6]^{2-}$							
K	217	195	243	78	115	100	
IPh_2	-	-	230		-	-	
Aqueous Solution [†]	207	190	-	-	97	-	

* Calculated values $86(\text{vs})\text{cm}^{-1}$, experimental value.

† Reference 35. § 338 cm^{-1} (w-m) in the infrared.

Table 3.2

Force constants for $M_2^I[\text{PtCl}_6]$ millidynes/Å

	K	F	H	A	B
$M^I=K$	1.83	0.13	0.08	0.22	0.04
Rb	1.80	0.11	0.10	0.215	0.035
Cs	1.75	0.10	0.10	0.215	0.04
Tl	1.80	0.145	0.065	0.225	0.04
Ag	1.89	0.05	0.15	0.32	0.08
NH_4	1.79	0.12	0.10	0.21	0.045
NMe_4	1.74	0.10	0.09	0.26	0.04
NEt_4	1.73	0.105	0.08	0.265	0.045
NBu_4^n	1.745	0.08	0.12	0.27	0.03
AsPh_4	1.73	0.10	0.09	0.25	0.05
IPh_2	1.70	0.09	0.11	0.30	0.035
$\text{K}_2[\text{PtBr}_6]$	1.57	0.12	0.09	0.13	-0.035

Table 3.3

Frequencies (cm^{-1}) and assignment for $\text{K}_2[\text{PtCl}_4\text{Br}_2]$

<u>IR</u>		<u>Raman</u>		
337(vs) } 319(s) }	$\nu(\text{Pt-Cl}) e_u$	337(vs) } 323(s) }	$\nu(\text{Pt-Cl})$	a_{1g} b_{1g}
248(m) } 234(w-m) }	$\nu(\text{Pt-Br}) a_{2u}$ a_{1g}	232(s) 201(w)	$\nu(\text{Pt-Br})$	a_{1g}
(sh)	$\delta(\text{PtCl}_4) e_u$	165(m)	$\delta(\text{Pt-Cl})$	b_{2g}
183(s)	$\pi(\text{PtCl}_4) a_{2u}$	$\delta(\text{Pt-Br})$	e_g
92(vs)	$\zeta(\text{PtBr})^+ L, e_u$			

Table [3.4].

Observed and calculated $\sin^2 \theta$ values for $K_2 [PtCl_4Br_2]$

$\sin^2 \theta$ (Observed)	$\sin^2 \theta$ (Calculated)	($h^2 + k^2 + l^2$)
•0182	•0184	3
•0245	•0243	4
•0488	•0485	8
•0670	•0677	11
•0740	•0737	12
•0965	•0941	16
•1150	•1153	19
•1209	•1213	20
•1456	•1455	24
•1640	•1637	27
•1948	•1949	32
•2129	•2119	35
•2176	•2180	36
•2425	•2422	40
•2603	•2607	43
•2660	•2662	44
•2907	•2907	48
•3085	•3090	51
•3160	•3150	52
•3394	•3395	56
•3968	•3572	59
•3880	•3877	64

Table [3.5]

Vibrational frequencies (cm^{-1}) of solid hexahalogenostannates

	ν_1	ν_2	ν_3	ν_4	ν_5	$[\nu_6]$	ν_L (ν_{1u} , IR)
$[\text{SnCl}_6]^{2-}$							
k	323	249	314	174	184	124	83
NH_4	317	250	310	180	179	113	122
Rb	316	214	312	173	171	107	72
Cs	309	243	310	171	165	102	72
NMe_4	307	-	298	172	-	-	76
NEt_4	305.5	-	318 276(sh)	161	-	-	68
NBu_4^n	306	-	320 290	158	-	-	
AsPh_4	-	-	284	161	-	-	
IPh_3	310 ^x	-	294 284(sh)	180(w) 162	-	89 [†]	
Aqueous Solution	311	229	-	-	158	-	

^x 311 in infrared

[†] Observed in infrared spectrum.

Table [3.6]

Vibrational frequencies (cm^{-1}) of solid hexahalogenoplumbates

	ν_1	ν_2	ν_3	ν_4	ν_5	$[\nu_6]$	ν_L (f.i.u. IR)
$[\text{PbCl}_6]^{2-}$							
NH_4	296	220	278	154	157	84	106,90(sh)
Rb	293	220	281	139	147	83	65
Cs	285	217	272	144	148	81	63
NMe_4	281	209	262	142	139	64	68
NEt_4	281	215	280 ^(sh) 259	138	144	80	
AsPh_4	279	211	247	133	139	75	
IPh_2	282 [†]	231	252 259	135	141	84	
Aqueous solution	285	212	-	-	137	-	

[†] 278 in infrared

Table [3.7]

Force constants (millidynes/Å) for solid
hexachlorostannates and plumbates.

	K	F	H	A	B
$[\text{SnCl}_6]^{2-}$					
K	1.07	0.27	0.03	0.04	0.01
NH_4	1.08	0.24	0.03^5	0.04	0.01^5
Rb	1.04	0.26^5	0.01	0.00	0.02
Cs	1.03	0.23	0.01^5	0.02	0.02
$[\text{PbCl}_6]^{2-}$					
NH_4	0.86	0.25	0.01	-0.02^5	0.03
Rb	0.89	0.24	-0.02	-0.04	0.02
Cs	0.86	0.22	-0.00^5	-0.02^5	0.02
NMe_4	0.77	0.22	-0.02	-0.01	0.03
NEt_4	0.80	0.21	-0.00^5	0.02	0.02
AsPh_4	0.73	0.21	-0.01^5	0.05	0.02
IPh_2	0.91	0.17	0.01	0.09	0.02

Table [3.8]

Vibrational frequencies (cm^{-1}) for the hexachlorotellurate(IV) anion in the solid state. (AH bands strong unless shown otherwise).

	Raman				Others
	ν_1	ν_2	ν_3	ν_4	
K	301	253	150	243	139(w-m), ν_4 ; 108(w-m), 98(w-m), ν_L
Rb	299	254	235	{330(sh) 251	63(m), ν_L
Cs	288	247	139	251	62(m), ν_L
NH_4	300	250	142	250	142(w-m), ν_4 ; 110, 98(w-m), ν_L
NMe_4	281	243	136	228 [†]	106(vw); 79(vs), ν_L
NEt_4	280	243	127	{282(w-m) 228	66(w-m), ν_L
PyH	283	-	146	{295(sh) 225	100(w), ν_L
AsPh_4	284 ^x	268 ^x	-	{248 237 223	156(w-m), 146(s) ν_4
IPh_2	291	252	-	{230 210 185	
Aqueous Solution	302P	263	137	-	

[†] Probably has two equal components, ca. 250, 212 cm^{-1}

[‡] In the infrared spectrum bands are also found at 288(m-s), 258(m-s) cm^{-1} , and are assigned to ν_1 and ν_2 respectively.

^x Observed in the infrared spectrum.

Table [3.9]

Vibrational frequencies (cm^{-1}) for hexabromo- and hexaiodo tellurate (IV) anions, in the solid state.

(All bands strong unless shown otherwise).

$[\text{TeBr}_6]^{2-}$	ν_1	ν_2	Raman		ν_3	I.R.	
			ν_5	Others		ν_3	Others
K	174	153	73(w)	90(vw)	198	100(m), 76(m)	
Rb	179	160	90	109(w)	195	95(vw)	
Cs	173	151	91(m)				
NH_4	180	155	83		198		
NMe_4	170	148	96(w)		180	104(vw), 68(m)	
NEt_4	168	144	-		180	65(m), 54(wm)	
PyH	173	157	-		178 149(sh)	73(w-m)	
Aqueous Solution	167P	146	73(m)				
$[\text{TeI}_6]^{2-}$							
NMe_4					154	106(m-s); 68(w), ν_L	
NEt_4					152 172(sh)	112(vw); 98(m), ν_L	
PyH					148	104(w-m)	

Table [3.10]

Force constants (millidynes/Å) for $M_2^I[\text{TeCl}_6]$,

	K	F	H	A	B	Value of ν_4	$[\nu_6], \text{cm}^{-1}$
	[TeCl ₆] ²⁻						
$M^I=\text{K}$	0.92	0.17	0.02 ^s	0.30	0.00	139	103
	0.93	0.17	0.02 ^s	0.29	-0.02	105	121
Rb	0.97	0.16	0.01	0.27	-0.03	63	119
Cs	0.95	0.14	0.02	0.23	-0.03	62	125
NH ₄	0.92 ^s	0.17	0.01	0.26	0.01	142	88
	0.93	0.17	0.01	0.25	-0.01	105	111
NMe ₄	0.86	0.13	0.03	0.28	-0.01	106	106
	0.86 ^s	0.13	-0.01	0.28	-0.01	79	81
NEt ₄	0.87	0.12	0.02	0.28	-0.02	66	111
PyH	0.90	0.11	0.05	0.33	-0.02	100	122

Table [3.11]

Force constants (millidynes/Å) for $M_2^I[\text{TeBr}_6]$.

	K	F	H	A	B	Value of ν_4	$[\nu_6]^\dagger$, cm^{-1}
	$[\text{TeBr}_6]^{2-}$						
K	0.86	0.10	0.04	0.17	0.01	100; $\nu_5=90$	57
	0.90	0.10	0.01	0.14	0.00	76; $\nu_5=73$	51
	0.90	0.10	0.04	0.14	-0.02	76; $\nu_5=90$	73
	0.86	0.10	0.01	0.17	0.02	100; $\nu_5=73$	22
Rb	0.91	0.09	0.04	0.23	0.00	$\nu_5=90$	61
	0.91	0.09	0.09	0.23	-0.02	$\nu_5=109$	87
NH_4	0.87	0.12	0.02	0.18	0.02	105	40
	0.90	0.12	0.02	0.15	-0.00	82	61
NMe_4	0.75	0.10	0.05	0.22	0.01	104	62
	0.80	0.10	0.05	0.17	-0.03	68	83
Net_4	0.77	0.11	0.05	0.14	-0.03	65	84
	0.77	0.11	0.05	0.13	-0.04	54	87

[†] Calculated values

Table [3.12]

Observed frequencies for $\text{H}_2\text{TeBr}_6 \cdot 2\text{H}_2\text{O}$ (cm^{-1})

Infrared	Raman
238 (broad, strong)	226 (strong)
222 (strong)	210 (strong)
210 (shoulder, weak)	[185 (weak)]
[190 (medium)]	[137 (medium-strong)]
	122 (medium-strong)
	85 (medium)

Bands in parentheses doubtful (see text).

Table [3.13]

Observed infrared frequencies of some $[\text{MCl}_6]^{3-}$ ions (cm^{-1})

	ν_3	ν_4	Others
$[\text{Co}(\text{pn})_3][\text{CrCl}_6]$	315	200	107
$[\text{Co}(\text{pn})_3][\text{MnCl}_6]$	342	183	107
$[\text{Co}(\text{pn})_3][\text{FeCl}_6]$	248	184	105
$[\text{Co}(\text{pn})_3][\text{InCl}_6]$	248	161	100
$[\text{Co}(\text{NH}_3)_6][\text{FeCl}_6]$	272, 248, 227	181, 160	129, 107, 90
$[\text{Co}(\text{NH}_3)_6][\text{IrCl}_6]$	302	195	100, 85
$(\text{NEt}_4)_3[\text{IrCl}_6]$	336, 317, 305	188, 171	112, 95, 85
$\text{K}_2[\text{MnCl}_6]$	358	200	102

CHAPTER FOUR

SQUARE-PLANAR IONS

CHAPTER 4 - SQUARE-PLANAR IONS

4.1 Prologue

Confusion exists in the literature over the numbering of the normal vibrations of square-planar molecules. It is conventional when numbering the normal modes, to label them in the order of occurrence in the character tables of Decius, Cross and Wilson³⁸. Thus, Nakamoto⁶⁹, for example, uses the wrong numbering system in his well known book. Much of the published data on square-planar ions uses this same system. The correct numbering of the representations of an ML_4 system is :- ν_1 (A_{1g}), ν_2 (B_{1g}), ν_3 (B_{2g}), ν_4 (A_{2u}), ν_5 (B_{2u}), ν_6 (E_u), and ν_7 (E_u). A_{2u} and E_u are the infrared active modes while all the g-modes are Raman active. These normal vibrations are shown in Figure [4.1].

The numbering of the normal modes for octahedral MX_6 molecules is also wrong but the convention used by Hertzberg⁷⁰ is too well established to be changed.

4.2 Introduction

The aims of the work in this chapter may be broadly divided into two categories. Firstly, the spectrum of $K_2 [PtCl_4]$ was examined in detail to help sort out the confusion that existed in the literature concerning assignments. To help this work a number of other simple chloroplatinites were investigated also, as well as some $[MK]^{n-}$ anions. In the second part of the chapter we discuss the effect of Magnus green type lattices on the spectrum of $[PtCl_4]^{2-}$ and related ions. In particular it was hoped to decide whether there was a vibrationally effective metal-metal bond in such systems. The $[PtI_4]^{2-}$ ion has also been characterised for the first time by incorporating it in a Magnus green type lattice. The spectra of $[Pt(NH_3)_4] [PtX_4]$, ($X = Cl, Br, I$) admit of two interpretations neither of which is wholly satisfactory.

4.3 Potassium chloroplatinite

The first investigation of $K_2 [PtCl_4]$ was by Adams and Gebbie¹² in 1963. They used a prototype Michelson interferometer at N.P.L. an instrument which at that time possessed only a limited resolving power. They reported bands at 320, 183 and 93 cm^{-1} , all bands being strong, while the ones below 200 cm^{-1} were also very broad. A three band spectrum is all that is predicted for an isolated $[PtCl_4]^{2-}$ ion and hence, quite naturally, the assignments made were $\nu_6 = 320$, $\nu_7 = 183$ and $\nu_4 = 93$ cm^{-1} . Fairly obviously ν_4 will fall below ν_7 since it is an out-of-plane deformation whilst ν_7 is in-plane.

Almost simultaneously a year later, Sacconi et al.⁴³ and Mathieu⁷¹ et al. both reported the spectra of $K_2 [PtCl_4]$, each group of workers disagreeing with the assignments made by Adams. Their data were in fair agreement, but their assignments were quite different. Their data, with their assignments, are given below.

(a) Mathieu.

322 (ν_6), 195,172,160 (ν_7), 111 (ν_4), 89 (ν_L).

(b) Sacconi.

325 (ν_6), 193 (ν_7), 175 (ν_4), 106 (ν_L).

It is clear that Adams failed to resolve the 133 cm^{-1} band into the two or three components that Sacconi or

Mathieu observed. Because of the disagreement between Sacconi and Mathieu, it was decided to measure the spectrum of $K_2 [PtCl_4]$ a number of times in order to substantiate any splittings or weak bands. The observed frequencies with our assignments are given below.

326 (ν_6), 194 (ν_7), 174.5 (ν_4), 108.5, 87.5, 59 (all ν_L).

It is evident from the assignments given that we support Sacconi's assignment and disagree with that of Mathieu. We do this for the following reasons.

1) The site-symmetry of $[PtCl_4]^{2-}$ in the potassium salt is the same as that of the free ion⁷². It is thus difficult to account for the triplet nature attributed to ν_7 by Mathieu. Thus the space group of $K_2 [PtCl_4]$ is D_{4h}^1 and the Bravais cell consists of one molecule only; this implies that the only degenerate vibrations are E-modes and only two bands would be expected from any splitting. Furthermore no splitting is predicted for ν_7 .

2) The band near 110 cm^{-1} assigned by Mathieu to ν_4 is absent in the spectrum of Magnus Green Salt, $[Pt(NH_3)_4][PtCl_4]$ (vide infra), and is thus more likely to be a lattice mode. Three translational lattice modes of the potassium ions are predicted and three have been observed by us, all of which we believe may be associated with the potassium ions.

3) Assignments are supported by the band width considerations; the band assigned to an A_{2u} mode is sharp and narrow, while those assigned to E_u modes are at least twice as broad. A similar band width effect is seen in (CO) bands for complexes of the type $M(CO)_3(\Pi\text{-arene})$.⁷³

4.4 Other single chloroplatinates.

Besides $K_2 [PtCl_4]$ a number of other single chloroplatinates $M_2^I [PtCl_4]$ ($M^I = Rb, Cs, Tl, Et_4N, Ph_2I, Ph_4As$) have been prepared and infrared spectra investigated. The salts $Na_2 [PtCl_4] \cdot nH_2O$, $Ba [PtCl_4] \cdot nH_2O$, $Pb [PtCl_4]$ and $Hg_2 [PtCl_4]$ which have also been studied, do not fit into the $M_2^I [PtCl_4]$ category. Assignments of fundamentals and other bands are given in table [4.1]. The Rb and Cs salts have been investigated previously⁴³, but are included here for the sake of completeness.

It is likely that each of the compounds $M^I [PtCl_4]$, ($M^I = Rb, Cs, Tl$) have the $K_2 [PtCl_4]$ structure. In accordance with this there is a smooth decrease in ν_6 , the platinum chlorine stretch, and in ν_7 , the in-plane deformation as the cation size is increased. ν_4 , the out-of-plane deformation, however, decreases rather more spectacularly from 175 cm^{-1} in $K_2 [PtCl_4]$ to 146 cm^{-1} in the thallium salt. Rather surprisingly the tetraethylammonium salt has ν_6 at the same position almost as the potassium salt and also ν_4 is higher by 4 cm^{-1} than in $K_2 [PtCl_4]$. Even less correlation is obtained when the tetraphenylarsonium salt is considered. Compared with $K_2 [PtCl_4]$, ν_6 is 20 cm^{-1} lower, ν_7 absorbs at the same frequency, and ν_4 is 25 cm^{-1} lower. Fairly obviously, the 'cation-effect' is more

complicated with square-planar complexes than with octahedral ions. Force-constant calculations would probably be useful to obtain a better understanding of the subject. However, calculations which require the incorporation of out-of-plane vibrations are notoriously difficult because of the difficulty of finding suitable internal coordinates.

In spite of these difficulties in finding convincing correlations, the effect of the unsymmetrical cation Ph_2I^+ , was rather similar to that noticed in octahedral systems. Thus ν_6 was quite definitely split into two components at 321 and 308 cm^{-1} giving a band centre of 315 cm^{-1} . ν_4 was not split but broader than the comparable band in other chloroplatinates. No bands which might have been Raman active fundamentals of $[\text{PtCl}_4]^{2-}$ were observed.

The only other monovalent cation chloroplatinate investigated was Na_2PtCl_4 . This, apparently, is hydrated and only poor spectra of it were obtained. The fundamentals of the anion were in each case the highest of all chloroplatinates investigated. Three low frequency bands, (144, 89, 54 cm^{-1}), must be attributed to lattice vibrations of the sodium ion. Since K^+ ions in $\text{K}_2[\text{PtCl}_4]$ translate at 110 cm^{-1} it is not impossible for Na^+ ions to translate at 144 cm^{-1} .

The three divalent cation chloroplatinates, $\text{Ba}[\text{PtCl}_4]$, $\text{Pb}[\text{PtCl}_4]$ and $\text{Hg}_2[\text{PtCl}_4]$ all had unusual spectra. The barium salt (from which many of the other salts were made), is hydrated. No splittings were observed, as might have been predicted, and no bands were unusually broad. The fundamentals appeared at reasonable frequencies, but a medium-strong band was observed also at 208 cm^{-1} . Tentatively this is attributed to a vibration associated with the torsion of the water molecules. Plumbic chloroplatinite, (not hydrated), also had ν_4 , ν_6 , and ν_7 in normal positions, but ν_6 was only a weak-medium broad band. Whether this is indicative of splitting is not certain, but certainly a medium feature at 350 cm^{-1} can be equated with ν_1 . Presumably mercurous chloroplatinite contains the Hg_2^{2+} ion, and the salt will obviously be of unusual structure. Difficulty was experienced in obtaining a spectrum of this compound; the only band observed (from a very thick mull) was at 285 cm^{-1} . Tentatively this is attributable to ν_6 .

Unfortunately, in spite of their promising colour, none of the solid chloroplatinites gave a Raman spectrum.

4.5 Other square-planar ions

Square-planar anion chemistry is a feature of the heavier d^8 ions; this type of configuration (in the case of halogeno complexes) is limited to Pt(II), Pd(II) and Au(III). Since simple salts containing the $[\text{PtI}_4]^{2-}$ or $[\text{PdI}_4]^{2-}$ ions are not properly characterised, only a limited number of these square-planar ions exist. They are namely, $[\text{PtX}_4]^{2-}$, (X = Cl, Br), $[\text{PdX}_4]^{2-}$, (X = Cl, Br), and $[\text{AuX}_4]^-$, (X = Cl, Br, I). Besides $\text{K}_2[\text{PtCl}_4]$, the spectra of $\text{K}_2[\text{PtBr}_4]$, $\text{K}[\text{AuCl}_4]$ and $\text{K}[\text{AuBr}_4]$ have been investigated elsewhere^{12, 43}. However, the spectra of $\text{K}_2[\text{PdX}_4]$, (X = Cl, Br) and $\text{K}[\text{AuI}_4]$ are reported here for the first time, (see table [4.2]. The spectrum of $[\text{PtI}_4]^{2-}$, which has been characterised with a complex cation associated with it, will be mentioned in a later section.

The spectrum of $\text{K}_2[\text{PtBr}_4]$ is worth mentioning here, because it was probably wrongly assigned. The assignments for it were directly dependent on those of $\text{K}_2[\text{PtCl}_4]$, which was also investigated at the same time¹². The assignments of $\text{K}_2[\text{PtCl}_4]$ are now known to be wrong (see section 4.3). The assignments of ν_6 and ν_7 to the bands at 233 and 135 cm^{-1} are still probably correct, but the interpretation of the two lower frequency bands (107, 80) is in doubt.

The proximity of ν_4 and ν_7 in $K_2[PtCl_4]$ suggest strongly that the band at 107 cm^{-1} should be attributed to ν_4 , and that at 80 cm^{-1} to ν_L . However, in direct conflict, the fact that potassium ions translate at 109 cm^{-1} in $K_2[PtCl_4]$, suggest that they should translate near this frequency in $K_2[PtBr_4]$; this requires assignation of the 107 cm^{-1} to ν_L and (presumably) the 80 cm^{-1} band to ν_4 . To make matters worse, it can be shown that one of the translational lattice modes in $K_2[PtBr_4]$ is of A_{2u} symmetry⁷⁴ (the others are E_u). It is quite likely therefore, that both the 107 cm^{-1} and the 80 cm^{-1} bands contain contributions from ν_L (A_{2u}) and ν_4 (A_{2u}). The only known simple iodo complex $K[AuI_4]$ was also studied in order to find out at which frequency the potassium ion translated. ν_6 (a sharp strong band, in line with other iodo complexes) appeared at 191 cm^{-1} and the only other bands observed were weak features at 70 and 54 cm^{-1} . Although $K[AuI_4]$ must adopt a different structure from the $K_2[PtCl_4]$ structure, it was thought that the K^+ ions would translate at roughly the same frequencies. However, no absorption was seen around 110 cm^{-1} ; thus in $K_2[PtBr_4]$, it is more likely that the 107 cm^{-1} band contains more contribution from ν_4 than ν_L . Tentatively the 70 cm^{-1} and 54 cm^{-1} bands in $K[AuI_4]$ are assigned to ν_7 and ν_4 , but again, it is probable that some lattice mode contribution

must be present in these bands.

The assignments for $K_2 [PdCl_4]$ follow from direct comparison with the platinum analogue; the low frequency bands at 111 and 90 cm^{-1} are attributed to lattice vibrations of the potassium ions. Except for a 20 cm^{-1} difference in ν_6 , the spectrum of $K_2 [PdBr_4]$ is almost identical with $K_2 [PtBr_4]$. As with the platinum compound it is a moot point whether the band at 106 cm^{-1} is wholly assigned to ν_4 or not. Besides the potassium salts of $[PdX_4]^{2-}$, ($X = Cl, Br$), $Na_2 [PdCl_4]$ was also investigated for comparison with $Na_2 [PtCl_4]$. Rather surprisingly, each of the fundamentals for the $Na_2 [PdCl_4]$ fall below those of the platinum analogue. This is probably because the palladium compound is anhydrous whereas the platinum one is hydrated. The lattice mode of the sodium ion in $Na_2 [PtCl_4]$ at 144 cm^{-1} was also high compared with its frequency in $Na_2 [PdCl_4]$ (132 cm^{-1}).

4.6 Summary of the Magnus Green and Magnus Pink problem.

Magnus Green salt (MGS) was first made in 1828 by Magnus⁷⁵ by the action of ammonia on PtCl_2 . Empirically the compound had the formula $\text{PtCl}_2 \cdot 2\text{NH}_3$, but was fairly obviously $[\text{Pt}(\text{NH}_3)_4][\text{PtCl}_4]$. MGS would be expected to be pink; $[\text{Pt}(\text{NH}_3)_4]^{2+}$ is colourless and $[\text{PtCl}_4]^{2-}$ is red. However, Jorgensen and Sorensen⁷⁶ noticed that a pink modification with the same analysis, [Magnus Pink salt (MPS)] could be prepared, and that this was easily transformed to MGS by hot water. They suggested that MPS was a monomer while MGS was a polymer. Cox et al.⁷⁷ examined both modifications by X-ray and concluded that MGS was not a polymer but contained discrete cations and anions. Although correct, the actual structure they postulated is now known to be incorrect. Cox et al.⁷⁷ also suggested that MPS when generally made was not MPS but Cleve's salt, $[\text{Pt}(\text{NH}_3)_3\text{Cl}]_2[\text{PtCl}_4]$, and that both Cleve's salt and MPS were easily converted to MGS. (Cleve's salt also analyses to $\text{PtCl}_2 \cdot 2\text{NH}_3$). It was also postulated that genuine MPS and Cleve's salt were structurally similar although no actual structures were suggested.

Yamada⁷⁸, (basing his theories on the structure of MGS postulated by Cox), took the first quantitative

dichroism measurements on MGS and the bromo analogue. He suggested that the anomalous colour was due to interaction between various planes of ions (giving apparently a bathochromic effect). He concluded that the interaction was caused by mutual disturbance between the electronic clouds of d -electrons which spread above and below the central platinum atoms. Yamada obviously neglected the compound $[\text{Pt}(\text{NH}_3)_4][\text{PdCl}_4]$ which does have the expected pink colour.

The accepted crystal structure of MGS was determined by Rundle et al.⁷⁹ who demonstrated that MGS crystallised in a tetragonal lattice with crystallographic symmetry $D_{4h}^6 - P4/MNC$. The Pt-Cl bond distance was 2.34 Å, the Pt-N distance 2.06 Å and the nearest platinum atoms were 3.25 Å apart. The structure adopted is of stacked ions (cation and anion in turn) with a staggered configuration of 28° between the individual planes. This is illustrated in figure [4.2]. Rundle et al. also took radial distribution measurements of both MGS and MPS. These are shown in Figure [4.3]. Referring to this figure, it is clear that both I and I' represent the Pt-Cl distance. II in MGS represents the Pt-Pt distance, but there is no analogous II' in MPS. It is possible that II' is overlaid by III', but even if this were so, it places the Pt-Pt

distance in MPS at more than 5 Å. Rundle also was of the opinion that the colour of MPS was identical with that of $[\text{Pt}(\text{NH}_3)_4]\text{Cl}_2$, but this is surely incorrect. No structure was suggested for MPS by Rundle.

Since MGS was first prepared, a number of analogous have also been made. Thus $[\text{Pt}(\text{NH}_2\text{R})_4][\text{PtCl}_4]$ ($\text{X} = \text{Me}, \text{Et}, \text{Pr}^n, \text{Bu}^n$), and many bromo and thiocyanato analogues have been made. Also systems have been made where different metals are present in each ion. For the single amines, the resultant colour is the expected one if the two different metal atoms are present, but generally green if metal atoms are the same. In the series $[\text{Pt}(\text{NH}_2\text{R})_4][\text{PtCl}_4]$ ($\text{R} = \text{H}, \text{Me}, \text{Et}$), both the amine and methylamine complexes have green colour but the ethylamine complex reverts back to the expected pink colour.

Miller⁸⁰ in 1961 examined the electronic spectra of a large range of Magnus Green type salts. He concluded that the reason for the structure adopted was NOT the formation of metal-metal bonds, but that this type of packing was merely electrostatically favourable. He also showed that this type of structure was not restricted to J^8 ions alone because (a) $[\text{Cu}(\text{NH}_3)_4][\text{PtCl}_4]$ was found to be isomorphous with MGS and (b) there was a copper analogue to nickel dimethylglyoxime. He demonstrated that

$[\text{Pt}(\text{Et.NH}_2)_4][\text{PtCl}_4]$ was not isomorphous with MGS.

In table [4.3] the properties of a number of the salts that he investigated are listed. Both the actual and expected colour, as well as the metal-metal bond distance is shown. The metal-metal bond distance is actually half the length of the c-axis of the tetragonal unit cell. Miller was of the opinion that metal-metal interaction between the planes might explain the anomalous colours but was probably restricted to compounds in which the metal-metal distance was less than 3.35 \AA . He based this figure of 3.35 \AA on the properties of the compound $[\text{Pt}(\text{NH}_3)_4][\text{Pt}(\text{SCN})_4]$ which would be expected to be orange, but is in fact red. Miller believed that the fact that the colour was only slightly different from the expected one, indicated that the metal-metal distance in this compound (3.35 \AA) was the critical distance for interaction.

Miller re-examined the problem in 1965⁸¹ extending the range of compounds studied. He claimed to demonstrate quantum mechanically, that metal-metal interaction did occur in all compounds with Magnus Green type lattices, even with those possessing normal colours. However, he still stood by his earlier opinion⁸¹ that this interaction was not responsible for the structure adopted. He also failed to index the powder photograph of $[\text{Pt}(\text{Et.NH}_2)_4][\text{PtCl}_4]$ again.

Williams et al.⁸² published a paper almost simultaneously with that of Miller⁸¹ which examined the electronic spectra of MPS as well as the normal⁸ Magnus Green type compounds. They postulated that the colours adopted were due to 'vibronic intensity-borrowing mechanism'. In this paper a Russian reference⁸³ is quoted in which a full X-ray structure showed that $[\text{Cu}(\text{NH}_3)_3][\text{PtCl}_4]$ was indeed isomorphous with MGS. The angle of stagger between the planes in the complex was the same as in MGS and the stereochemistry of the ligands were square-planar. Williams claimed that the absence of hydrogen-bonding in Magnus Green type complexes (concluded from infrared studies in the $\nu(\text{N-H})$ region) indicated that the staggering of the planes was such, merely to satisfy the packing requirements of the hydrogen atoms.

Although $[\text{Pt}(\text{Et.NH}_2)_4][\text{PtCl}_4]$ did not have the MGS structure, Williams thought that metal-metal interaction was still not precluded and that higher amine complexes might possess a quasi -Magnus Green structure.

The same paper reported a near infrared band at 6000 cm^{-1} in MGS, which was attributed to intermolecular electron transfer transitions. It is also stated that the ligand field bands should be affected by changes in the Ungerade (u) vibrations. Since the E_u stretching vibration,

$\nu(\text{Pt-Cl})$ decreases from 325 cm^{-1} in $\text{K}_2[\text{PtCl}_4]$ to 310 cm^{-1} in MGS, it is claimed that the amplitude of this vibration is greater in MGS (than K_2PtCl_4), leading to an enhancement of intensity. In $\text{K}_2[\text{PtCl}_4]$, it is suggested that the A_{2u} and B_{2u} out-of-plane bending modes are active in vibronic coupling, but in MGS they are inhibited by the proximity of the ions (which should not affect the E_u vibration). Overall, Williams et al., are of the opinion that the electronic spectra of $[\text{PtA}_4][\text{PtCl}_4]$ tends towards that of $\text{K}_2[\text{PtCl}_4]$ as the size of A becomes very large. In support of this Williams et al. have recently quoted Prout⁸⁴ who claims to have found a metal-metal distance in $[\text{Pt}(\text{Et.NH}_2)_4][\text{PtCl}_4]$ of 3.40\AA . Thus the metal-metal distances in MGS, $[\text{Pt}(\text{Et.NH}_2)_4][\text{PtCl}_4]$ and $\text{K}_2[\text{PtCl}_4]$ are 3.26, 3.40 and 4.10\AA respectively.

The summary above shows that the nature of the metal-metal interaction in MGS type compounds is still uncertain and that no structure has been postulated for MPS. It was thought therefore to be of interest to (a) determine whether there was a vibrational active (antisymmetric) metal-metal bond in these complexes, and (b), seek any structural hints from the spectrum of MPS. The complexes studied however are worthy of a separate study for their own sake, since they are as yet little studied below 250 cm^{-1} .

The assignments of frequencies observed for all compounds of MGS type are shown in Tables [4.4] to [4.7]. The arrangement of the Tables is thus :-

(a) Table [4.4a], assignment of $[\text{PtX}_4]^{2-}$ bands in $[\text{ML}_4][\text{PtX}_4]$.

(b) Table [4.4b], assignment of $[\text{ML}_4]^{2+}$ kernel bands in $[\text{ML}_4][\text{PtX}_4]$.

(c) Table [4.5], assignment of N-H bands in $[\text{ML}_4][\text{PtX}_4]$.

(d), (e), and (f). Tables [4.6a], [4.6b], and [4.7] refer to the spectra of the analogous $[\text{ML}_4][\text{PdX}_4]$ compounds.

L refers to the ligand in the cation; high frequency modes other than those associated with N-H are not reported.

Some spectra are sketched in Figures [4.4] and [4.5].

Poor spectra only, were observed for a number of the

compounds studied. The only previously reported spectra

for compounds of this type are for MGS by Mathieu *et al.*⁷¹

and for MGS and the palladium analogue by Clark and

Williams⁸⁵. In the Tables [4.4], [4.7], all bands are strong

unless otherwise stated.

4.7 Spectra of Magnus Green type compounds.

The assignments for the spectrum of MGS published by us in 1965⁸⁶, is the one given in the tables in this chapter, but in fairness it should be mentioned that a re-investigation of the spectrum casts doubt on this assignment. Mathieu *et al.*⁷¹ have recorded the spectrum of $[\text{Pt}(\text{NH}_3)_4]\text{Cl}_2$; the $[\text{PtN}_4]$ kernel has the frequencies 510 (ν_6), 236 (ν_7) and 150 (ν_4). A consideration of these data, taken jointly with the present data from $\text{K}_2[\text{PtCl}_4]$ ($\nu_6 = 325$, $\nu_7 = 194$, $\nu_4 = 174$) suggests the following assignments in MGS :- $[\text{Pt}(\text{NH}_3)_4]^{2+}$ 234 (ν_7), 141.5 (ν_4); $[\text{PtCl}_4]^{2-}$ 310 (ν_6), 198 (ν_7), 175 (ν_4). However, section 4.4 has shown that the cation effect appears to be more active in ν_4 (bend) than ν_6 (stretch). In $\text{Fl}_2[\text{PtCl}_4]\nu_6$ is only 8 cm^{-1} lower than in $\text{K}_2[\text{PtCl}_4]$, but ν_4 is about 30 cm^{-1} lower at 146 cm^{-1} . Since ν_6 for the anion in MGS, is at 310 cm^{-1} it is very possible that the band at 141.5 might be ν_4 for the anion rather than the cation. The spectrum of the bromo analogue, $[\text{Pt}(\text{NH}_3)_4][\text{PtBr}_4]$ was taken in order to help assignments, the band near 145 cm^{-1} disappeared completely. This would seem to indicate that this band is halogen sensitive; indeed it obviously is x-sensitive but the author prefers to discuss

the spectra considering this band to be an anion vibration. If the 140 cm^{-1} band is taken as being ν_4 for the $[\text{PtCl}_4]^{2-}$ anion, then grave doubt must be cast on Mathieu's assignments of the spectrum of $[\text{Pt}(\text{NH}_3)_4]\text{Cl}_2$. In MGS, ν_7 would have to be assigned to the band at 266 cm^{-1} and ν_4 to the one at 234 cm^{-1} .

There are two things wrong with using the bromide as a comparison. The first thing is not serious and is merely instrumental; the deformation modes for the $[\text{PtBr}_4]^{2-}$ ion are very low and not always observable with the interferometer. The other problem is caused by the structure adopted by MGS type compounds; the out of plane deformations (ν_4 , A_{2u}) will probably be very sensitive to the nature of the counterions. Thus, it will be more difficult for a nitrogen atom than a halogen atom to move out of plane. This should be reflected by an increase in frequency of ν_4 for the cation as larger halogen atoms are placed in the anion, thus ν_4 for the cation in $[\text{Pt}(\text{NH}_3)_4][\text{PtBr}_4]$ has been assigned to a band at 185 cm^{-1} . The fact that ν_4 for the cation in MGS is close to that in $[\text{Pt}(\text{NH}_3)_4]\text{Cl}_2$ need not necessarily be surprising because these two compounds have entirely different structures. The in-plane deformation (ν_7) is not affected.

In order to confirm the above theory concerning the

sensitivity of ν_4 , an attempt to make $[\text{Pt}(\text{NH}_3)_4][\text{PtI}_4]$ was made. This was successful. Addition of $[\text{Pt}(\text{NH}_3)_4]^{2+}$ ions to a solution of $\text{K}_2[\text{PtCl}_4]$, to which excess KI had been added, yielded a green solid that analyses to $\text{PtI}_2 \cdot 2\text{NH}_3$. The colour is itself interesting; the solution of K_2PtI_4 was itself black, and thus some metal-metal interaction is indicated by the green colour. However, the metal-metal distance is almost certainly greater than the limiting value of 3.35\AA set by Miller⁸⁰ for metal-metal interaction to occur. X-ray data on this compound would be useful.

In $[\text{Pt}(\text{NH}_3)_4][\text{PtI}_4]$, the 185 cm^{-1} band present in the bromide disappeared (the band at 180 cm^{-1} is attributed to ν_6 , the platinum-iodine stretch) but a new band at 228 cm^{-1} (not present in MGS either) can be attributed to ν_4 in the cation. The change in ν_4 in going from MGS to the iodide is thus 90 cm^{-1} ; this value is very large and the assignment made for this series of complexes depends entirely on whether such an increase is possible. The deformation modes in Magnus Green iodide were observed at 56 cm^{-1} (ν_7) and 40 cm^{-1} (ν_4). These bands were confirmed with an FS-620 interferometer which had a 100 micron beam splitter (and thus spectral region studied was $10\text{-}100\text{ cm}^{-1}$). Recently Hendra⁸⁷ reported the Raman spectra of a large number of square-planar ions in the solid state. Apparently however,

the reported spectrum of $K_2 [PtI_4]$ was in fact that of $K_2 [PtI_6]$,⁸⁸ for which the same three band spectrum is predicted.

An attempt to make the complex $[Pt(NH_3)_4][PdI_4]$ was not wholly successful because the black solid obtained always had poor analysis figures. However, the spectrum could be interpreted on the basis that $[Pt(NH_3)_4][PdI_4]$ was the major constituent. Thus the palladium-iodine stretch ν_6 , was observed at 198 cm^{-1} whilst ν_4 the palladium-nitrogen out-of-plane deformation absorbed at 238 cm^{-1} .

Metal-metal bonds stretches are generally very strong and sharp in the infrared. Two weak features were observed in the MGS spectrum at 82.5 and 74 cm^{-1} , but these can be attributed to lattice modes (of uncertain nature) rather than metal-metal bonds. Also no discontinuous change was noticed in the spectra of the species $[Pt(R.NH_2)_4][PtCl_4]$, ($R = H, Me, Et$), as $R=H$ was replaced by $R=Me$ and then $R=Et$. It is therefore concluded that there is no vibrationally active metal-metal bond in Magnus Green type compounds. No comment is required on the cation part of the spectra (except that already mentioned); the coordinated ammonia bands are reported as a matter of course. It is worth mentioning however that in many cases, ν_6 the metal-nitrogen

stretch was too weak to be observed.

No structural hints are supplied by the spectrum of MPS. The platinum-chlorine stretch was at 322 cm^{-1} , 12 cm^{-1} higher than in MGS. Three band spectra were observed for both the cation and anion parts and thus it is likely that both $[\text{Pt}(\text{NH}_3)_4]^{2+}$ and $[\text{PtCl}_4]^{2-}$ are in fact present in MPS.

An interesting feature of the spectrum of Cleve's salt, $[\text{Pt}(\text{NH}_3)_3\text{Cl}]_2[\text{PtCl}_4]$ is that three bands were observed in the metal-chlorine stretching region (319 , 330 and 344 cm^{-1}). This observation can be correlated with presence of chlorine atoms in two different environments. The structure of Cleve's salt is unknown, but from its very nature must contain ions of low site symmetry. Thus the degenerate E_u mode (ν_8) of the anion is split into a doublet with components at 319 and 330 cm^{-1} giving an average value of $\nu(\text{Pt-Cl})$ of 325 cm^{-1} . The 344 cm^{-1} band is almost certainly $\nu(\text{Pt-Cl})$ of the cation; taking into account that the cation has a dipositive charge whilst the anion has a double negative charge, it is very likely that $\nu(\text{Pt-Cl})$ for the cation will be higher than $\nu(\text{Pt-Cl})$ for the anion. No spectral data on the $[\text{Pt}(\text{NH}_3)_3\text{Cl}]^+$ ion is available for reference.

4.8 Conclusions.

The infrared spectra of $K_2 [PtCl_4]$ and of a number of other simple chloroplatinates have been assigned; the interpretation of the spectrum of $K_2 [PtCl_4]$ supported that made by Sacconi et.al.⁴³ The spectra of various other square planar ions have also been assigned, although for bands at lower frequencies than 150 cm^{-1} , lattice mode contributions to the spectra were seen to be complicated.

The spectra of some MGS type compounds can be interpreted on the basis that there is no metal-metal bond that is vibrationally active. The $[PtI_4]^{2-}$ ion has the expected spectrum.

MPS probably contains both $[Pt(NH_3)_4]^{2+}$ and $[PtCl_4]^{2-}$ ions, $\nu(Pt-Cl)$ and $\nu(Pt-N)$ are 12 and 10 cm^{-1} higher respectively than the corresponding bands in MGS. The absorption in the $\nu(Pt-Cl)$ region in Cleve's salt can be interpreted on the basis of a low site symmetry for the ions present in the salt.

One large problem set by this chapter has been the exact positions of the in-plane and out of plane deformations of square-planar systems. It seems very strange that for the $[PtN_4]^{2+}$ and $[PtCl_4]^{2-}$ systems that ν_7 is higher in the first system than in the second system while the reverse is true of the ν_6 modes. Unfortunately, not enough square-

planar systems are available for complete studies to be made. Except for those already mentioned the only other common square-planar systems are encountered in thiourea complexes of some metalloids and in some cyanide complexes.

4.9 Experimental

MGS type compounds were made by mixing aqueous solutions of the counterions at 0°C.⁸⁰ MPS was prepared by the method of Cox et.al.⁷⁹ To an aqueous solution of $[\text{Pt}(\text{NH}_3)_4]\text{Cl}_2$, to which one quarter of its volume of 0.88 NH_3 had been added, neutral $\text{K}_2[\text{PtCl}_4]$ was added whereupon the product precipitated. MPS has the calculated analysis of N, 8.7% and Cl, 23.5% while the found analysis had N, 8.75% and Cl, 23.5%.

$[\text{Pt}(\text{NH}_3)_4][\text{PtI}_4]$ was prepared by mixing equimolecular solutions of $[\text{Pt}(\text{NH}_3)_4]^{2+}$ and $[\text{PtI}_4]^{2-}$ ions; $[\text{PtI}_4]^{2-}$ ions were made by adding excess KI to $\text{K}_2[\text{PtCl}_4]$ solution. Calculated, N 5.3%, I 52%, Pt 40%; found, N 5.31%, I 51.94% Pt 39.8%, $[\text{Pt}(\text{NH}_3)_4][\text{PtI}_4]$ was prepared in a similar manner but reasonable analysis figures could not be attained.

Cleve's salt was prepared according to Tschugaev's method.⁸⁹

Spectrometers used have been mentioned previously (Section [3.9]).

FIGURE 4.1

Normal modes of a square-planar MX_4 molecule.

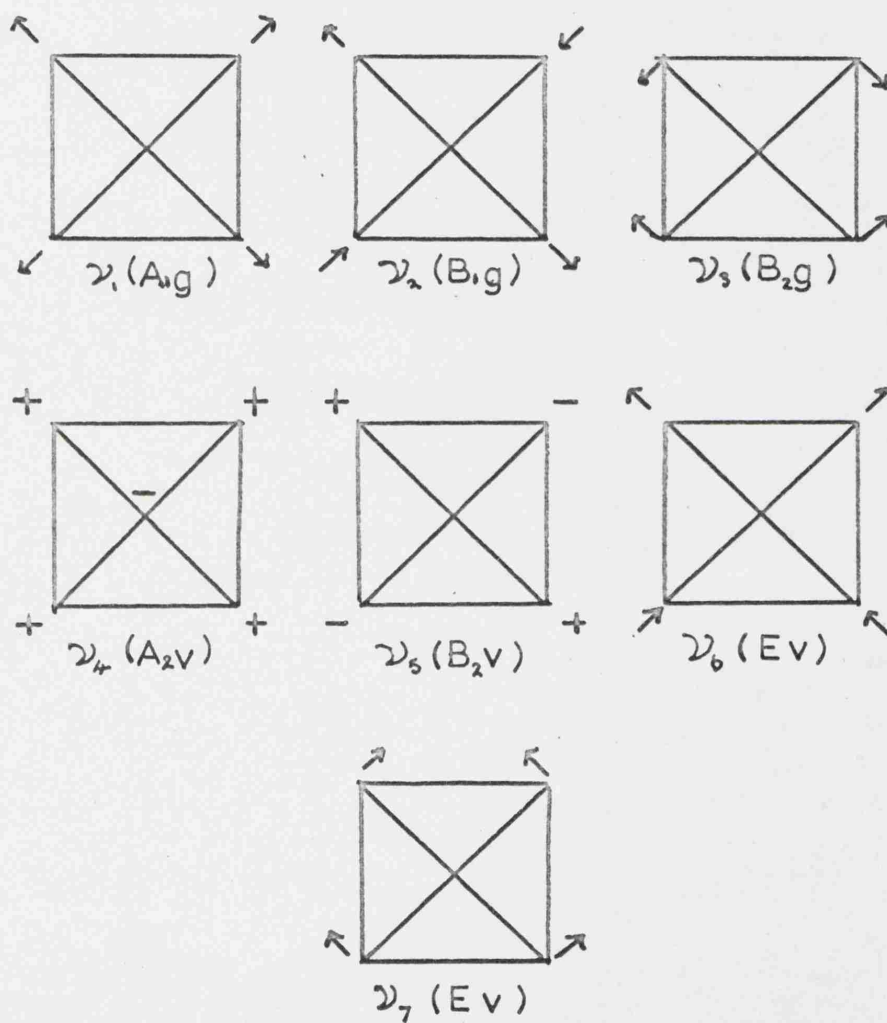
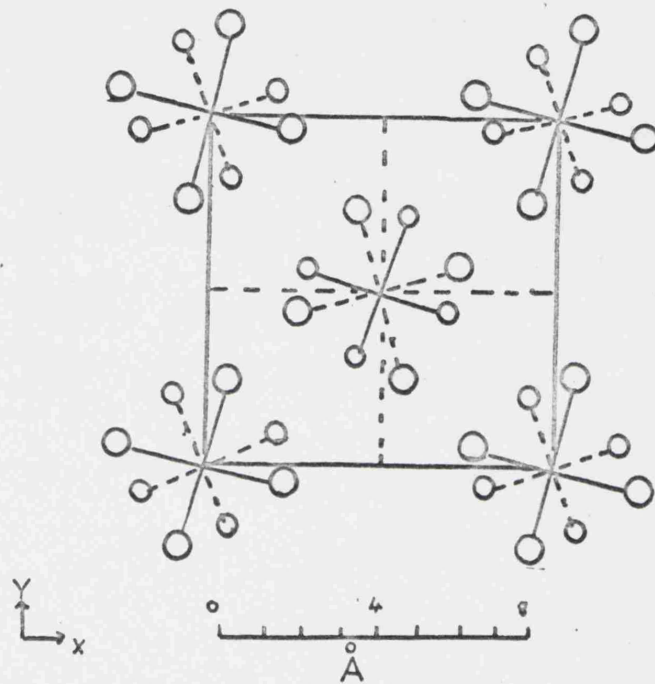


FIGURE 4.2

Crystal structure of Magnus Green Salt

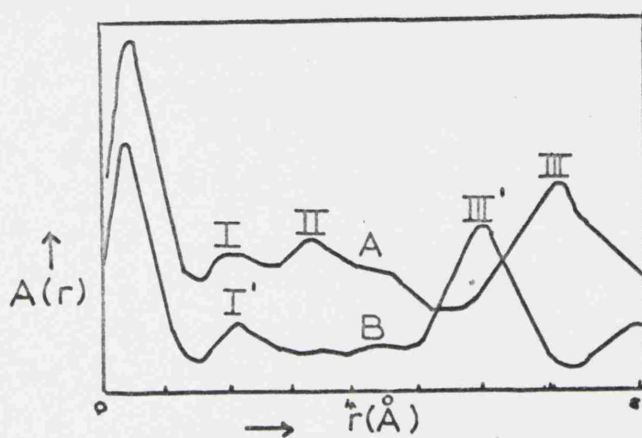


(001) Projection. Solid lines indicate $Z=0$,
broken ones $Z=1/2$

Large circles represent Cl, small ones
represent N

FIGURE 4.3

Radial distribution functions of Magnus Green
Magnus Pink Salts.



A=MGS

B=MPS

(after Rundle *et.al*, JACS., 1957, 79 3017)

FIGURE 4.4

Far-infrared spectra of $(\text{Pt}(\text{NH}_3)_4)(\text{PtX}_4)_2$, ($X = \text{Cl}, \text{Br}, \text{I}$).



FIGURE 4.5

Far-infrared spectra of $(M(\text{NH}_3)_4)(\text{PtCl}_4)$, ($M = \text{Pt, Pd, Cu}$).

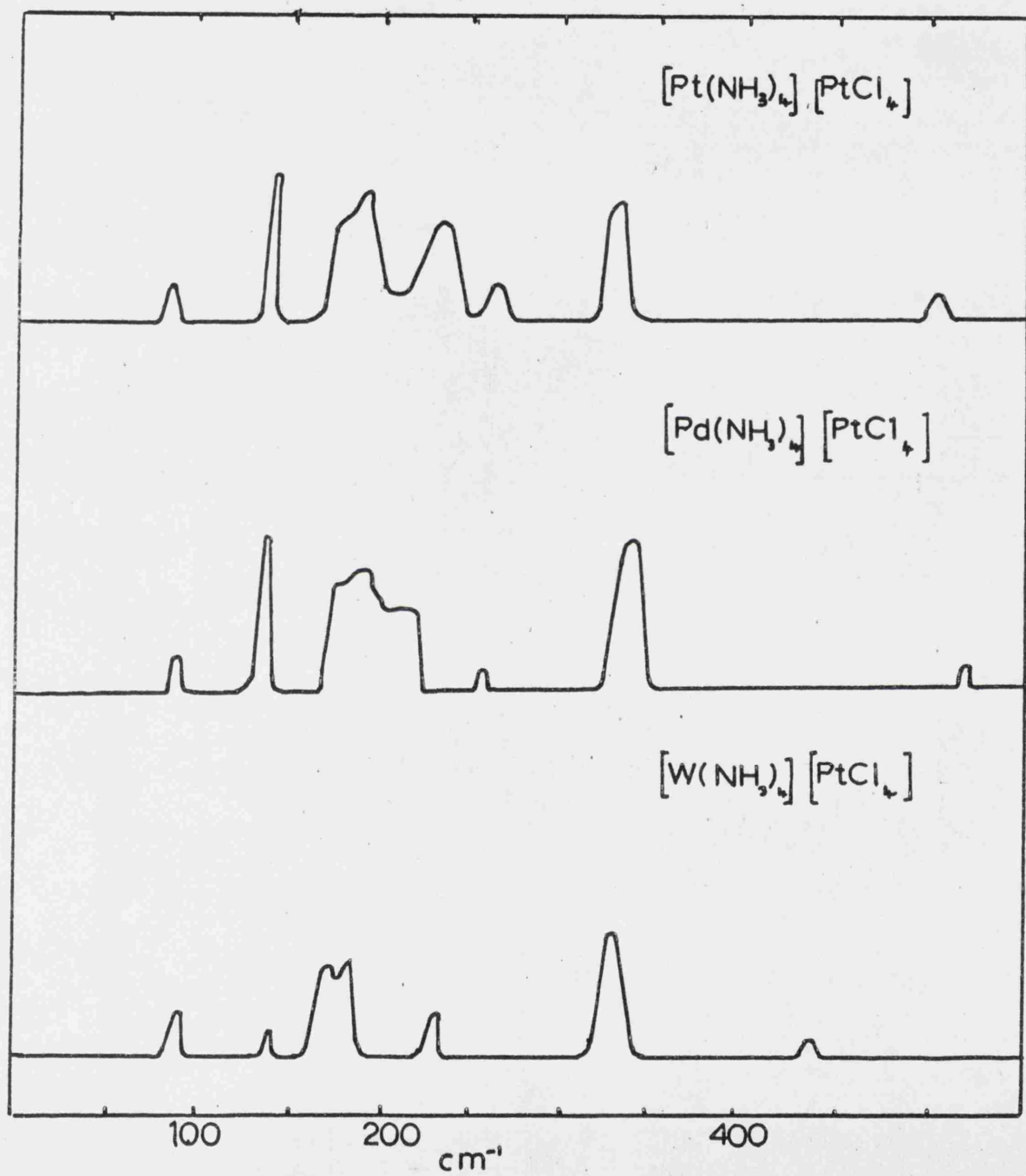


Table [4.1]

Assignments for some simple chloroplatinites

<u>Cation.</u>	ν_6	ν_7	ν_4	Other bands
Na ⁺ (hydrated)	327	209 _m	190	144, 89, 54
Et ₄ N ⁺	326	190	181	-
K ⁺	326	194	174.5	108.5, 87.5, 59
Rb ⁺	324	187	168	-
Cs ⁺	320	183	161	-
Ba ²⁺ (hydrated)	319	173	154	208 _m
Te ⁺	318	182	146	-
Pb ²⁺	315 _m	176	146	350 _{w-m}
Ph ₂ I ⁺	321, 308	177 (broad)	145	-
Ph ₄ As ⁺	305	193	151	-
"Mg ⁺ "	285 _w	-		260 _{vw}

All bands strong unless indicated.

Table [4.2]

Assignments for some simple square-planar ions (cm^{-1})

	ν_6	ν_7	ν_2	Other bands
$\text{K}_2 [\text{PtBr}_4]$	233	135	106	81
$\text{Na}_2 [\text{PdCl}_4]$	322	183	159	132, 80
$\text{K}_2 [\text{PdCl}_4]$	332	190.5	168	111, 90
$\text{K}_2 [\text{PdBr}_4]$	294	136 μ	106m	81w
$\text{K}[\text{AuI}_4]$	191	70m	54m	

All bands strong unless stated otherwise.

Table [4.3]

Properties of some Magnus Green type complexes (from ref. 81).

<u>Compound</u>	<u>Colour</u>	<u>Expected Colour</u>	<u>Metal-metal distance (Å)</u>
$[\text{Pd}(\text{NH}_3)_4][\text{PdCl}_4]$	Pink	Pink	3.245
$[\text{Pt}(\text{NH}_3)_4][\text{PdCl}_4]$	Pink	Pink	3.225
$[\text{Cu}(\text{NH}_3)_4][\text{PtCl}_4]$	Purple	Purple	3.230
$[\text{Pd}(\text{NH}_3)_4][\text{PtCl}_4]$	Pink	Pink	3.250
$[\text{Pt}(\text{NH}_3)_4][\text{PtCl}_4]$	Green	Pink	3.230
$[\text{Pt}(\text{Me.NH}_2)_4][\text{PtCl}_4]$	Green	Pink	3.245
$[\text{Pd}(\text{NH}_3)_4][\text{PdBr}_4]$	Red	Red	3.370
$[\text{Pt}(\text{NH}_3)_4][\text{PtBr}_4]$	Green	Red	3.310
$[\text{Pt}(\text{Me.NH}_2)_4][\text{PtBr}_4]$	Green	Red	3.305
$[\text{Pd}(\text{NH}_3)_4][\text{Pd}(\text{SCN})_4]$	Pink	Pink	3.345
$[\text{Pt}(\text{NH}_3)_4][\text{Pt}(\text{SCN})_4]$	Red	Orange	3.350
$[\text{Pt}(\text{Et.NH}_2)_4][\text{PtCl}_4]$	Pink	Pink	Not tetragonal

Table [4.4a]

Assignments for $[\text{PtX}_4]^{2-}$ in MGS type complexes(X = Cl, Br, I)

	ν_6	ν_7	ν_4
$[\text{Pt}(\text{NH}_3)_4][\text{PtCl}_4]$ (MGS)	310	198	175
$[\text{Pd}(\text{NH}_3)_4][\text{PtCl}_4]$	320	187	174
$[\text{Cu}(\text{NH}_3)_4][\text{PtCl}_4]$	320	184	175
$[\text{Pt}(\text{NH}_3)_4][\text{PtCl}_4]$ (MPS)	322	188	178
$[\text{Pt}(\text{NH}_3)_3\text{Cl}][\text{PtCl}_4]^{\dagger}$	330, 319		
$[\text{Pt}(\text{Me.NH}_2)_4][\text{PtCl}_4]$	313	One band observed at 187 cm^{-1} m	
$[\text{Pt}(\text{Et.NH}_2)_4][\text{PtCl}_4]^*$	312	-	-
$[\text{Pt}(\text{NH}_3)_4][\text{PtBr}_4]$	222	One band at 95 cm^{-1} m	
$[\text{Cu}(\text{NH}_3)_4][\text{PtBr}_4]$	228	One band at 105 cm^{-1} m-s	
$[\text{Pt}(\text{Me.NH}_2)_4][\text{PtBr}_4]$	217	139	105
$[\text{Pt}(\text{Et.NH}_2)_4][\text{PtBr}_4]$	220	-	-
$[\text{Pt}(\text{Br.NH}_2)_4][\text{PtBr}_4]$	219	-	-
$[\text{Pt}(\text{NH}_3)_4][\text{PtI}_4]^*$	180	56	40

 $^{\dagger} \nu(\text{Pt-Cl})$ in cation at 344 cm^{-1}

* Known not to be isomorphous with MGS

* Low frequency bands (56, 40) obtained from FTC-100.

Table [4.4b]

Assignments for $[ML_4]^{2+}$ in MGS complexes with Pt
in anion

ν_8	ν_7	ν_4
500w	234	141.5
-	266	144
435w	238w-m	146.5m
510	250 or 267	154
502w	253	144
496w	-	140 or 152
456w	272	155,wm
-	247m	185
440w	235	185
491,503w	268	-
-	264	-
-	267m	195m
-	255	228

Table [4.5]

NH frequencies in MGS type compounds containing Pt in anion.

$[\text{Pt}(\text{NH}_3)_4][\text{PtCl}_4]$	3260,3170; 1624,1536; 1310; 824
$[\text{Pd}(\text{NH}_3)_4][\text{PtCl}_4]$	3305,3198; 1624,1572; 1272; 776
$[\text{Cu}(\text{NH}_3)_4][\text{PtCl}_4]$	3305,3265,3190; 1600; 1310,1245; 688
$[\text{Pt}(\text{NH}_3)_4][\text{PtCl}_4](\text{MPS})$	3250,3180; 1588; 1330,1348; 856
$[\text{Pt}(\text{NH}_3)_3\text{Cl}][\text{PtCl}_4]$	3250,3190; 1580; 1340,1308; 922,808
$[\text{Pt}(\text{Me.NH}_2)_4][\text{PtCl}_4]$	3235,3170,1575; 1344,1268; 698.
$[\text{Pt}(\text{Et.NH}_2)_4][\text{PtCl}_4]$	3235,3200,3170; 1585; 1253; 734
$[\text{Pt}(\text{NH}_3)_4][\text{PtBr}_4]$	3260,3170; 1604; 1296; 780
$[\text{Cu}(\text{NH}_3)_4][\text{PtBr}_4]$	3300,3220; 3190; 1600; 1312,1292, 1256; 688
$[\text{Pt}(\text{Me.NH}_2)_4][\text{PtBr}_4]$	3200; 1592; 1248,1300; 698.
$[\text{Pt}(\text{Et.NH}_2)_4][\text{PtBr}_4]$	3208,3193,3165; 1570; 1238; 722
$[\text{Pt}(\text{Bu.NH}_2)_4][\text{PtBr}_4]$	3260,3168; 1570; 1304,1283,1215; 727
$[\text{Pt}(\text{NH}_3)_4][\text{PtI}_4]$	3230,3163,1608; 1318; 816

(N-H) 3200 cm^{-1} (NH_3) 1600 cm^{-1} 1300 (NH_3) 1300,

(NH_3) 800 cm^{-1}

Table [4.6a]

Assignments for $[\text{PdX}_4]^{2-}$ in MGS type compounds(X = Cl, Br, I).

Compound	ν_6	ν_7	ν_4
$[\text{Pd}(\text{NH}_3)_4][\text{PdCl}_4]$	326	197	188
$[\text{Pt}(\text{NH}_3)_4][\text{PdCl}_4]$	332	224	164
$[\text{Pd}(\text{NH}_3)_4][\text{PdBr}_4]$	262	-	-
$[\text{Cu}(\text{NH}_3)_4][\text{PdBr}_4]$	262 m-s		One band at 110 m
$[\text{Pd}(\text{Me.NH}_2)_4][\text{PdBr}_4]$	250		One band at 105 m
$[\text{Pt}(\text{NH}_3)_4][\text{PdI}_4]$	198	-	

Table [4.6b]

Assignments for $[ML_4]^{2+}$ in MGS complexes with Pd in anion.

Compound	ν_6	ν_7	ν_4
$[Pd(NH_3)_4][PdCl_4]$	490w	260	147
$[Pt(NH_3)_4][PdCl_4]$	491w	245m	137
$[Pd(NH_3)_4][PdBr_4]$	-	262	186 w-m
$[Cu(NH_3)_4][PdBr_4]$	468w	-	186
$[Pd(Me.NH_2)_4][PdBr_4]$	498w	-	190
$[Pt(NH_3)_4][PdI_4]$	-	254	238m

Table [4.7]

NH frequencies in MGS complexes containing
Pd in anion.

$[\text{Pd}(\text{NH}_3)_4][\text{PdCl}_4]$	3305,3185; 1624,1580; 1277; 779
$[\text{Pt}(\text{NH}_3)_4][\text{PdCl}_4]$	3310,3190; 1600; 1246; 752.
$[\text{Pd}(\text{NH}_3)_4][\text{PdBr}_4]$	3282,3170; 1608; 1197,1164; 648,695
$[\text{Cu}(\text{NH}_3)_4][\text{PdBr}_4]$	3400,3280,3220; 1608; 1279,1245; 776
$[\text{Pd}(\text{Me.NH}_2)_4][\text{PdBr}_4]$	3275,3235,3190; 3165; 1586; 1240; 680
$[\text{Pt}(\text{NH}_3)_4][\text{PdI}_4]$	3235,3160; 1608,1530; 1319; 818

$$\nu(\text{N-H}) \sim 3200 \text{ cm}^{-1}, \quad \delta_s(\text{NH}_3) \sim 1600 \text{ cm}^{-1}, \quad \delta_s(\text{NH}_3) \sim 1300 \text{ cm}^{-1},$$

$$\rho_r(\text{NH}_3) \sim 800 \text{ cm}^{-1}$$

CHAPTER FIVE

TETRAHEDRAL ANIONS

CHAPTER 5. TETRAHEDRAL ANIONS

5.1 Introduction

The first halogeno complexes of thallium(III) were made by Meyer⁹⁰ in 1900. The elements of group III A appear to be able to form various complex halides of the form $[MX_n]^{3-n}$ ($n = 3, 4, 5, 6$) as well as various aquated halogenocomplexes, and thus subsequent reports on TlX_4^- ions have been sometimes conflicting.^{91, 92} The situation was summarised by Cotton⁹³ who also authentically characterised for the first time the tetra coordinated species TlX_4^- , ($X = Cl, Br, I$). He also demonstrated that $(Ph_4As)[TlCl_4]$ was isostructural with $(Ph_4As)[FeCl_4]$ and thus $[TlCl_4]^-$ was also tetrahedral. The compounds $(Bu_4^+N)[TlX_4]$, ($X = Cl, Br$), were also shown to be isomorphous with each other. However, Atoji *et.al.*⁹⁴ have claimed that X-ray evidence shows that some tetrahalothallates are square-planar. Infrared and Raman spectra of $[TlX_4]^-$ ions provide an elegant method of distinguishing between tetrahedral and square-planar configurations and these complexes were made in order to obtain their spectra. Since this work was completed, Spiro^{96, 95} has published data in close agreement with that reported below.

5.2 Results and Discussion.

The infrared and Raman frequencies observed for the complex studied are given in table [5.1], with assignments made on the assumption of a tetrahedral structure. The spectra of the tetraethylammonium salts are shown in Figure [5.1].

The major differences in the spectra of tetrahedral and square-planar ions will occur because the tetrahedral ion does not have a centre of inversion. Thus, coincidences between Raman and infrared spectra are to be expected for tetrahedral ions, while there should be none for square-planar ions. For $K_2[PtCl_4]$ the highest Raman stretch occurs at 335 cm^{-1} and the infrared stretch is only 10 cm^{-1} lower. Good Raman spectra were obtained from the yellow $(Et_4N)[TlBr_4]$ and red $(Et_4N)[TlI_4]$. In each case coincidences were observed with the infrared spectra; a Raman band at 183 cm^{-1} in $(Et_4N)[TlBr_4]$ was matched by one in the infrared at 185 cm^{-1} , while the corresponding bands in the iodide occurred at 149 and 146 cm^{-1} respectively. It is concluded that these ions are tetrahedral and not square-planar.

It is impossible to use correlation tables to compare the spectra of tetrahedral and square-planar ions, because T_d and D_{4h} point groups lie in separate branches at the

symmetry-hierarchy^{9 6} (see Figure [5.2]). However, the number of expected bands for each symmetry group is shown below :-

$$T_d \quad 2 \text{ I.R.} \quad 4 \text{ R.} \quad ; \quad D_{4h} \quad 3 \text{ I.R.} \quad 3 \text{ R.}$$

It should therefore be also possible to decide which configuration is adopted by merely counting the number of bands in the spectra. For the thallium complexes, (except for iodide), however, most bands were split to some extent and therefore this method failed. Nevertheless, it is believed that the coincidences observed argue strongly for a tetrahedral configuration, and the spectra will be discussed on this assumption. For a tetrahedral complex MX_4 , the bands expected are $\nu_1(A)$, $\nu_2(E)$, ν_3 and ν_4 (both F_2), ν_1 and ν_3 are stretching vibrations, all bands are Raman active but only the F_2 -modes infrared active. The form of the normal vibrations are shown in Figure [5.3].

None of the chlorides $R[TlCl_4]$, ($R = Me_4N$, Et_4N , Ph_4As), (all white) gave a good Raman spectrum. ν_3 for the tetramethylammonium salt was very broad, possessed structure and was centred at 302 cm^{-1} . A doublet at 98 and 115 cm^{-1} (both strong) is assigned to ν_4 . The possibility of one component being a lattice mode is discounted on the evidence presented in Chapter three;

Me_4N^+ would be expected to translate at about the same frequency as Cs^+ , and Cs^+ generally translates at less than 80 cm^{-1} . No Raman signal at all was obtained from this compound. In contrast $(\text{Et}_4\text{N})[\text{TlCl}_4]$ gave a Raman signal of sufficient intensity to be able to observe ν_1 and ν_3 . The strength and sharpness of the band at 312 cm^{-1} unambiguously assigns itself as ν_1 ; ν_3 was of only medium intensity, quite broad and centred at 290 cm^{-1} . This value of ν_3 compares quite well with the corresponding value in the infrared spectrum, i.e. 293 cm^{-1} . This was quite broad, but not as broad as ν_3 in the Me_4N^+ salt. ν_4 was very similar to the ν_4 in $(\text{Me}_4\text{N})[\text{TlCl}_4]$: thus a band at 110 cm^{-1} had a shoulder at 93 cm^{-1} . For the tetraphenylarsonium salt ν_3 appeared as a distinct doublet (at 306 , and 292 cm^{-1}), as did ν_4 . The fact that all three tetrachlorothallates had this near 90 cm^{-1} lends further evidence for its assignation as a component of ν_4 , rather than a lattice mode. It seems likely from the spectral evidence that in the compounds investigated there is some distortion in the crystal; whether this is due to packing of the organic group or an actual lowering of T_d symmetry is not certain. In $(\text{Ph}_4\text{As})[\text{FeCl}_4]$ it was found in fact, that the actual tetrahedron, $[\text{FeCl}_4]$, was slightly flattened along one axis.

The interpretation of the spectra of the bromides follows closely that of the chlorides. No Raman spectrum was obtained from the Me_4N^+ and Ph_4As^+ salts but $(\text{Et}_4\text{N})[\text{TlBr}_4]$ gave a good signal. ν_3 for the $(\text{Me}_4\text{N})[\text{TlBr}_4]$ was split into a definite triplet (main strong peak at 199 cm^{-1} with shoulders either side at 186 and 207 cm^{-1}). The strong band at 102 cm^{-1} is rather high for ν_4 , considering the position in the chlorine analogue. In table [5.1] this band is listed under ν_4 , but really this is rather doubtful. In $(\text{Et}_4\text{N})[\text{TlBr}_4]$ ν_4 was quite broad, and overlaid by the polythene band; thus the figure of 78 cm^{-1} is only an approximate one. ν_3 was split into two very strong features at 173 and 185 cm^{-1} . ν_1 and ν_2 are much closer together in the Raman spectra of $(\text{Et}_4\text{N})[\text{TlBr}_4]$ than in the chloride; thus ν_1 was a very sharp and strong at 192 cm^{-1} while ν_2 was of only weak-medium intensity at 182 cm^{-1} . This value of ν_2 compares well with the infrared value. For $(\text{Ph}_4\text{As})[\text{TlBr}_4]$ only a poor spectrum could be obtained and only ν_3 was observed with certainty in the infrared; this had the same shape as the Me_4N^+ salt and was centred at 196 cm^{-1} .

The Raman spectrum of $[\text{TlI}_4]^-$ in its tetraethylammonium salt showed the same trend as the bromide when compared to the chloride. (i.e. proximity of ν_1 and ν_2). In this case

however ν_1 fell below ν_3 at 130 cm^{-1} . As with the bromide ν_1 was very sharp and strong, while slits of 0.15 mm were necessary to resolve ν_3 (at 149 cm^{-1}). In sharp contrast to the other halothallates ν_3 in the infrared was very sharp (at 146 cm^{-1}), ν_4 was observed as a medium sharp feature at 60 cm^{-1} . For the tetraphenylarsonium salt only ν_3 (at 148) was observed from the infrared spectrum. However, the spectra of the tetraethylammonium salt was good enough to suggest that there is no distortion in the iodothallate salts.

5.3 Conclusions.

The spectra of the tetrahalothallates $[\text{TlX}_4]^-$, (X = Cl, Br, I), have been observed and assigned on the basis of a tetrahedral configuration. In no cases were ν_2 and ν_4 observed in the Raman spectra. It is concluded that there is some distortion in the chloro and bromo complexes but not in the iodothallates. The observed frequencies observed here compare well with those of the indium analogues already in the literature. ⁹⁸⁻¹⁰¹

5.4 Experimental

All compounds were prepared according to the preparations given by Cotton.⁹³ The salt $(Et_4N)[TlI_4]$ which had not been prepared previously had satisfactory analysis figures.

Spectra were taken on instruments mentioned previously (see Section 3.9).

FIGURE 5.1

Vibrational spectra of $(\text{NEt}_4)(\text{TX}_4)$, ($X = \text{Cl}, \text{Br}, \text{I}$).

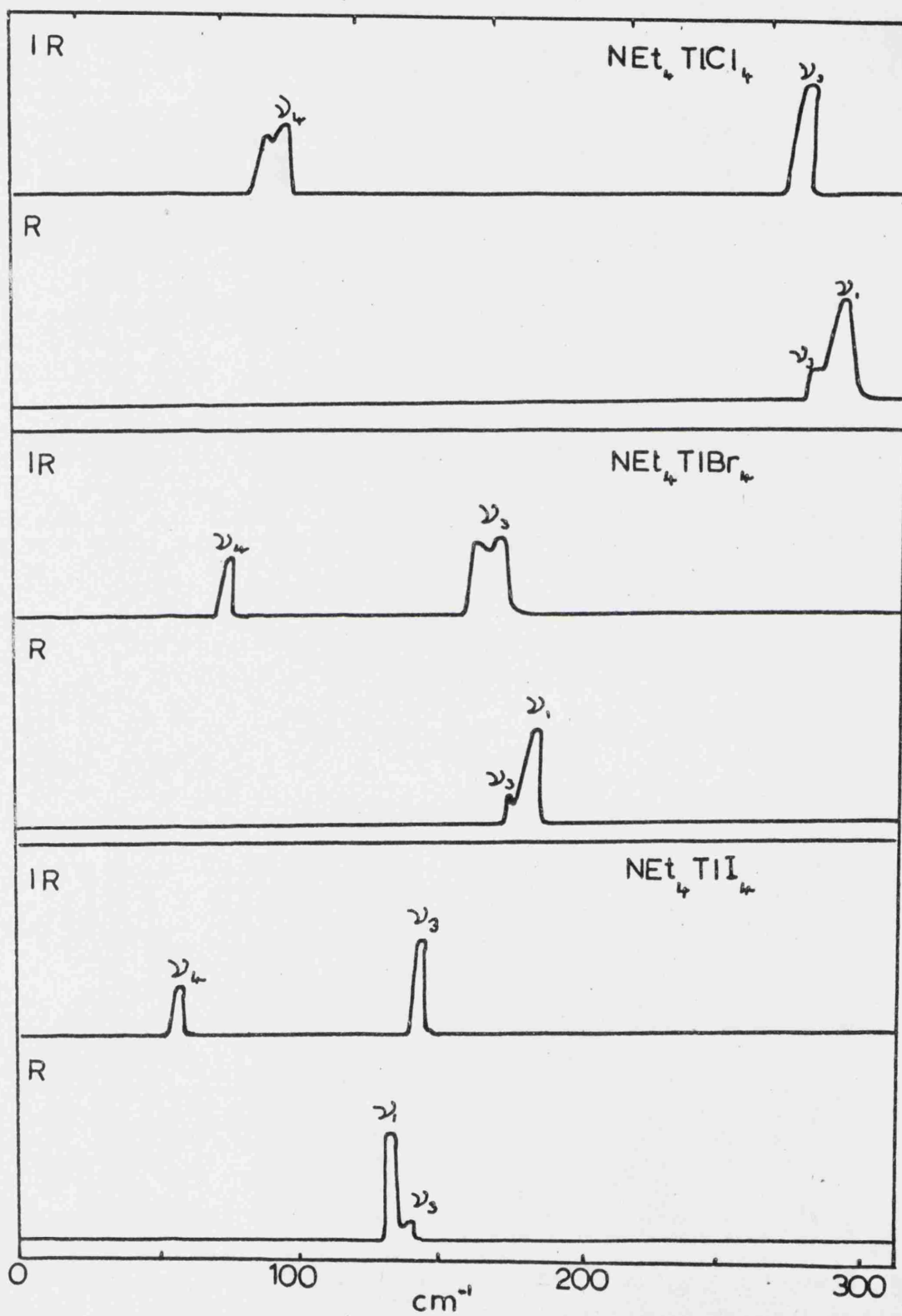


FIGURE 5.2

The symmetry-hierarchy diagram of Jorgenson.

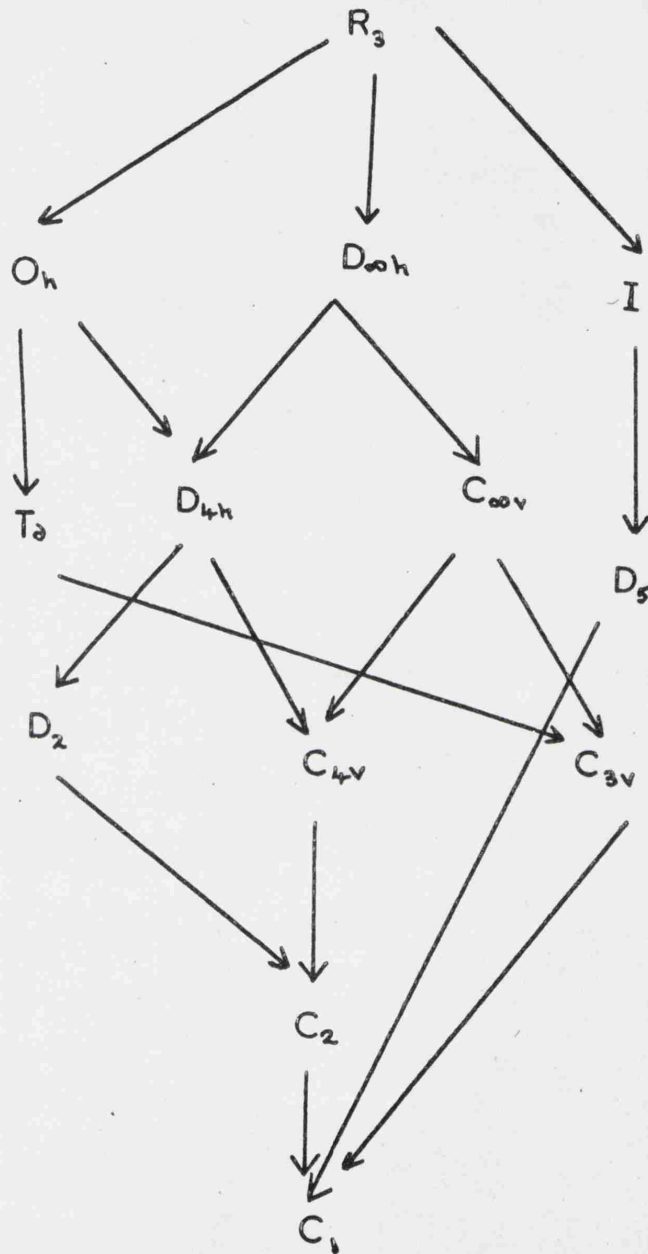


FIGURE 5.3

Normal modes of a tetrahedral MX_4 molecule.

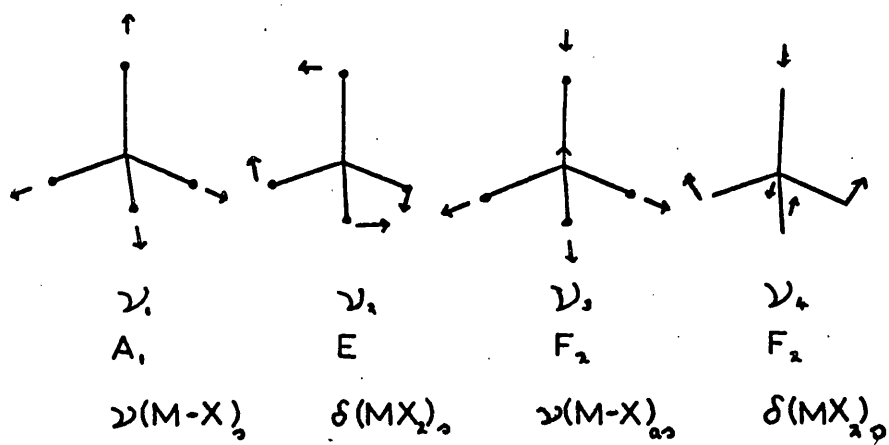


Table [5.1]

Observed frequencies for some tetrahalothallates(III)
(in cm^{-1})

	ν_1	ν_3	ν_4
$(\text{Me}_4\text{N})[\text{TlCl}_4]$		302(IR)	115,98(IR)
$(\text{Et}_4\text{N})[\text{TlCl}_4]$	312	293(IR) 290(R)	110,93(IR)
$(\text{Ph}_4\text{As})[\text{TlCl}_4]$		306,292(IR)	107,93(IR)
$(\text{Me}_4\text{N})[\text{TlBr}_4]$		207,199,186(IR)	102(IR)
$(\text{Et}_4\text{N})[\text{TlBr}_4]$	192	185,173(IR) 183(R)	78(IR)
$(\text{Ph}_4\text{As})[\text{TlBr}_4]$		196(IR)	
$(\text{Et}_4\text{N})[\text{TlI}_4]$	130	146(IR) 149(R)	60
$(\text{Ph}_4\text{As})[\text{TlI}_4]$		148(IR)	

CHAPTER SIX

TUNGSTEN CHLORIDE PENTAFLUORIDE

CHAPTER 6. TUNGSTEN CHLORIDE PENTAFLUORIDE6.1 Introduction

Chapter three dealt with the spectra of octahedral anions typified by PtCl_6^{2-} . With most cations it was found that the spectra obeyed the normal octahedral selection rules. However, with the diphenyliodonium cation and sometimes with the tetraphenylarsonium cation the spectra (especially the infrared) were more compatible with C_{3v} site symmetry for the anion. Thus ν_1 became infrared active, ν_3 split and ν_6 the inactive mode was sometimes observed directly. The central metal atom in the anion still would have, however, six halogen atoms around it situated octahedrally. This 'apparent distortion' of the octahedron can be useful sometimes in helping make assignments. It is possible to achieve 'distortions' chemically by substituting a different halogen into the octahedron for one of the original halogens. If an atom X in MX_6 is replaced by a similar one Y then the symmetry of the octahedron is reduced to C_{4v} . The relaxation of selection rules for this symmetry group would help in making assignments for MX_5Y when compared with MX_6 .

No well established anionic complexes of the type $[\text{MX}_5\text{Y}]^-$ are known where both X and Y are halogens. The first neutral complex of this type made was SF_5Cl .¹⁰²

Woodward et.al.¹⁰³ assigned the complete vibrational spectrum of this molecule. All mention of SF₅Cl elsewhere in this Chapter (except where otherwise stated) refers to his work. The fundamentals assigned for this compound are given in table [6.1]. The modes associated with each ν_i ($i = 1, 2, \dots, 11$) will be given in the next section. The second example of a neutral MX₅Y molecule was prepared by Cohen et.al.¹⁰⁴ and was WF₅Cl. This system is sufficiently different from SF₅Cl to warrant a separate study. Considerable differences are to be expected in the spectra of the two molecules because sulphur and tungsten have a) entirely different atomic weights (32 and 184) and b) come from completely different parts of the periodic table. Samples of WF₅Cl were kindly supplied by Dr. G. W. Fraser.

6.2 Expected molecular vibrations.

For an octahedral molecule MX_6 the irreducible representation is :-

$$\Gamma = A_{1g} + E_g + 2F_{1u} + F_{2g} + F_{2u}$$

It is more convenient to separate the stretching vibrations from the deformation modes thus :-

$$\Gamma = A_{1g}(\nu_1) + E_g(\nu_2) + F_{1u}(\nu_3) + F_{1u}(\nu_4) + F_{2g}(\nu_5) + F_{2u}(\nu_6).$$

Using the correlation tables to transform from D_h to C_{4v} (via D_{4h}) one finds $A_{1g} \rightarrow A_1$, $E_g \rightarrow A_1 + B_1$, $F_{1u} \rightarrow A_1 + E$, $F_{2g} \rightarrow B_2 + E$ and $F_{2u} \rightarrow B_1 + E$. Thus for WF_6Cl the irreducible representation is

$$\Gamma = 3A_1(\nu_1, \nu_2, \nu_4) + B_1(\nu_3) + E(\nu_5) + A_1(\nu_6) + B_1(\nu_7) + B_2(\nu_8) + 3E(\nu_9, \nu_{10}, \nu_{11}).$$

The selection rules for C_{4v} symmetry require all modes except A_2 to be Raman active and all except the B modes to be infrared active. The infrared spectrum of WF_6Cl should therefore contain 8 fundamentals, 4 of which are stretches. All 11 fundamentals should be Raman active including the 5 stretching vibrations. The individual contributions to the irreducible representation of the

various stretches and deformations are : -

$$\Gamma \nu_{(W-F)} = A_1 (\nu_1)$$

$$\Gamma \nu_{(W-Cl)} = A_1 (\nu_3)$$

$$\Gamma \nu_{(WF_4)} = A_1 (\nu_2) + B_1 (\nu_5) + E (\nu_8)$$

$$\Gamma \delta_{(W-F)} = E (\nu_9)$$

$$\Gamma \delta_{(W-Cl)} = E (\nu_{11})$$

$$\Gamma \delta_{(WF_4)} = B_2 (\nu_7) + E (\nu_{10})$$

$$\Gamma \pi_{(WF_4)} = A_1 (\nu_4) + B_1 (\nu_6)$$

There are no redundancies in these representations since all eleven vibrations are accounted for. The approximate forms of these modes are shown in Figure [6.1]. In this Figure + indicates movement of an atom above the horizontal plane of the octahedron while - indicates the opposite.

6.3 Experimental.

The infrared spectra were measured on either a PE-225 or FS-520 interferometer. Above 400 cm^{-1} KBr windows and plates were used for the gas cell. The cold cell for this region used the same windows but the cold finger plate was made of AgCl. Below 400 cm^{-1} both gas cell and cold cell used polythene windows and plates.

The Raman spectrum of the liquid was measured with an LR-1 which uses He/ne laser excitation at 6328\AA using the cold cell designed by Dr. D. M. Adams, and described in Chapter 2. The temperature of the liquid was maintained at -25°C except when room temperature measurements were required.

The bands observed are listed in table [6.2] with their intensities and polarisation state if of medium intensity or stronger. Band contours are also shown. The assignment of fundamentals discussed in the next section are listed in table [6.3]; in cases of infrared and Raman coincidences the gas infrared figure is quoted. For convenience the ReF_6Cl assignment is given in the same table.

6.4 Infrared Spectrum of Gas.

This spectrum is shown in Figure [6.2a]. In the metal-fluorine stretching region three bands were observed; a medium strong one at 743 cm^{-1} definitely PQR with splitting 12.5 cm^{-1} , a very strong one at 703 cm^{-1} again PQR with splitting 13 cm^{-1} and a medium strong band at 667 cm^{-1} . This third band had an unusual shape looking like a normal PQR system with two Q branches. These three bands correspond to ν_1 , ν_2 , and ν_3 but not necessarily in this order. ν_1 is the axial tungsten fluorine stretch, A_1 mode, a parallel vibration which should therefore show PQR structure. ν_2 is the symmetric tungsten fluorine stretch involving the equatorial fluorine atoms, strictly this is an A_1 perpendicular vibration and should not exhibit PQR structure. ν_3 is the degenerate equatorial fluorine tungsten stretch, E mode and perpendicular. In SF_5Cl Woodward found $\nu_3 > \nu_1 > \nu_2$ but in WF_5Cl it is far more likely to find $\nu_1 \gg \nu_2 > \nu_3$. The breadth of the 667 cm^{-1} band compared to the other two suggest in fact that this is the E vibration. This mode is one of two stretches that involve tungsten atom movement and this should lower its frequency considerably compared to ν_1 and ν_2 . The analogous vibration in octahedral complexes is ν_3 the triply degenerate stretch. This would therefore also be expected to show considerable

central mass dependence. For SF_6 ν_1 is at 775 while ν_3 appears at 940 cm^{-1} ; in WF_6 ν_1 absorbs at 769 cm^{-1} but ν_3 is considerably lower at 712 cm^{-1} . Since the symmetric stretches (ν_1) in SF_6 and WF_6 are very similar it is reasonable to expect ν_2 in WF_5Cl to be close to that in SF_5Cl . ν_2 in SF_5Cl occurs at 703 cm^{-1} and therefore the 703 cm^{-1} band in WF_5Cl can also be assigned to ν_2 . In fact the description of this mode (symmetric equatorial fluorine-tungsten stretch) cannot be an exact one; such a vibration would not normally be expected to be infrared active but it is very difficult to construct a vibration of MX_5L that is (a) a stretching vibration, and (b) an A_1 mode, and therefore both Raman and infrared active. Both the axial stretches [$\nu(\text{M-X})$ and $\nu(\text{M-L})$] satisfy these conditions but three A_1 vibrations are required. It is possible that Coriolis interaction is interfering with the normal vibrations in WF_5Cl . This hypothesis is supported by the fact that the band assigned to ν_2 shows PQR structure (although it is a perpendicular vibration) and the band assigned to ν_3 also has a peculiar band shape. ν_1 should show a slight central atom mass dependence and would therefore be expected at lower frequency than 834 cm^{-1} , where it occurs in SF_5Cl . The PQR band at 743 cm^{-1} is therefore assigned to ν_1 .

The medium strong band at 400 cm^{-1} is assigned to ν_4 the tungsten chlorine stretching vibration. This is an A_1 parallel vibration and should exhibit PQR structure, but the only observed structure was attributable to Cl^{37} . In SF_5Cl ν_4 was assigned to a band at 404 cm^{-1} . This was not observed in the infrared because measurements only went to 500 cm^{-1} . It is not known therefore whether this band shows PQR structure or not. In ReF_5Cl the situation is reversed; the rhenium-chlorine stretch does show PQR structure while the rhenium fluorine stretches do not appear to show any structure at all. The very high position of the tungsten chlorine stretch will be considered later when the information given by the PQR splittings is also discussed. Supporting evidence that the 400 cm^{-1} band is due to the tungsten chlorine bond is indicated by the placing of the rhenium-chlorine stretch at 390 cm^{-1} .

The degenerate sulphur chlorine deformation $\nu_{11}(E)$ in SF_5Cl was assigned to the lowest band in the Raman spectrum at 270 cm^{-1} . The most reasonable band to assign to this vibration in WF_5Cl is at 228 cm^{-1} (medium strong). This is still 50 cm^{-1} higher than the deformation mode in $(\text{Et}_4\text{N})[\text{WCl}_6]$. The stretching mode is 80 cm^{-1} higher than in the above chloro tungstate. The best evidence for the

assignment of this band will be given in the discussion of the spectrum of the solid.

Three bands, 302 cm^{-1} (medium), 278 cm^{-1} (weak-medium) and 254 cm^{-1} (very strong) are left to assign. All occur in the metal fluorine deformation region. The infrared active bands expected are (a) ν_9 (E) the degenerate tungsten fluorine (axial) deformation, (b) ν_{10} (E) the degenerate in plane tungsten fluorine (equatorial) deformation and (c) ν_3 (A_1) the symmetric out of plane tungsten fluorine (equatorial) deformations. This last mode is the only parallel vibration and therefore the only one expected to show PQR structure. The only band that exhibits any shape is the one at 254 cm^{-1} which shows "residual" PQR structure but no definite splitting. This is assigned to ν_3 . This band should be quite low because it is an "out of plane" mode and all four fluorines approach the chlorine atom simultaneously. Woodward placed ν_3 in SF_5Cl at 600 cm^{-1} : this is quite reasonable considering that ν_4 in SF_6 occurs at 615 cm^{-1} . ν_4 in WF_6 occurs at 256 cm^{-1} . No help is given in deciding which of the remaining two bands is assigned to ν_9 and which to ν_{10} . In SF_5Cl Woodward (for no obvious reason) assigned ν_9 to a band at 579 cm^{-1} and ν_{10} to one at 442 cm^{-1} . Consideration of the modes involved

however suggest that it is more likely to find ν_{10} greater than ν_9 and tentatively the band at 302 cm^{-1} is assigned to ν_{10} and that at 278 cm^{-1} to ν_9 .

No bands were observed below 200 cm^{-1} , all infrared active fundamentals have been assigned in the gas phase spectrum but a number of bands were observed above 750 cm^{-1} . A weak medium band at 784 cm^{-1} is assigned to $2\nu_4$ (A_1). The four very weak bands observed above 1100 cm^{-1} are given the following tentative assignments :

- | | | | |
|----|------|-----------------|---|
| a) | 1180 | $\nu_1 + \nu_4$ | (A_1) |
| b) | 1238 | $2\nu_5$ | ($A_1 + B_1 + B_2$) |
| c) | 1330 | $2\nu_8$ | ($A_1 + B_1 + B_2$) |
| d) | 1395 | $2\nu_2$ | (A_1) or $\nu_2 + \nu_8$ (E) or $\nu_1 + \nu_8$ (E) |

6.5 Infrared Spectrum of Solid.

The spectrum is shown in Figure [6.2b]. The site symmetry of WF_6 in the solid phase has recently been shown to be C_1 . Thus the spectrum of WF_6 in the solid can be expected to be more complicated than the gas phase (or liquid) spectrum. Degenerate vibrations can be expected to split and Raman active frequencies should appear in the infrared. It is quite likely that the site symmetry of WF_6Cl will also be C_1 in the solid, or even lower, and that the same sort of complication in the infrared might reasonably occur.

The spectrum of the solid was taken at 77°K. A thin film of solid was obtained by condensing the vapour onto a cold finger. As expected all band shape normally attributed to PQR effects disappeared in the spectrum of the solid. The tungsten-fluorine stretching region was more complex than in the gas phase spectrum. The two bands observed in the gas phase spectrum above occurred at 734 and 704 cm^{-1} in the solid but with apparently reversed intensities. The 734 cm^{-1} band was in fact the most intense absorption in the entire spectrum while the 704 cm^{-1} band was only of medium intensity. This band at 704 cm^{-1} actually was part of a complex of absorptions between 705 cm^{-1} and 635 cm^{-1} , none of the features of

which were completely resolved. The band assigned to ν_8 at 667 cm^{-1} in the gas spectrum split into a doublet centred around 668 cm^{-1} in the solid. The two peaks occurred at 665 and 678 cm^{-1} and were of strong intensity and the splitting supports the assignment because ν_8 is an E-mode and would be expected to be resolved into two components in the solid spectrum. A new strong band appeared at 640 cm^{-1} and the most likely assignment of this band is ν_5 (B_1). This is one of the three Raman active bands that are not infrared active. This particular mode is out of phase stretching vibration of the equatorial fluorine atoms.

ν_4 , the tungsten chlorine stretch appeared at 390 cm^{-1} in the spectrum of the solid; there was still a shoulder on it in accordance with ^{37}Cl splitting. The bands assigned to ν_{10} and ν_9 in the gas phase spectrum appeared at 293 and 278 cm^{-1} respectively. The higher band was of medium intensity but the 278 cm^{-1} band was only weak. Both are degenerate vibrations and should show signs of splitting in the solid. The 293 cm^{-1} band was quite definitely split into a doublet and the 278 cm^{-1} band might have been split but it was too weak to be able to show splittings.

Below 250 cm^{-1} the bands seemed to have coalesced. The band at 254 cm^{-1} in the gas spectrum appeared only as a

medium band at 243 cm^{-1} in the solid. The metal chlorine wag (ν_{11}) was assigned to a band at 228 cm^{-1} in the spectrum of the gas. This is a degenerate vibration and should show some asymmetry in the solid spectrum. Two bands (not really describable as a doublet) were observed at 225 cm^{-1} and 209 cm^{-1} . The low frequency band was slightly more intense than the higher one. It is still probable however that these both originate from the E-mode and that unusual distortion effects account for the difference in intensity of the two bands.

No bands were observed either below 200 cm^{-1} or above 750 cm^{-1} . This supports the assignation of bands in the gas spectrum as combinations or overtones. This is quite important for the gas phase band at 784 cm^{-1} which might conceivably have been one of the tungsten-fluorine stretching vibrations.

6.6 Raman Spectrum of Liquid.

This spectrum is shown in Figure [6.2c].

In his study of SF_5Cl Woodward obtained generally very good agreement between the bands common to both the Raman and infrared spectra. This is perhaps slightly surprising because the infrared spectrum was obtained from a gas at room temperature while the Raman sample was a liquid held at -50°C . It would be reasonable to expect fairly large differences between the same band observed in both infrared and Raman when the two spectra were obtained from different physical states. The largest discrepancy that Woodward had to contend with was 20 cm^{-1} (834 Raman , 854 cm^{-1} infrared). Coincidence of the spectra of WF_5Cl are not as conclusive as in SF_5Cl but nevertheless the only satisfactory interpretation of the Raman data is a C_{4v} structure for WF_5Cl .

Above 700 cm^{-1} two bands (744 cm^{-1} vs, 703 cm^{-1}) were observed. Both were strongly polarised and this confirms the infrared assignments to the corresponding bands as ν_1 and ν_2 (both A_1) respectively. It is perhaps surprising that two A_1 modes can exist with such a small percentage difference of frequencies (5%) between them without interacting, and consequently becoming more widely separated. It is also interesting to note that the

intensities of ν_1 and ν_2 in the Raman spectrum are reversed in intensity compared with the gas spectrum in the infrared. A medium intensity band occurred at 661 cm^{-1} with a shoulder on the low frequency side at 644 cm^{-1} . Both the medium band and the shoulder appeared to be depolarised. The band at 661 cm^{-1} obviously corresponds to that attributed to ν_8 in the infrared at 667 cm^{-1} . No absorption at 644 cm^{-1} was observed in the infrared spectrum of the gas but an intense absorption occurred at 640 cm^{-1} in the infrared spectrum of the solid film. This band was tentatively assigned to ν_8 (B_1) the only Raman active stretch in the spectrum. It is surprising that it is so weak in the Raman but it is still the only reasonable assignment.

Two bands were observed around 400 cm^{-1} . A very strong feature occurred at 407 cm^{-1} while a medium intensity band absorbed at 377 cm^{-1} . The former band was clearly polarised while the second one was depolarised. The band at 407 cm^{-1} is clearly ν_4 (A_1), the metal-chlorine stretch. The first overtone of this band was also observed at 820 cm^{-1} ; this is also of class A_1 but was too weak to yield polarisation data. The band at 377 cm^{-1} is a new feature not present in the infrared spectrum of either the gas or solid. This band is one of the two remaining

B modes to be assigned (the first one assigned was the 644 cm^{-1} band). The description of these two modes are a) ν_6 (B_1) the in phase anti symmetric out of plane deformation of the equatorial fluorine atoms and (b), ν_7 (B_2) the scissors in plane deformation of the same fluorine atoms. Actually the terms 'in plane' and 'out of plane' have no real meaning in this molecule. In SF_5Cl Woodward found $\nu_7 > \nu_6$. The most similar modes of an octahedral molecule are ν_5 and ν_6 respectively. As expected here 'in plane' $\nu_5 >$ 'out of plane' ν_6 (in fact simple theory requires $[\nu_5/\nu_6]^2 = 2$). In WF_5Cl however the 'out of plane' B_2 mode involves movement of two fluorine atoms towards the bulky chlorine atom simultaneously. Thus it is quite likely that $\nu_6 \sim \nu_7$ or even $\nu_6 > \nu_7$. Thus no definite assignment is given to this band at 377 cm^{-1} ; it is either ν_6 (B_1) or ν_7 (B_2).

The medium strong band observed at 307 cm^{-1} which is depolarised is presumably ν_{10} the tungsten fluorine in plane deformation observed at 302 cm^{-1} in the infrared. Bands observed below 300 cm^{-1} were, with one noticeable exception, all weak and the exact maxima of these bands are sometimes doubtful. A shoulder was present on the low frequency side of the 307 cm^{-1} band at 290 cm^{-1} . This is probably ν_9 the tungsten fluorine wag observed at

278 cm^{-1} in the infrared spectrum of the gas. It is possible that this band could be ν_6 or ν_7 but unlikely considering the position of the other band assigned to ν_6 or ν_7 at 377 cm^{-1} . The strong features observed at 254 and 228 cm^{-1} in the gas infrared spectrum occurred at 257 and 227 cm^{-1} in the Raman. The 257 cm^{-1} band attributed to ν_3 should be polarised but it is too weak to take measurements on. The band at 227 cm^{-1} coincides with that in the infrared assigned to ν_{11} the tungsten chlorine wag.

A disturbing feature of the Raman spectrum was the appearance of two bands below 200 cm^{-1} , a weak one at 182 cm^{-1} and a medium strong feature, depolarised, at 123 cm^{-1} . The most difficult band to explain is the higher one at 182 cm^{-1} ; it is conceivable that it is the metal-chlorine wag ν_{11} and that the 228 cm^{-1} band is one of the metal fluorine deformation modes. There are several reasons however why this interpretation is unlikely. Perhaps the most important one is the absence of an absorption in the 1175-185 cm^{-1} region in the infrared. Also the complete set of fundamentals in the infrared have been assigned satisfactorily assuming the 227 cm^{-1} is in fact ν_{11} . This band splits in the spectrum of the solid sample and it is very unlikely that any other absorption

predicted for that region could split. The possible assignment of the 182 cm^{-1} band as the missing B mode (ν_8 or ν_7) is also unlikely.

The frequency quoted at 123 cm^{-1} for the strong band in that region was for a temperature of -25°C . At room temperature this band absorbs nearer 116 cm^{-1} . It is quite inconceivable that this absorption can be due to a fundamental internal vibration of the octahedron WF_5Cl . It is most unlikely also that it is due to a combination band between two other fundamentals because it is quite an intense absorption. A tentative assignment for this band in view of the marked temperature dependence is that it represents a "liquid lattice mode"; a vibration of the pseudo lattice that exists in many liquids. Such bands are known in the infrared spectra of liquids¹⁰⁸ but have not been reported previously for Raman spectra. Further work on this and related systems is obviously required before this tentative assignment can be confirmed.

6.7 Infrared Spectrum of rhenium chloride pentafluoride gas.

A sample of ReF_5Cl was kindly supplied by Dr. D. F. Stewart. This is an intense red liquid which is far more unstable than its tungsten analogue. Both the neat liquid and solutions of it in CFCl_3 were too intense in colour to yield Raman spectra. Sometimes the more intense bands due to CFCl_3 were actually observed but none due to ReF_5Cl were. The infrared spectrum of the gas was obtained however and thus will briefly be described.

In the metal-fluorine stretching region three bands were observed with the same sort of intensities as the tungsten analogues in WF_5Cl . These were at 732, 689 and 640 cm^{-1} and are attributed to ν_1 , ν_2 and ν_3 respectively. No PQR structure was observed for any of these bands. The reasons for the lowering of frequencies by 11, 14 and 27 cm^{-1} respectively for these three bands compared to WF_5Cl is presumably due to the presence of the extra electron on the rhenium atom. (W_5Cl is a d^0 system).

The rhenium chlorine stretching vibrations quite obviously occurred at 388 cm^{-1} ; this was a strong band with classic PQR structure and splitting 13 cm^{-1} . The first overtone of this was not observed in the spectrum

unlike WF_5Cl where $2\nu_4$ was observed.

The bands that occurred at 302 and 278 cm^{-1} in WF_5Cl were found at 330 and 278 cm^{-1} in ReF_5Cl . For the same reasons as with WF_5Cl these bands are assigned to ν_{10} and ν_9 respectively. The symmetric out of plane deformation of the ReF_4 system occurred at 250 cm^{-1} while the rhenium chlorine wag was found at 227 cm^{-1} .

6.8 Structural conclusions from the gas phase spectrum of WF_5Cl .

ν_3 the infrared active metal halogen stretch in potassium hexachlorotungstate(IV)²¹ occurs at 324 cm^{-1} , in the rubidium and caesium salts it appears at 308 and 306 cm^{-1} respectively. For tetraethylammonium hexachlorotungstate(V)²⁰ the corresponding band is at 329 cm^{-1} , 23 cm^{-1} higher than in the above caesium salt the cation of which NEt_4^+ is most comparable. It is not surprising to find ν_3 in $[WCl_6]^{2-}$ lower than in $[WCl_6]^-$. The extra negative charge increases the size of the anion giving a larger metal chlorine distance and hence a lower stretching frequency. This increase in size of an anion by the addition of negative charge is well known and X-ray evidence can be given in verification of it. No structure determinations are available for chlorotungstates but an almost comparable actinide system has had a crystal structure determination. In uranium hexachloride¹⁰⁶ the uranium-chlorine bond length is 2.42 \AA while in caesium hexachloroplutinate(IV)¹⁰⁷, $[Cs_2(PuCl_6)]$ the plutonium chlorine distance is 2.62 \AA . It is likely that the analogous uranium salt would leave an even larger bond length than the plutonium compound because ionic radii of uranium ions are slightly bigger than plutonium ions.

Preliminary work by R. G. Churchill in the department indicates that neutral tungsten hexachloride has ν_3 around 370 cm^{-1} . The bond length in solid WCl_6 ¹⁰⁸ is 2.26 \AA , presumably smaller than in the anionic chlorotungstates. ν_4 the tungsten chlorine stretch in WF_5Cl has been unambiguously assigned to a band at 400 cm^{-1} ; this assignation was supported by (a) the intensity of the band in both the infrared and Raman spectra, (b) the presence of the Cl^{37} isotope effect and (c) the polarisation data on this band. It was mentioned earlier that this position is almost exactly the same place where the sulphur-chlorine stretch occurs in SF_5Cl . This is most unexpected at first sight because sulphur only has an atomic weight of 32 compared to that of 184 in tungsten. This indicates that the tungsten-chlorine bond distance in WF_5Cl is considerably shorter than in WCl_6 .

Quantitative information can be gained from the band contours of the infrared gas spectrum. For symmetric molecules Gerhard and Dennison have shown that if the parallel moments of inertia are of the same order of magnitude as the perpendicular one then PQR structure can be expected for parallel vibrations.¹⁰⁹ This is the reverse of the case in linear molecules; there, molecules

do not have a moment of inertia parallel to the main axis and this causes parallel vibration to be of the type PR and perpendicular ones PQR. For heavy molecules the individual splittings in the P and R branches become so small that the structure of the outer branches collapse and appear just as broad contours. For such molecules the PR splitting $\Delta\nu$ is defined as the frequency separation between the two maxima of these contours. Gerhard has shown that with the knowledge of one of the two different moments of inertia of a symmetric molecule and the PR separation of a parallel band it is possible to calculate the unknown moment of inertia.

Suppose that the moments of inertia of a symmetric molecule are A, A and C. Assume that the parallel moment of inertia C is known. Define B such that $B = A/C - 1$ and therefore $A = C(B + 1)$. The relation between $\Delta\nu$ and A is:-

$$\Delta\nu = \frac{S(B)}{\pi Q} [KT/A]^{1/2} \quad [1]$$

Here Q is the velocity of light, K is the Boltzmann constant, and T is the absolute temperature.

Empirically, S(B) can be found to 0.5% accuracy by the relation :-

$$\log_{10} S(B) = .721/(B+4)^{1.13}, \quad [2]$$

this relation holding to this accuracy for the range $-0.5 \leq B \leq +100$. Substituting [2] in [1] and replacing A by $C(B+1)$ gives

$$\Delta\nu = \frac{10}{\pi Q} \left[.721/(B+4)^{1.13} \right] \cdot [KT/C(B+1)]^{1/2} \quad [3]$$

K, T, C, Q are known and $\Delta\nu$ can be measured. It is a simple matter to write a computer program to determine the value of B that gives the correct value of $\Delta\nu$. From the value of B, A can be calculated.

For WF_6Cl ν_1 the axial metal fluorine stretch occurs at 743 cm^{-1} with PQR splitting 12.5 cm^{-1} . The spectrum was obtained from the PE-225 and the temperature in the beam at 743 cm^{-1} was 35°C . C, the parallel moment of inertia in WF_6Cl is given by $C = 4 M_F R_{W-F}^2$ where M_F is the weight of the fluorine atom and R_{W-F} is the tungsten fluorine bond distance. The most recent determination¹¹⁰ of the tungsten fluorine bond distance in WF_6 is 1.826 \AA ; this value is probably very close to that in WF_6Cl and this value will be assumed in the calculations that follow. Taking the atomic weight of fluorine as 18.99, C is given by

$$C = 4 \times (19/6.023 \times 10^{23}) \times 1.826^2 \times 10^{-16} \text{ gm. cm}^2,$$

or $C = 420.7 \text{ g. cm}^2$.

The value of B which gives the required PQR splitting with the above value of C is .36. The perpendicular moment of inertia A is given immediately by $A = C(B+1)$ as 572.5 g. cm². In terms of the geometry of the molecule A is given by $A = 3M_F R_{W-F}^2 + M_{Cl} R_{W-Cl}^2$. The only unknown quantity in this equation is the tungsten-chlorine bond distance and this comes out to 2.10 Å. It is very difficult to quote the limits of accuracy of this figure but Woodward in his study of SF₆Cl was able to calculate a sulphur chlorine bond distance that was only .03 Å different from the more exact microwave calculations.¹¹¹ It is important to note that the value calculated above for the tungsten chlorine bond distance is 0.15 Å less than in WCl₆ but the sulphur chlorine distance in SF₆Cl is quite normal compared with the simple chlorides of sulphur.

The spectrum of the gas has therefore given two arguments to the fact that the tungsten chlorine bond distance is anomalously short. There is a third piece of evidence that indicates a short bond distance : WF₆Cl is a pale yellow liquid. Both SF₆ and WF₆ are colourless and so is SF₆Cl, the bond length of which is known to be normal. WF₆Cl is a d⁰ system and no colour is to be expected from tungsten(VI); it is probable therefore that the

tungsten-chlorine bond is partly double bonded and consequently imparting colour to the molecule. The rhenium analogue ReF_5Cl is a d^1 system and its deep red colour is not surprising.

In WF_5Cl presumably the very electronegative fluorine atoms withdraw electrons inductively from the tungsten atom. There will therefore be a greater electron density between the fluorine atoms and the tungsten atom than between the tungsten and chlorine atom. As mentioned above the tungsten atom is d^0 and can readily accept electrons into its d orbitals. Thus besides the normal σ bond between chlorine and tungsten there will probably be also a π -bond, the electrons of which are supplied by the chlorine atom.

FIGURE 6.1

Normal modes of an MX_5L molecule (symmetry C_{4v}).

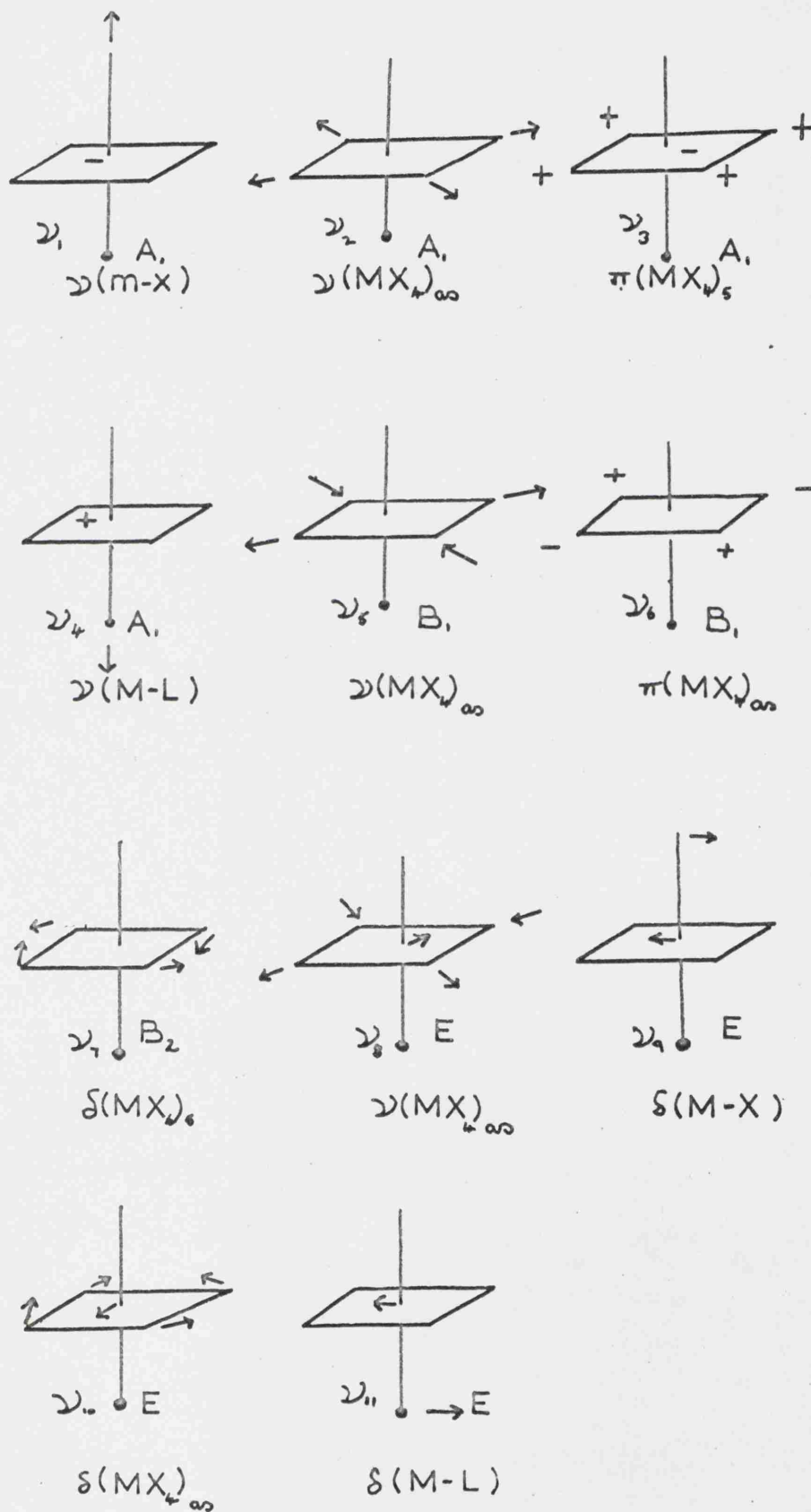


FIGURE 6.2
Vibrational spectra (750-200 cm^{-1}) of WF_5Cl .

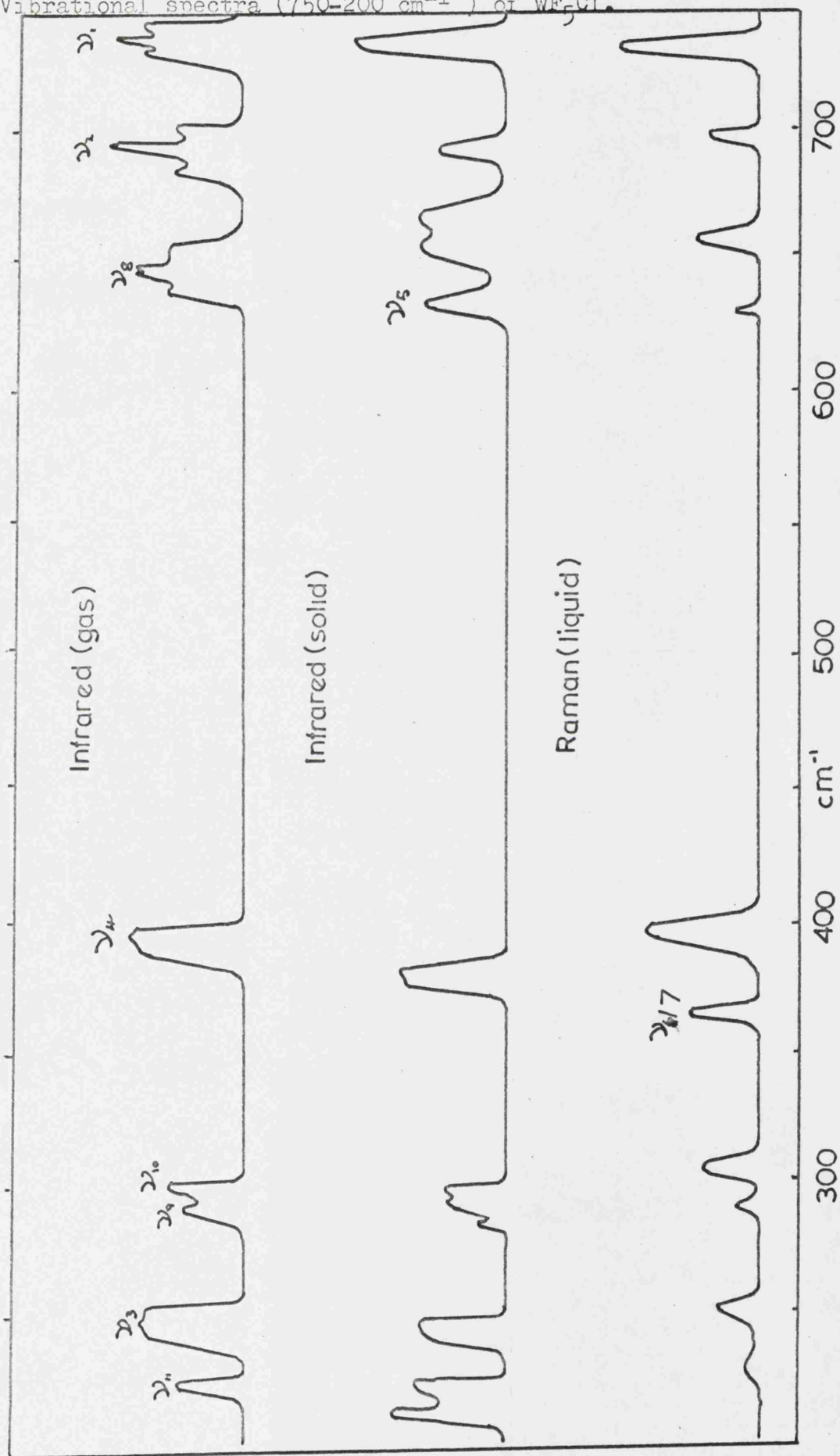


Table [6.1]

Fundamental vibrations of SF₅Cl

Frequency (cm ⁻¹)	Assignment
844	ν_1 (a ₁) axial SF stretch
704	ν_2 (a ₁) SF ₄ square stretch
600	ν_3 (a ₁) SF ₄ out of plane deformation
404	ν_4 (a ₁) S-Cl stretch
624	ν_5 (b ₁) SF ₄ square stretch
396	ν_6 (b ₁) SF ₄ out of plane deformation
504	ν_7 (b ₂) SF ₄ in plane deformation
916	ν_8 (e) SF ₄ square stretch
578	ν_9 (e) SF wag
442	ν_{10} (e) SF ₄ in plane deformation
211	ν_{11} (e) S-Cl wag

Table [6·2]

Observed bands in WF_5Cl in cm^{-1}

(a) Gas, infrared.

1395 (v.w), 1330 (v.w), 1238 (v.w), 1180 (v.w),
 784 (w.m), 743 (m.s) PQR, 703 (v.s) PQR,
 667 (m.s) "PQR", 400 (m.s), 302 (m), 278 (w.m),
 254 (v.s) "PQR", 228 (m.s).

(b) Solid, infrared.

743 (v.s), 704 (m), 671 (s), 640 (s), 390 (s),
 296 (m), 289 (m), 278 (w), 243 (m.s), 225 (m), 209 (m.s)

(c) Liquid, Raman.

820 (w), 744 (v.s) P, 703 (m) P, 661 (m) DP,
 644 (w), 407 (s) P, 377 (m) DP, 307 (m) DP,
 290 (w), 257 (w), 227 (w), 182 (w), 123 (m.s) DP.

Table [6.3]

Fundamental vibrations of WF_5Cl and ReF_5Cl

	WF_5Cl	ReF_5Cl
ν_1	743	732
ν_2	703	689
ν_3	254	250
ν_4	400	389
ν_5	644	-
ν_6	377 [⊗]	-
ν_7	377 [⊗]	-
ν_8	667	640
ν_9	278	278
ν_{10}	302	330
ν_{11}	228	227

[⊗] 377 band either ν_6 or ν_7 .

CHAPTER SEVEN

CUPRIC HALIDE-QUINOXALINE COMPLEXES

CHAPTER 7. CUPRIC HALIDE-QUINOXALINE COMPLEXES7.1 Introduction.

Copper(II) compounds have a d^9 configuration and provide one of the best opportunities for observing the Jahn-Teller effect. For a d^9 ion in would-be octahedral surroundings, appreciable distortions should occur, and for Cu(II) there are extensive data to bear this out. In all cases investigated so far it has been found that the distorted octahedron consists of two trans long bonds and four short ones. Generally analogous Zn(II) complexes, where the Jahn-Teller effect is inoperative, show expected undistorted octahedral or cubic structure. Also it is not always certain whether some square-planar copper(II) complexes are manifestations of extreme tetragonal distortions or not.

Because of these distortions the structures formed by copper(II) compounds are quite often rather novel. Quinoxaline and its derivatives form a series of compounds with copper(II) halides of varying stoichiometries and Dr. A. E. Underhill kindly provided samples of these for far-infrared study. It was expected that far-infrared investigation might provide pointers to the various

structures adopted. Before the infrared evidence is given the structure and spectra of the parent halides are discussed.

7.2 Structure and spectra of CuX_2 and CuX_2py_2 ($\text{X} = \text{Cl}, \text{Br}$).

It is usual to discuss together the structures of cupric and palladous chlorides. In both compounds the metal and halogen atoms form an infinite chain in which each metal atom is surrounded by four coplanar bridging halogen atoms.¹¹²

In PdCl_2 the Pd-Cl distance in the chain is 2.31 \AA and the angle between two chlorines and palladium is 87° ; CuCl_2 has almost identical parameters. Here, however, the similarity between the two structures ends because the chains pack in entirely different fashions. In PdCl_2 the chains are isolated, and the crystal structure is probably dominated merely by packing requirements. The chains in CuCl_2 are packed in such a way as to form secondary Cu-Cl bonds between the chains 2.95 \AA apart. Thus each copper atom has a tetragonally distorted array of six chlorine atoms around it. The next nearest chlorine atoms from palladium in PdCl_2 after those at 2.3 \AA are situated at the corners of a rectangle, which is perpendicular to the plane of the main chain, and 3.25 \AA array.

The infrared spectra of these compounds have been measured by Adams *et.al.*¹¹³ between 400 and 160 cm^{-1} . For PdCl_2 bands at $348, 340, 297, 187$ and 174 cm^{-1} were

observed. Only the 340 and 174 cm^{-1} frequencies were assigned, the former to $\nu(\text{Pd-Cl})$ and the latter to $\delta(\text{PdCl}_2)$. CuCl_2 appeared to have only two regions of absorption in the spectral range studied. The higher frequency band at 329 cm^{-1} was assigned to $\nu(\text{Cu-Cl})$ the stretching vibrations between the copper atoms, and chlorine atoms in the chain. No definite interpretation of the lower band at 277 cm^{-1} was given. Two suggestions were however put forward. The less likely one suggested that the unusually close proximity of the chains made infrared active a mode not normally active. This is unlikely since any relaxation of the selection rules would probably be reflected by the appearance of more than just one band in the region $400\text{-}160\text{ cm}^{-1}$. The second suggestion was that this band was due to the stretch of the long copper-chlorine bond. This is equivalent to interpreting this band as an "interchain mode". This latter description is more in keeping with the structure and was the one that was used in the tentative assignment of this band.

The assignation of a band to a 'long bond' stretch has not been completely accepted but nevertheless several workers have successfully based interpretations of the spectra of copper halide complexes on this assumption.

For example Goldstein et.al.¹¹⁴ examined a series of compounds derived from the parent ion CuCl_2py_2 . This compound also has an infinite chain structure but each copper atom has two trans pyridine groups attached such that the N-Cu-N axis is normal to the chain. The chain is distorted in such a way that the chlorine bridges are unsymmetrically placed between the copper atoms. This is illustrated in Figure [7.1]. Thus the environment of each copper atom is that of six ligands arranged around it at the vertices of a distorted octahedron. The published far-infrared data for CuX_2py_2 ($X = \text{Cl}, \text{Br}$) is shown in table [7.1]. For the chloride the bands at 287 and 229 cm^{-1} were attributed to the short and long bond stretches respectively. This data will be discussed in a later section.

7.3 Extant data on quinoxaline complexes of copper(II)

The complex $\text{CuCl}_2 \cdot \text{py}_2$ has been known since 1888¹¹⁵ but only recently have the complexes formed between copper(II) and other heterocyclic bases been extended. In 1961 the complexes between copper halides and pyrazines were first described¹¹⁶. These complexes were generally polymeric containing both halogen and pyrazine bridges. They were however usually unstable, and investigation of them was difficult, being easily reduced to the copper(I) state.

Recently Underhill¹¹⁷ formed complexes between either quinoxaline (Q) or substituted quinoxalines and copper(II) seemingly analogous to those formed by pyrazine. The stoichiometry and properties of these complexes were heavily affected by the number and nature of substituents on the quinoxaline ligand. The structure and numbering of the atoms in the quinoxaline molecule is shown in Figure [7.2].

Quinoxaline and 2,3 dimethylquinoxaline (Dmq) formed complexes of the type QCuX_2 while 2 methylquinoxaline (mq) and 2,3 diphenylquinoxaline (Dpq) formed species with stoichiometry C_2CuX_2 (X = Cl, Br). Reflectance spectra of these complexes suggested that they fell in two groups.¹¹⁸ The evidence indicated that the spectra of QCuCl_2 and

(mq)₂CuCl₂ were similar to each other and also to (py)₂CuCl₂, while the spectra of DmqCuCl₂ and (Dpq)₂CuCl₂ were also similar to each other. This indicated that while the first two compounds were probably polymeric the second two were not and were possibly just monomers with lower co-ordination numbers around copper. This was confirmed with molecular model studies which showed that the methyl and phenyl substituents on quinoxaline had profound steric effects. Thus the model of Mq showed that the N atom adjacent to the methyl group could not approach as close as the observed Cu-N distance (2.0 Å) in CuCl₂py₂ without some steric hindrance between the hydrogen atoms of the methyl group, the 8-H atom of the quinoxaline, and the chlorine atom of the chain. Models involving quinoxaline itself showed that this was able to form an analogous complex to CuCl₂(py)₂ and in addition was able to co-ordinate with both nitrogen atoms. Both Dmq and Dpy were unable to approach copper atoms joined to short Cu-Cl bonds but were able to co-ordinate to copper atoms joined to two long Cu-Cl bonds.

7.4 Infrared evidence.

(a) Copper-Halogen frequencies. The far-infrared frequencies of Q, Mq, Dmq, Dpq, QCuX_2 , $(\text{Mq})_2\text{CuX}_2$, DmqCuX_2 and $(\text{Dpq})_2\text{CuX}_2$, (X = Cl, Br) are shown in tables [7.2a] and [7.2b] with possible assignments. The spectra of the dmq series is also shown in Figure [7.3]. The spectra of $\text{CuX}_2(\text{py})_2$ (X = Cl, Br) measured by Goldstein are given in table [7.1] with his assignments.

As mentioned above it is not known for certain whether the long Cu-X "bonds" give rise to a stretching frequency, even in those cases in which ultraviolet spectra clearly indicate the presence of a tetragonal crystal field. Whereas palladous chloride was seen to exhibit only one band due to Pd-Cl stretching, copper(II) chloride was seen to have two, viz., 329, 277 cm^{-1} . The suggestion that the lower of these bands was possibly associated with the long Cu-Cl bond led to an analogous interpretation of the spectrum of $\text{CuCl}_2(\text{py})_2$ although here both frequencies were very low, viz., 287, 229 cm^{-1} . What is certain is that since all halogen atoms in the cupric halides are in bridging positions, any Cu-Cl or Cu-Br frequency higher than those of the cupric halides are associated with Cu-Cl or Cu-Br terminal bonds. This criterion clearly indicates that the complexes DmqCuX_2 and

(Dpq)₂CuX₂ have terminal Cu-X bonds. Thus they have bands assignable to ν (Cu-X) (terminal) at 368 and 345 cm⁻¹ respectively in the chlorides and at 278 and 269 cm⁻¹ in the bromides. Furthermore, the next lowest X-sensitive bands in their spectra are at comparable positions (156,44 X = Cl, and 105,98 cm⁻¹ X = Br), though much lower than those of QCuX₂ and (Mq)₂CuX₂. This can be taken as good evidence that the two pairs of complexes have different structures. Since the QCuX₂ and (Mq)₂CuX₂ only have apparently bridging (Cu-X) it is likely that these are both halogen bridged polymeric species. The bridging frequencies are in fact very close to those in the parent copper halides. The absence of bridging frequencies in the Dmq and Dpq series imply that these are probably monomeric or at least cannot be polymeric with halogen bridges. Polymeric species involving bridging quinoxalines cannot yet be discounted.

The variation of the lower X-sensitive frequencies (i.e. those less than 220 cm⁻¹) can be explained by postulating varying amounts of Cu-X long-bond interaction. If square-planar molecules CuX₂L₂ are so packed in the crystal that long Cu-X bonds can be formed giving the metal atom a distorted octahedral environment of four short and two long bonds, then the in-plane and out-of-plane

deformation modes, $\delta(\text{CuX}_2)$ and $\pi(\text{CuX}_2)$, will both be raised in frequency as the strength of the Cu-X long bond is increased. At the same time, $\nu(\text{Cu-X})$ values should drop as the halogen atoms take on more bridging character; this is exactly the observed trend. Thus the Q and Mq complexes for which long Cu-X bonds are postulated have $\delta(\text{CuX}_2)$ around 190 cm^{-1} (X = Cl) and 140 cm^{-1} (X = Br) while the corresponding bands in the Dmq and Dpq series are near 150 and 100 cm^{-1} respectively. Also $\pi(\text{CuCl}_2)$ is observable in both the Q and Mq compounds (near 95 cm^{-1}) while only the Dmq complex has the comparable band observable and is below 90 cm^{-1} .

(b) $\nu(\text{Cu-N})$ and Internal Vibrations of the Ligands.

Each of the organic ligands has in-plane and out-of-plane skeletal deformation modes which may be at frequencies down to about 150 cm^{-1} although they may not necessarily be infrared active in the free ligand. Thus, it is quite likely that an in-plane vibration will interact with stretching of the copper nitrogen bonds, giving rise to delocalised normal modes; i.e. it may not be correct to assign any one band to $\nu(\text{Cu-N})$ alone. There are further complications; for the ligands Q and Dmq, which it is suggested co-ordinate through both nitrogen atoms, changes

in position and intensity of the internal modes seem probable, whilst for D_{pq} the loss of symmetry consequent upon coordination through just one nitrogen atom would cause four, previously inactive, out-of-plane skeletal modes to become infrared active. For Mq , which is less symmetric anyway than D_{pq} , neither of these complications should arise.

The general features of the spectra confirm the above predictions. In the Mq complexes, the ligand modes can be clearly identified at approximately the same frequencies and relative intensities in $(Mq)_2CuX_2$. These occur near 135, 180, 285 and 300 cm^{-1} . Apart from the bands and the X-sensitive ones there is one X-insensitive band (208, X = Cl; 200, X = Br) not present in the ligand spectrum, and this is maybe associated with $\nu(Cu-N)$. In the compounds $DmqCuX_2$, the ligand spectrum is considerably modified; in particular, a band at 166 cm^{-1} is shifted slightly and reduced to low intensity, whilst a band at 278 cm^{-1} appears to be shifted about 60 cm^{-1} to the long-wavelength side. Alternatively, the band around 220 cm^{-1} could be $\nu(Cu-N)$; it would then be assumed that the 278 cm^{-1} ligand band is of vanishingly small intensity in the complexes.

For the quinoxaline complexes, similar changes occur, although here there are X-insensitive bands which do not

originate in the ligand spectrum. Tentatively the bands at 246 (X = Cl) and 244 (X = Br) are assigned to $\nu(\text{Cu-N})$.

Although the spectra of Dpq and its compounds are complex, they are particularly valuable in that they enable one to place, quite clearly, an upper limit about 220 cm^{-1} on any mode involving $\nu(\text{Cu-N})$ where the substituted quinoxaline complexes are considered.

(c) Conclusions. The above evidence, taken as a whole, suggests that in these complexes there is absorption in the region $200\text{--}250 \text{ cm}^{-1}$ which is associated, at least in part, with $\nu(\text{Cu-N})$ motion. This range extends a little below that found by Goldstein et.al. for substituted pyridine complexes, and may be taken as additional support for the above assignments, as a simple mass effect would cause a shift in this direction.

From the X-sensitive frequencies, a consistent explanation is offered of the results, which requires that C and Mq complexes have similar structures in which there is appreciable "Cu-X long bond" interaction, whilst in the Dmq and Dpq complexes there is no such association involving the halogen atoms.

7.5 General discussion.

The evidence of the far-infrared spectra taken in conjunction with the reflectance spectra and molecular model studies leads to the following structural conclusions.

(a) The complexes $QCuX_2$. The far-infrared spectra of these pair of compounds are very similar to those reported for $CuX_2(py)_2$. To account for this, and the different stoichiometry of the Q complex, it is easiest to postulate bridging quinoxaline molecules as well as bridging halogens. Thus the structure is most likely to be a two dimensional network as shown in Figure [7.4].

(b) The complexes $(Mq)_2CuX_2$. The reflectance spectra again suggested that these complexes were similar to the analogous pyridine complexes and in this case the same stoichiometry was found. This is supported by the far-infrared spectra, which indicate bridging rather than terminal halogens. Since the molecular models indicated steric hindrance at the 1-N atom when this is coordinated to a copper atom, which is itself joined to a bridging halogen atom, it is likely that an entirely analogous structure to CuX_2py_2 is

adopted with coordination through the 4-N atom.

This is illustrated in Figure [7.5].

(c) The complexes $DmqCuX_2$. Reflectance spectra suggested that these complexes were either square-planar or very strongly tetragonally distorted octahedral coordination around the copper atom but did not therefore distinguish between these two possibilities. The far-infrared spectra showed the presence of terminal halogens only and a different structure to $CuX_2 \cdot py_2$. To account for these facts and the stoichiometry it is required to postulate bidentate coordination by Dmq with the resulting polymeric structure shown in Figure [7.5].

(d) The complexes $(Dpq)_2CuX_2$. Bidentate coordination by Dpq is impossible in this case and the reflectance spectra indicated a square planar system. This is entirely supported by the far-infrared spectra which showed the presence of terminal halogens only. Also the presence of only one $\nu(Cu-X)$ frequency suggests a trans rather than cis configuration. It also rules out a tetrahedral configuration. The structure postulated for this is indicated in Figure [7.5].

The complexes described here show that 2-substituents on a ligand can have a very significant effect on the structure of a complex. Apparently complexes of cobalt(II) and nickel(II) halides with these ligands form a much more limited range of structures. The facility with which copper(II) halides form these complexes is therefore probably due to the preference of the copper(II) ion for a distorted octahedral or square-planar environment, which will reduce steric effects due to the 2-substituent.

Epilogue.

Since this work was completed, P. J. Lock¹¹⁹ of this department has made an extensive study of chloro and bromo complexes of copper. He has concluded that spectra of copper(II) complexes can be explained without the need to postulate "long Cu-X bonds". In cases where two stretching frequencies have been observed in the ν (Cu-X) region he has described these as both belonging to internal stretching modes of a chain. Whether this description is correct or not the structural conclusions found above will not be affected. Although the mechanism of assignation of the individual bands may be wrong the majority of assignments will still stand.

FIGURE 7.1

Structure of CuX_2py_2 .

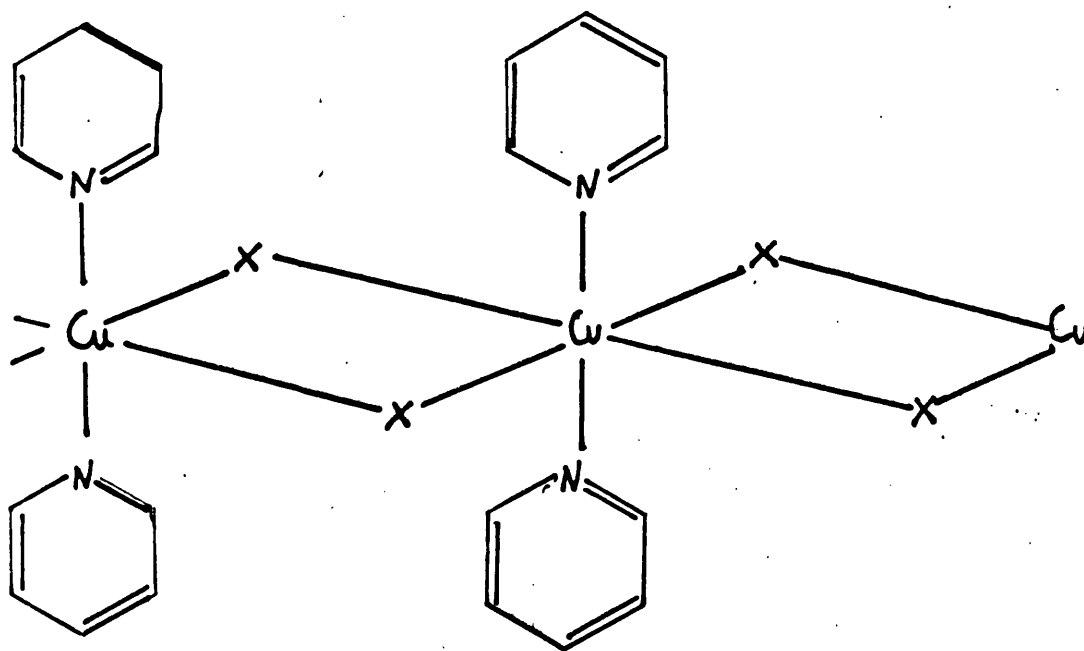


FIGURE 7.2

Conventional numbering of the quinoxaline ring.

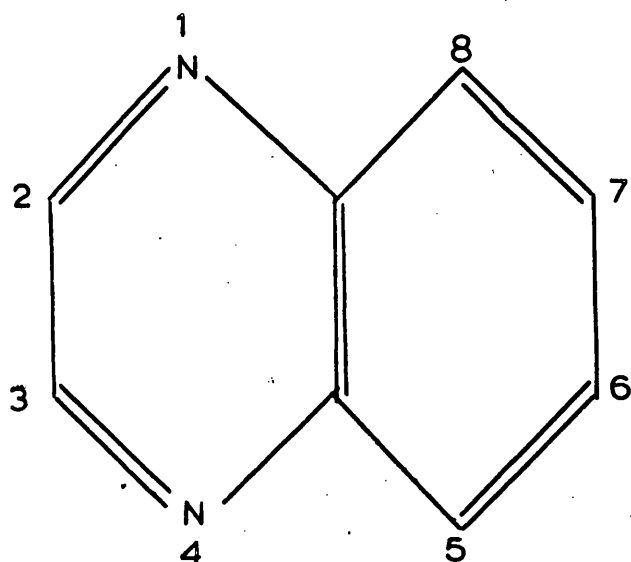


FIGURE 7.3
Far-infrared spectra of $(dmq)CuX_2$, ($X = Cl, Br$), and dmq .

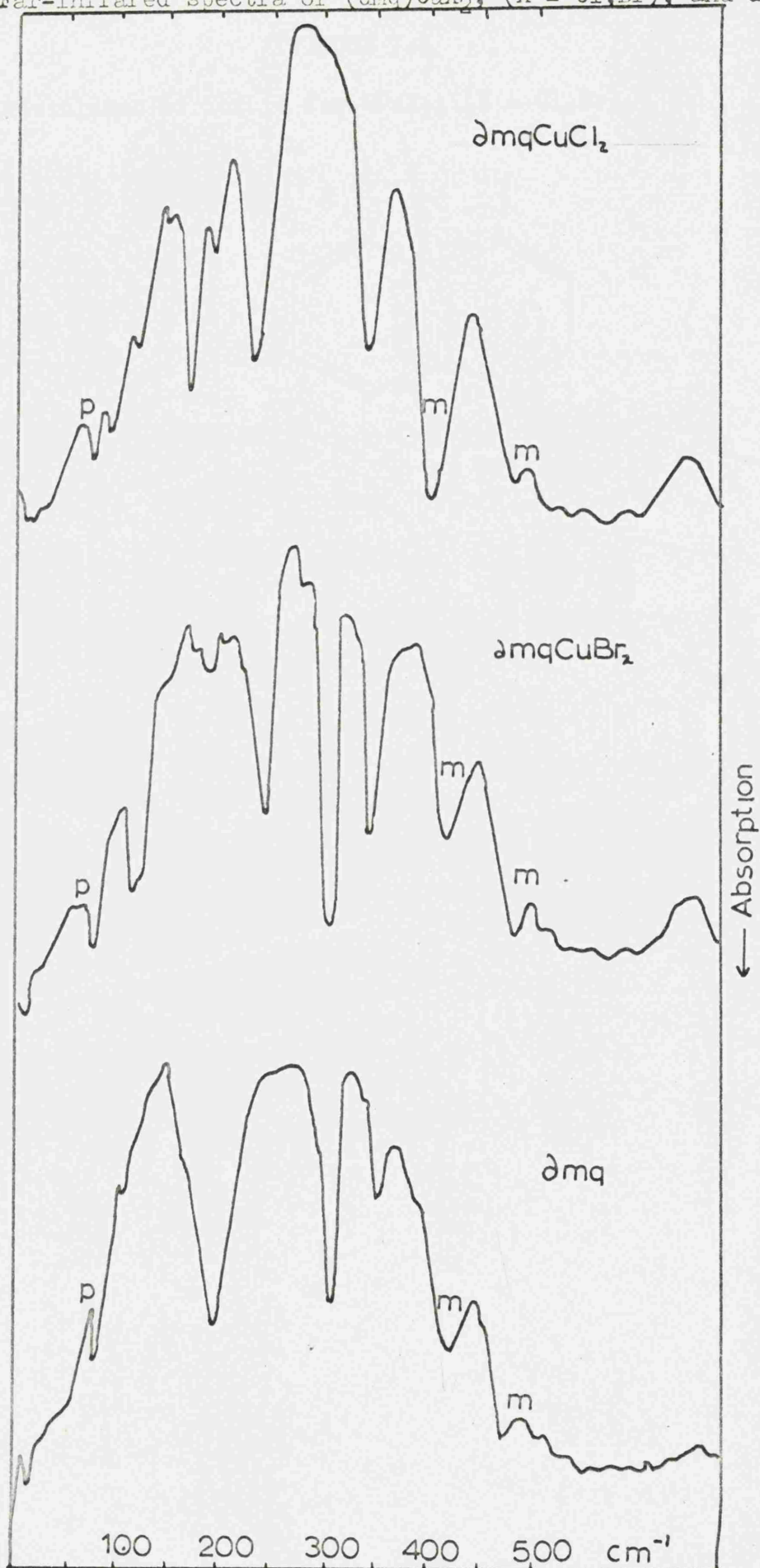


FIGURE 7.4

Postulated structure for $QCuX_2$, ($X = Cl, Br$).

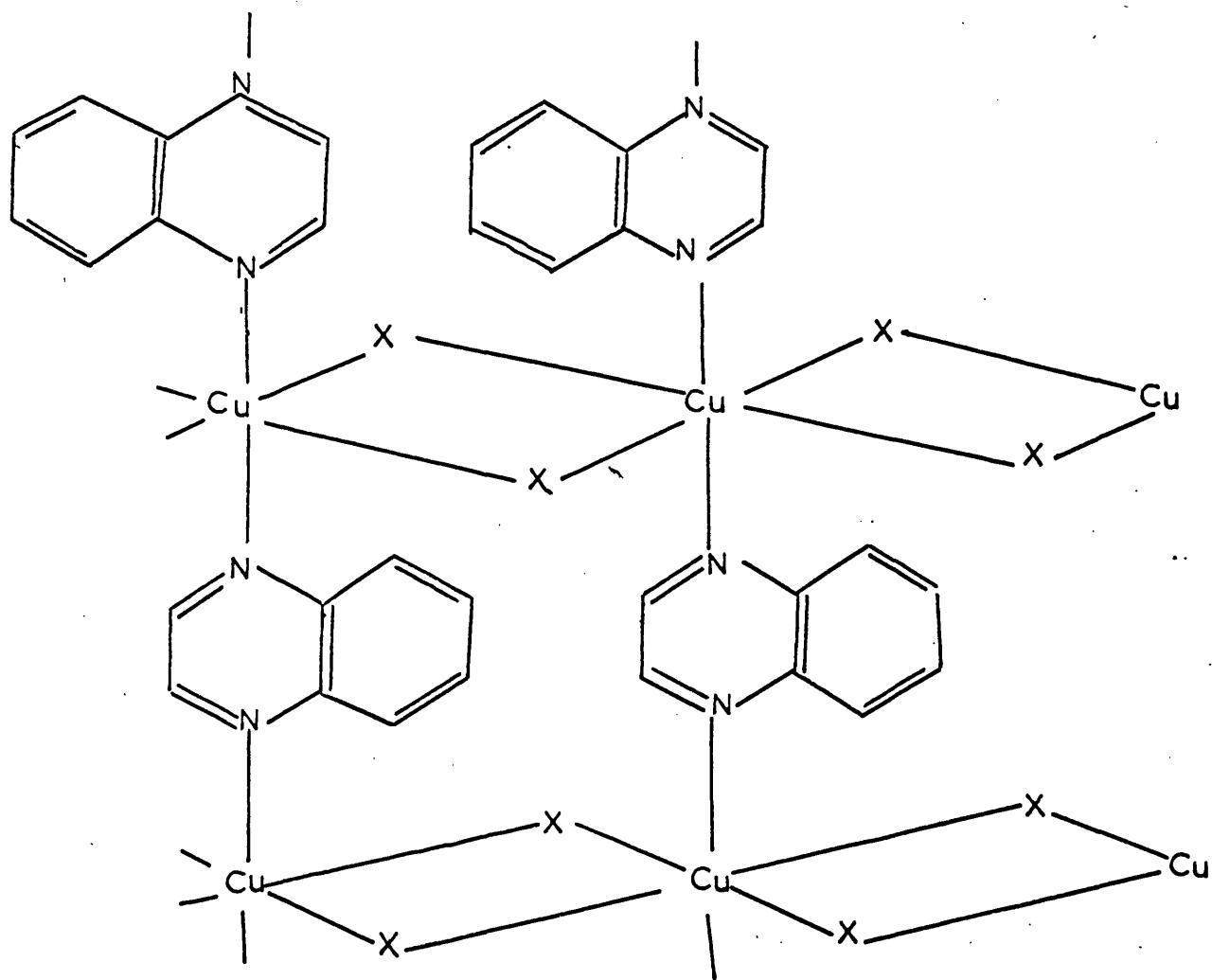
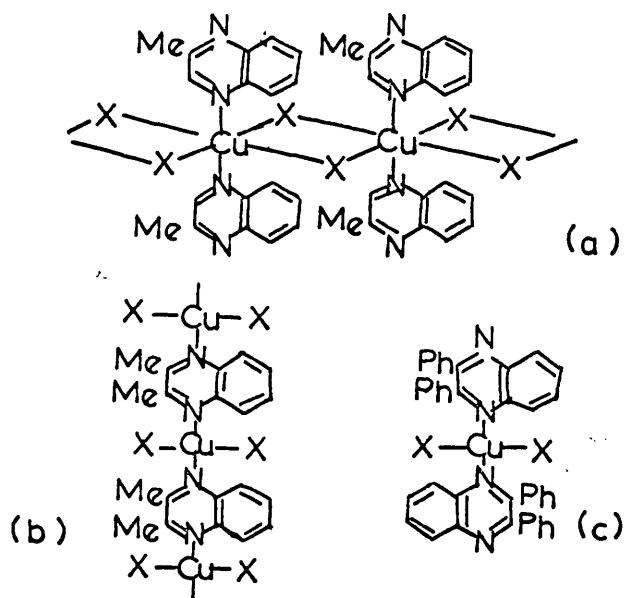


FIGURE 7.5

Postulated structures for $(mq)_2CuX_2$, $(\partial mq)CuX_2$,
and $(\partial pq)_2CuX_2$, (X = Cl, Br).



(a) $(mq)_2 CuX_2$

(b) $(\partial mq) CuX_2$

(c) $(\partial pq)_2 CuX_2$

Table 7.1

(Cu-X) and (Cu-N) vibrations of CuX_2PY_2 (X = Cl, Br) (cm^{-1}).
(from ref. 114).

	CuCl_2PY_2	CuBr_2PY_2
$\nu(\text{Cu-X})$	287 229	256 204
$\delta(\text{Cu-X})$	177	132
$\nu(\text{Cu-N})$	266	268
$\delta(\text{Cu-N})$	200	196
$\pi(\text{Cu-X})$	90	60

Table [7.2a].

Far-Infrared Absorption Frequencies (cm^{-1}) of some
Cu(II) Quinoxaline Complexes in the Solid State

CuX ₂ Q			CuX ₂ (mQ) ₂		
Q	X = Cl	X = Br	mQ	X = Cl	X = Br
	88 w	88 w			
	98 m			90.5	
	129 m	115 w		107 sh	102 s
	147 m	141 ush			
	180 vs	138 m		217 m	132 m
184 s	172 ush	172 s			
			137 m	138 m	139 m
205 sh	195 ush	193 w	188 vs	173 m	181 m
	220	211 w			
	246 s	244 sh		208 sh	200 s
			276 vs	286 m	294 s
			293 sh	300 sh	305 sh
	324 vs	255 s		320 s	252 s
		274 w			

† tentative assignments

ush = unresolved
shoulder

Table [7.2b].

CuX ₂ (dmQ)			CuX ₂ (dpQ) ₂			
dmQ	X = Cl	X = Br	dpQ	X = Cl	X = Br	
	88 m	-				$\pi(\text{Cu-X})^{\dagger}$
	110 w	112 sh				
	139 w	137 w	97 w	115 w	110 w	
	156 s	106 m		144 sh	98 m	$\delta(\text{Cu-X})$
166 s	178 w	176 w		138 m	139 m	
				168 m	165 m	
				194 sh	188 m	
			192 s	202 m	201 m	
	214 s	220 s		217 s	220 s	$\chi(\text{Cu-N})^{\dagger}$
278 s			307 m	298 ush	298 w	
320 m	315 s	315 s	332 m	315 m	317 m	
	368 vs	278 vs		337 s	269 s	$\nu(\text{Cu-X})$
			360 s	345 ush	349 m	

REFERENCES

REFERENCES

- 1 M.J.E. GOLAY, Rev. Sci. Inst., 1947,18,357.
- 2 H.M. RANDALL, J.Opt.Soc.Am., 1954,44,97.
- 3 R.W. WOOD & A. TROWBRIDGE, Phil.Mag., 1910,20,770.
- 4 H.A. GEBBIE & G.A. VANASSE, Nature, 1956,178,432.
- 5 A. MICHELSON, Phil.Mag.Ser., 1891,31,256.
- 6 H. RUBENS & R.W. WOOD, Phil.Mag., 1911,21,249.
- 7 P. FELLGETT, J.Phys.Radium, 1958,19,187.
- 8 J. CONNES, Rev.Optique, 1961,40,45.
- 9 ibid., 1961,40,116.
- 10 ibid., 1961,40,171.
- 11 ibid., 1961,40,231.
- 12 D.M. ADAMS & H.A. GEBBIE, S.A., 1963,19,925.
- 13 P.L. RICHARDS, Applied Optics, 1965,4,111.
- 14 C.H. PERRY, R. GEICK, & E.F. YOUNG, Applied Optics, 1966,5,1171.
- 15 D.M. ADAMS, S.A., 1962,18,1039.
- 16 J.B. CORNELL, Ph.D. thesis,Leicester, 1967.
- 17 K. LIVINGSTON, Private Communication.
- 18 D.M. ADAMS, Proc. Chem. Soc., 1961,335.
- 19 L.A. WOODWARD & J.A. CREIGHTON, S.A., 1961,20,711.
- 20 D.M. ADAMS, J. CHATT, J.M. DAVIDSON, & J. GARRATT, J., 1963,2189.
- 21 D.M. ADAMS, H.A. GEBBIE, & R.D. PEACOCK, Nature, 1963,199,278.
- 22 K.W. BAGNALL, D. BROWN, & J.G.H. du PREEZ, J., 1964,2603.
- 23 K.W. BAGNALL & D. BROWN, J., 1964,3021.

- 24 J. HIRAISHI, I. NAKAGOWA, & T. SHIMANOUCI, S.A.;
1964,20,819.
- 25 I.R. BEATTIE, G.P. McQUILLAN, L. RULE, & M. WEBSTER,
J., 1963,1514.
- 26 L.A. WOODWARD & M.J. WARE, S.A., 1963,19,775.
- 27 M.Le POSTELLOC, J.P. MATHIEU, & H. POULET, J., Chim.Phys.,
1963,60,1319.
- 28 N.N. GREENWOOD & B.P. STRAUGHAN, J(A)., 1966,962.
- 29 I.R. BEATTIE, T. GILSON, K. LIVINGSTON, V. FAWCETT, &
G.A. OZIN, J(A)., 1967,712.
- 30 D.H. BROWN, K.R. DIXON, C.M. LIVINGSTON, R.H. NUTTALL, &
D.W.A. SHARP, J(A)., 1967,100.
- 31 T.W. SPIRO, Inorg.Chem., 1967,6,569.
- 32 O. REDLICH, T. KURTZ, & P. ROSENFELD, J.C.P., 1934,2,619.
- 33 L.A. WOODWARD & L.E. ANDERSON, J., 1957,1284.
- 34 J.A. CREIGHTON & L.A. WOODWARD, T.F.S., 1962,58,1077.
- 35 L.A. WOODWARD & J.A. CREIGHTON, S.A., 1961,17,594.
- 36 L.A. WOODWARD & M.J. WARE, 1964,20,711.
- 37 L.A. WOODWARD & M.J. TAYLOR, J., 1960,4473.
- 38 E.B. WILSON, J.C. DECIUS, & P.C. CROSS, "Molecular
Vibrations", McGraw-Hill, 1955.
- 39 N. BJERRUM, Verhandl.Dent.Physik.Ges.,1914,16,737.
- 40 D.M. DENNISON, Phil.Mag.,1926,1,195.
- 41 H.C. UREY & C.A. BRADLEY, Phys.Rev., 1931,38,1969.
- 42 E. ADRIAN & T.N. MARGULIS, Inorg.Chem., 1967,6,210.
- 43 A.SABATINI, L. SACCONI, & V. SCETTINO, Inorg.Chem.,
1964,3,1775.
- 44 S. ABRAMOWITZ & I.W. LEVIN, Inorg.Chem., 1967,6,538.

- 45 R.A. ROBINSON & R.H. STOKES, "Electrolyte Solutions", Butterworths, 1959.
- 46 R. KLEMENT, Z.Anorg.Chem., 1927, 164, 195.
- 47 A.F. WELLS, "Structural Inorganic Chemistry", Oxford, 1962.
- 48 R.J. GILLESPIE & R.S. NYHOLM, Quart.Rev., 1957, 11, 339.
- 49 J.L. HOARD & B.N. DICKENSON, Z.Krist., 1933, 84, 436.
- 50 G.ENGEL, Z.Krist., 1935, 90, 341.
- 51 E.E. AYNSLEY & A.C. HAZELL, Chem.& Ind., 1963, 611.
- 52 I.D. BROWN, Canad.J.Chem., 1964, 42, 2758.
- 53 R.W.G. WYCKOFF, "Crystal Structures", Interscience, 1965.
- 54 D.M. ADAMS & P.J. LOCK, J(A)., 1967, 145.
- 55 N.N. GREENWOOD, B.P. STRAUGHAN, & A.E. WILSON, J(A)., 1966, 1479.
- 56 G.C. HAYWOOD & P.J. HENDRA, J(A)., 1967, 643.
- 57 J.W. GEORGE, N. KATSAROS, & K.J. WYNNE, Inorg.Chem., 1967, 6, 903.
- 58 D.S. URCH, J., 1964, 5775.
- 59 R. RIPON & R. PALADE, Ann.Sci.Univ.Jassy, 1948, 30, 155.
- 60 W.E. HATFIELD, R.C. FAY, C.E. PFLUGER, & T.S. PIPER, J.A.C.S., 1963, 85, 265.
- 61 A.BELLANCA, Periodico Mineral, 1947, 16, 73.
- 62 ibid., 1948, 16, 199.
- 63 P.C. MOEWS, Inorg. Chem., 1966, 5, 5.
- 64 J. LEWIS, R.S. NYHOLM, & G.A. RODLEY, J., 1965, 1483.
- 65 D.T. CROMER & R.K. KLINE, J.A.C.S., 1954, 76, 5282.
- 66 T. KAATZ & M. MARCOVICH, Acta Cryst., 1966, 21, 1011.

- 67 L.P. LINDERMAN & M.K. WILSON, Z.Physik.Chem., 1956,2,29.
- 68 "Inorganic Syntheses", Volume 2, 1946.
- 69 K. NAKAMOTO, "Infrared Spectra of Inorganic and Co-ordination Complexes", Wiley, 1963.
- 70 G. HERZBERG, "Infrared and Raman Spectra of Polyatomic Molecules", Van Nostrand, 1945.
- 71 H. POULET, P. DELORME, & J.P. MATHIEU, S.A., 1964,20,1855.
- 72 W. THEILACKER, Z.Anorg.Chem., 1937,234,161.
- 73 D.M. ADAMS, J., 1964,1771.
- 74 J. HIRAIISHI & T. SHIMANOUCI, S.A., 1966,22,1483.
- 75 MAGNUS, Pogg.Ann., 1828,14,204.
- 76 JØRGENSEN & SORENSEN, Z.Anorg.Chem., 1906,48,441.
- 77 E.G. COX, F.W. PINKARD, W. WARDAW, & G.H. PRESTON, J., 1932,2527.
- 78 S. YAMADA, J.A.C.S., 1951,73,1579.
- 79 M. ATOJI, J.W. RICHARDSON, & R.E. RUNDLE, J.A.C.S., 1957,79,3017.
- 80 J.R. MILLER, J., 1961,4452.
- 81 ibid., 1965,973.
- 82 P. DAY, A.F. ORCHARD, A.J. THOMSON, & R.J.P. WILLIAMS, J.C.P., 1965, 42,1973.
- 83 M. BUKOVSKA & M.A. PORAI-KOSHITS, Kristallografiya, 1960,5,137.
- 84 P. DAY, A.F. ORCHARD, A.J. THOMSON, & R.J.P. WILLIAMS, J.C.P., 1965,42,3763.
- 85 R.J.H. CLARK & C.S. WILLIAMS, J(A)., 1966, 1425.
- 86 D.M. ADAMS & D.M. MORRIS, Nature, 1965,208,1973.
- 87 P.J. HENDRA, Nature, 1966,212,179.

- 88 W.P. GRIFFITHS, Private Communication.
- 89 TSHUGAEV, J., 1915,1247.
- 90 R.J. MEYER, Z.Anorg.Chem.,1900,24,321.
- 91 G.J. SUTTON, Austral. J.Chem., 1958,11,120.
- 92 F.Y. KULBA, V.E. MIRONOV, C. TSUNG, & Z.G. FILIPPOVA, Zh.Neorgan.Khim., 1962,8,672.
- 93 F.A. COTTON, B.F.G. JOHNSON, & R.M. WING, Inorg.Chem., 1965,4,502.
- 94 T. WATANABE, Y. SANTO, R. SHIONO, & M. ATOJI, First Congress of the International Union of Crystallography,1948.
- 95 T.G. SPIRO, Inorg.Chem., 1965,4,1290.
- 96 C.K. JORGENSON, "Orbitals in Atoms and Molecules", Academic Press, 1962.
- 97 B. ZASLOW & R.E. RUNDLE, J.P.C., 1957,61,490.
- 98 A. DAVISON, M.L.H. GREEN, & G. WILKINSON, J., 1961,3172.
- 99 L.T. REYNOLDS & G. WILKINSON, J.I.N.C., 1956,2,246.
- 100 F.C. WILSON & D.P. SHOEMAKER, J.C.P., 1957,27,809.
- 101 F.C. WILSON & D.P. SHOEMAKER, Naturwiss, 1956,43,57.
- 102 H.L. ROBERTS & N.H. RAY, J.,1960,665.
- 103 L.H. CROSS, H.L. ROBERTS, P. GOGGIN, & L.A. WOODWARD, T.F.S., 1960,56,945.
- 104 B. COHEN, A.J. EDWARDS, M. MERCER, & R.D. PEACOCK, Chem.Comm., 1965,322.
- 105 G.W. CHANTRY, H.A. GEBBIE, B. LASSIER, & G. WYLLIE, Nature, 1967,214,163.
- 106 W.H. ZACHARIASEN, Acta Cryst., 1948,1,285.
- 107 ibid, 1948,1,268.
- 108 J. GAUNT, T.F.S., 1954,50,546.

- 109 S.L. GERHARD & D.M. DENNISON, Phys.Rev., 1933,43,197.
- 110 B. WEINSTOCK & J.G. MALM, Proceedings of the Second United Nations International Conference on the Peaceful Uses of Atomic Energy, Geneva, 1958,28,125.
- 111 R. KEWLEY, K.S.R. MURTY, & T.M. SUGDEN, T.F.S., 1962,58, 1284.
- 112 A.F.WELLS, J., 1947,1690.
- 113 D.M. ADAMS, M. GOLDSTEIN, & E.F. MOONEY, T.F.S., 1963,59,2228.
- 114 M. GOLDSTEIN, E.F. MOONEY, A.ANDERSON, & H.A. GEBBIE, S.A., 1965,21,105.
- 115 W. LANG, Ber., 1888,21,1578.
- 116 A.B.P. LEVER, J. LEWIS, & R.S. NYHOLM, Nature, 1961,189,58.
- 117 A.E. UNDERHILL, J., 1965,4336.
- 118 D.E. BILLING, A.E. UNDERHILL, D.M. ADAMS, & D.M. MORRIS, J(A)., 1966,602.
- 119 D.M. ADAMS & P.J. LOCK, J(A)., 1967,620.